DUPLO Deliverable D6.3

Full-Duplex Radios for Local Access, final report

Project Number:	**316369**
Project Title	**Full-Duplex Radios for Local Access – DUPLO**
Deliverable Type:	**PU**

Contractual Date of Delivery:	**May 31, 2015**
Actual Date of Delivery:	**June 8, 2015**
Editor(s):	**Kari Rikkinen (UOULU)**
Author(s):	**Kari Rikkinen (UOULU), Ari Pouttu (UOULU), Visa Tapio (UOULU), Hirley Alves (UOULU), Björn Debaillie (IMEC), Cristina Lavin (TTI), Mir Ghoraishi (UniS), Jawad Seddar (TCS), Dirk Jan van den Broek (UT)**
Work package:	**WP6**
Estimated person months:	**8**
Security:	**PU**
Nature:	**Report**
Version:	**1.0**

Abstract: This deliverable provides summary on main results from research on full-duplex transceiver techniques and system level solutions conducted in the DUPLO project. The developed RF, antenna, analog and digital baseband solutions for full-duplex transceiver and their performance characteristics are given. Numerical results from conducted system level studies and developed radio resource management and protocol solutions are also presented. Furthermore, the implemented proof-of-concept platform and its measured performance characteristics are introduced.

Keyword list: full-duplex, self-interference, transceiver, antenna, RF circuits and systems, baseband, system performance

Executive Summary

This document provides summary on main results from research on full-duplex transceiver techniques and system level solutions conducted in the DUPLO project.

The Full-Duplex Radios for Local Access – DUPLO project is a concerted effort with partners from industry and academia that addresses the challenge of developing transceiver techniques and system level solutions for full-duplex operation in small area radio systems. The project started in November 2012, and concludes in May 2015.

DUPLO has studied potential full-duplex transceiver techniques for radio devices, aiming to solutions which are attractive in terms of form-factor, system integration, process technology and operation flexibility. Three RF/antenna/analog solutions have been developed. These solutions cover a SI-cancelling front-end, a dual-polarized antenna structure and an electrical balance duplexer. Compared to the state-of-the-art, the developed designs differ mainly in terms of form-factor and integration potential in compact or portable radio system devices. This is significant advance for the DUPLO solutions, since the previously published techniques mainly rely on physical dimensions (i.e. antenna spacing) and/or require bulky component.

Main emphasis in the digital baseband solutions related studies has been in search for novel algorithms to improve self-interference cancellation capability in the presence of transceiver non-linearity, and in performance improvements with joint RF and digital cancellation. Furthermore, precoding techniques and baseband algorithms full-duplex MIMO systems have been analysed and developed.

The DUPLO proof-of-concept hardware demonstrator integrates sub-set of the designs into a complete full-duplex transceiver solution enabling performance measurements in realistic dynamic indoor operation environment. Two different full-duplex radio transceivers have been implemented within DUPLO project, i.e. single-port antenna demonstrator and dual-port antenna demonstrator. Conducted performance measurements indicate that the achievable self-interference cancellation capability is around 65 dB and 90 dB in 20 MHz bandwidth, with single port antenna solution and dual port antenna solution, respectively. As proof-of-concept for the functional operation, two short distance point-to-point link demonstrators with each two DUPLO full-duplex transceivers have been successfully showcased in VTC-2015 Spring DUPLO Workshop.

DUPLO system level studies have focused on full-duplex transmission in small cell radio system operation environment. Potential use cases are full-duplex BS serving half-duplex UEs, full-duplex UE, device-to-device connections, relaying, and transmission in mesh networks. Numerical results from conducted performance studies in network level indicate that in small area systems full-duplex transmission can provide system level performance gains over half-duplex even with moderate self-interference cancellation levels (70 dB…90 dB). However, better self-interference cancellation capability in the full-duplex transceiver is beneficial in expanding the competitive operation range of full-duplex transmission. Maximum observed system level capacity gain of full-duplex over half-duplex in small cell networks varies from 40% to 80% depending on the study assumptions.

Radio resource management is crucial when aiming to utilize full-duplex transmission efficiently in wireless networks. Several algorithms have been devised to tackle problems such as spectral efficiency maximization, scheduling, co-channel interference, power allocation etc. Advanced relaying schemes, protocol solutions for mobile ad-hoc networks and network level management solutions are also covered.

The DUPLO work on full-duplex technology development has gained lot of attention outside the project, and has been well received for multiple top-tier publications and conferences in various domains. DUPLO has organized two workshops on full-duplex technology, the first in conjunction with Crowncom 2014 and the second with VTC-2015 Spring conference.

Authors

Partner	Name	Email
University of Oulu (UOulu)	Kari Rikkinen	krikkine@ee.oulu.fi
	Ari Pouttu	apo@ee.oulu.fi
	Visa Tapio	vita@ee.oulu.fi
	Hirley Alves	halves@ee.oulu.fi
TTI Norte, SL (TTI)	Cristina Lavin	clavin@ttinorte.es
Interuniversitair Micro-Electronica Centrum vzw (IMEC)	Björn Debaillie	bjorn.debaillie@imec.be
Universiteit Twente (UT)	Dirk Jan van den Broek	j.d.a.vandenbroek@utwente.nl
University of Surrey (UniS)	Mir Ghoraishi	m.ghoraishi@surrey.ac.uk
Thales Communications & Security SA (TCS)	Jawad Seddar	jawad.seddar@thalesgroup.com

Table of Contents

Abbreviations

ADC	Analog to Digital Converter
AGC	Automatic Gain Control
AWGN	Additive White Gaussian Noise
BER	Bit Error Rate
BPSK	Binary Phase Shift Keying
BS	Base Station
BW	Bandwidth
CCI	Co-Channel Interference
CMOS	Complementary Metal Oxide Semiconductor
CP	Cyclic Prefix
CSI	Channel State Information
CTS	Clear to Send
DL	Downlink
DUPLO	full-DUPlex radios for LOcal access
EBD	Electrical Balance Duplexer
EC	European Commission
EVM	Error Vector Magnitude
FD	Full Duplex
FDD	Frequency Division Duplexing
FDHD	Full Duplex Dual Hop
FDJD	Full Duplex Joint Decoding
FP7	Seventh Framework Programme
HD	Half Duplex
IEEE	Institute of Electrical and Electronics Engineers
IBFD	In-Band Full-Duplex
IIP	Intermodulation Intercept Point
IP	Internet Protocol
LNA	Low Noise Amplifier
LTE	Long Term Evolution
LTS	Long Training Sequence
MAC	Media Access Control
MANET	Mobile Ad-hoc Network
MMSE	Minimum Mean Square Error
MIMO	Multiple Input Multiple Output
OFDM	Orthogonal Frequency Division Multiplexing
OFDMA	Orthogonal Frequency Division Multiple Access
PA	Power Amplifier
PC	Personal Computer
PCB	Printed Circuit Board
PHY	Physical layer
QAM	Quadrature Amplitude Modulation
QPSK	Quadrature Phase Shift Keying
RF	Radio Frequency
RTS	Request to Send
RX	Receiver
SAW	Surface Acoustic Wave
SE	Spectral Efficiency
SI	Self Interference
SIC	Self Interference Cancellation
SINR	Signal to Interference and Noise Ratio
SIR	Signal to Interference Ratio

SISO	Single Input Single Output
SOI	Silicon on Insulator
STS	Short Training Sequence
TDD	Time Division Duplexing
TX	Transmitter
UDP	User Datagram Protocol
UE	User Equipment
UL	Uplink
USB	Universal Serial Bus
VM	Vector Modulator
WARP	Wireless Open Access Research Platform
WLAN	Wireless Local Area Network
WP	Work Package

1. INTRODUCTION

The evolution of wireless communication networks with ever-increasing data traffic call for air interface enhancements to exploit the finite radio resources more efficiently. The foreseen need to support thousand-fold increase in traffic volume with future 5G wireless network solutions compared to today's standards emphasizes the importance of system capacity enhancement as one major target for system solution development. Future 5G networks are aimed to provide capabilities for very high achievable data rates, very low latency, ultra-high reliability, and the possibility to handle extreme device densities, in cost and energy efficient manner [1][2]. Full-duplex wireless transmission is considered as a promising air interface technique for future wireless systems at it tackles key issues such as spectral efficiency, link level capacity and latency [1].

In the full-duplex (FD), or more explicitly *in-band* full-duplex wireless (IBFD) transmission concept, a wireless terminal is allowed to transmit and receive simultaneously in the same frequency band. The concept sets high requirements to the transceiver implementation due to self-interference phenomena (i.e., transmit signal leaking into its own receiver), but when successfully solved, it provides significant improvements to wireless systems operation [3]. Enabling wireless devices to operate in full-duplex mode offers the potential to double their spectral efficiency in terms of transmitted bits per second per Hz. Full-duplex can provide more flexibility in spectrum usage. Same frequency resources can be used for one directional transmission or bi-directional transmission. Full-duplex can complement legacy half-duplex systems based on time division duplexing (TDD) or frequency division duplexing (FDD). Beyond spectral efficiency and physical layer, full-duplex concepts can be advantageously utilized in higher layers, such as the access layer. Full-duplex transmission can reduce air interface delays and facilitate improved collision detection/avoidance mechanisms on contention based networks.

In-band full-duplex wireless has a long history, and the concept has been utilized already in 1940s with full-duplex radars [4]. Terrestrial wireless communication systems like cellular mobile and WiFi have not yet largely utilized full-duplex transmission. In these systems, full-duplex has been used in some special cases, e.g., relaying applications [5]. However, interest in applying full-duplex to future evolution of wireless systems has risen significantly during past few years. Potential use cases proposed for full-duplex in the literature include relaying, self-backhauling, microwave backhaul links, mesh networks, cognitive radio, access points/base stations and devices in Wi-Fi and mobile systems [3][6]-[10]. Short-range systems (e.g., femto or pico cells in mobile wireless systems and Wi-Fi systems) are especially feasible operation environments for full-duplex because the self-interference requirements are much more relaxed in these environments compared to large cell systems. This facilitates implementation of full-duplex technology to compact commercially attractive wireless devices.

The Full-Duplex Radios for Local Access - DUPLO project [11] is a research project within the Seventh Framework Programme for research and technological development (FP7) of the European Commission (EC). The DUPLO project is a concerted effort with partners from industry and academia that addresses the challenge of developing transceiver techniques and system level solutions for in-band full-duplex operation in small area radio systems. The project started in November 2012, and concludes in May 2015.

DUPLO has studied potential full-duplex transceiver techniques for *compact* radio devices such as small cell access points, tablets, smart phones, and smart glasses. Three RF/antenna design

solutions for full-duplex radios have been developed, fabricated and validated. The first design is based on self-interference cancelling transceiver front-end structure [19]. The second design is an antenna technique based on dual-polarized microstrip patch antenna structure, complemented with an active analog cancellation network [17]. The third design is based on electrical balance duplexer circuit which connects with a single port antenna [17]. The DUPLO RF/antenna solutions are designed with the aim to enable their integration into the compact radio device as a separate module, or on the radio chip (system on chip, SoC). In that respect, DUPLO is in the leading edge in developing and presenting solutions for integrated design targeted specifically for in-band full-duplex operation [27][28][38]. Main emphasis in the digital baseband solutions related studies has been in search for novel algorithms to improve self-interference cancellation performance in the presence of transceiver non-linearity, and in performance improvements with joint RF and digital cancellation.

The DUPLO transceiver solutions (including RF and antenna designs, and digital baseband algorithms) for compact full-duplex transceiver are developed to tackle the main design challenges such as high self-interference cancellation requirement, dynamic operation environment, and feasibility for compact devices. The DUPLO solutions are validated based on an integrated proof-of-concept hardware demonstrator. As proof-of-concept for the functional operation, a short distance point-to-point link with two DUPLO full-duplex transceivers has been successfully demonstrated in VTC'2015 Spring DUPLO Workshop [14].

At system level, the DUPLO focus has been in small area radio systems. System level studies are conducted to evaluate attainable gains of using full-duplex transceivers in different network nodes and to study radio resource management and protocol solutions for networks deploying full-duplex transmission in the air interface. Key findings from conducted radio resource management and protocols studies are reported in multiple journal and conference papers [30]-[34].

This document provides a summary on the main results of the technical work conducted in DUPLO WPs 1-6, and provides further conclusions on the potential and future development needs of in-band full-duplex transmission in wireless systems.

The outline of the remainder of this document is as follows:

- In chapter 2, the DUPLO scenarios and technical approach are presented, based on system requirements defined in DUPLO WP1 [15].
- Chapter 3 introduces the developed RF/antenna and digital baseband solutions and their observed performance, based on technical work conducted in DUPLO WP2 [16]-[19] and DUPLO WP3 [20][21].
- Chapter 4 presents main results from the conducted system level studies in DUPLO WP4 [22]-[24].
- Chapter 5 introduces the DUPLO proof-of-concept hardware demonstrator and its measured performance characteristics, as studied in DUPLO WP5 [25][26].
- Chapter 6 discusses potential future development opportunities.
- Finally, chapter 7 provides summary and conclusions on the DUPLO project conducted work and results.

2. CHALLENGES AND TECHNICAL APPROACH

The in-band full-duplex transmission scheme differs fundamentally from conventional duplexing schemes, i.e., frequency division duplexing and time division duplexing, which are used in legacy wireless communication systems. While the conventional duplexing schemes are based on orthogonal spacing of transmit and receive signals (either in frequency or time domain), the full-duplex concept enables a wireless terminal to transmit and receive simultaneously in the same frequency band. Full-duplex offers the potential to improve the radio system performance, but sets also challenges for wireless transceiver implementation as well as system deployment.

2.1. Full-duplex transceiver

Simultaneous transmission and reception at the same frequency band creates *self-interference (SI)* (transmit signal leaking into its own receiver, see Figure 1.) problem in the transceiver. The self-interference deteriorates receiver (RX) performance unless it is significantly reduced (ideally down to noise floor level). The total self-interference reduction requirement depends on the deployment scenario, and can be more than 100 dB to get full gain out of full-duplex transmission. To achieve this challenging requirement, the self-interference reduction needs to be implemented constructively in multiple stages across the full-duplex transmitter (TX) chain (antenna, RF, and baseband). Furthermore, these techniques should be self-adaptive to maintain the requirements over different propagation conditions and environments.

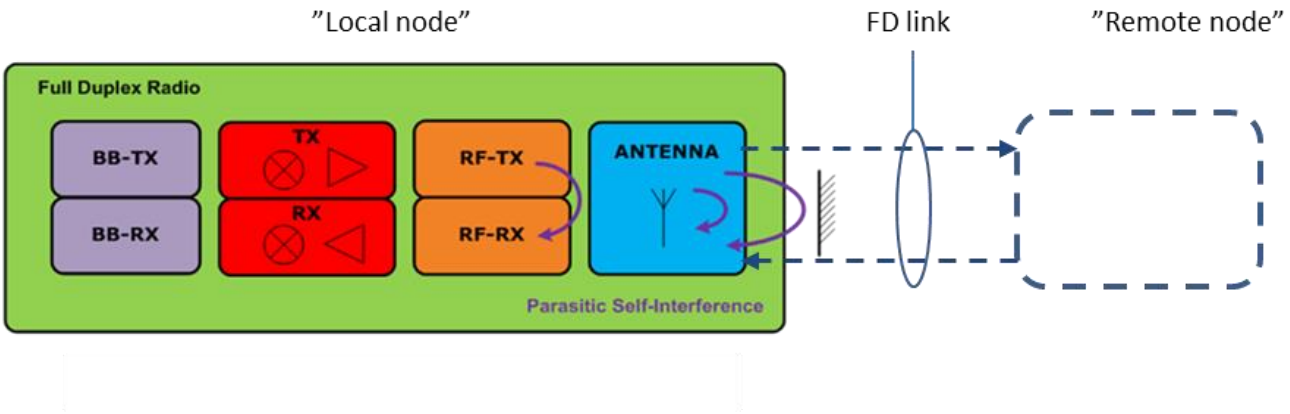

Figure 1. Self-interference in the full-duplex transceiver

DUPLO targets solutions for wireless radios to facilitate full-duplex operation in *compact* commercially attractive communication devices. The focus in RF/antenna circuit development is in solutions can offer substantial self-interference isolation or cancellation and can be integrated into the compact radio device as a separate module, or integrated on the radio chip. The full-duplex radio solutions presented in literature mainly rely on physical dimensions (i.e., antenna spacing) or require bulky components [12][6], hampering dense integration. The focus in digital baseband algorithm development is in search for efficient solutions to improve self-interference cancellation performance in the presence of transceiver non-linearity, channel estimation, and performance improvements with joint RF and digital cancellation.

2.2. System scenarios

‘

DUPLO has selected small cell radio system operation environment as the main framework for system level studies. Other scenarios studied in the DUPLO project include public safety networks and mesh networks [15]. Densification of network deployments is already trend in 4G, and the development continues with 5G. Small cells improve spatial re-use of spectral resources and facilitate low transmit powers for data transmission, even with high data rates. Small cells are attractive application areas for full-duplex transmission because the self-interference reduction requirements are much more relaxed in these operation environments compared to macro cells. This facilitates implementation of full-duplex technology to compact commercially attractive wireless devices.

Potential use cases for full-duplex transmission in wireless networks are radio connections in LTE and future 5G small indoor or outdoor radio cells (e.g., femto or pico cells), device-to-device connections, relaying, transmission in mesh networks, and (self-)backhauling connections. All these scenarios, except the last one, have been included in the DUPLO system studies. In a small radio cell, full-duplex capable base station can serve half-duplex terminals, or both base station and terminals are operating in full-duplex mode. In all cases, the main target is to improve spectral efficiency beyond legacy half-duplex (FDD or TDD) connections utilizing the full-duplex capability in some or all of the network nodes.

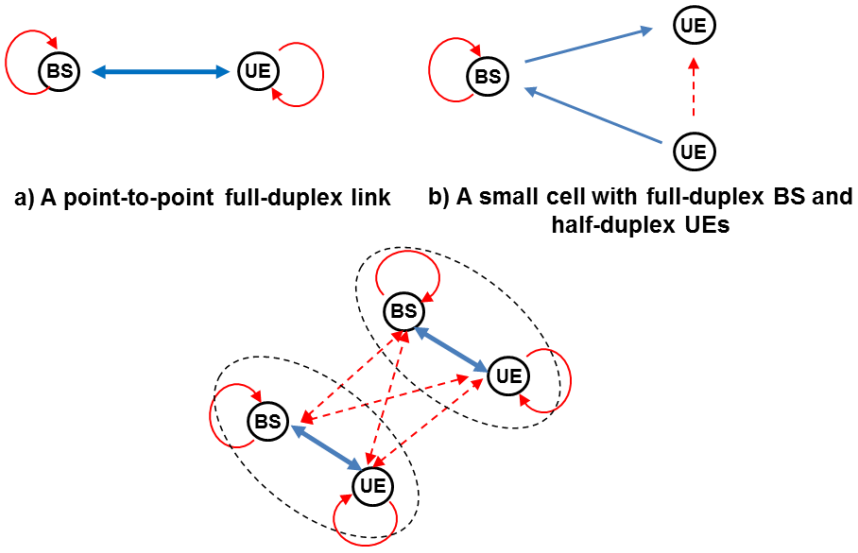

a) A point-to-point full-duplex link

b) A small cell with full-duplex BS and half-duplex UEs

c) Two neighboring small cells with full-duplex BS and UEs

Figure 2. Full-duplex deployment scenarios. The solid blue lines denote the desired signal channels, the solid red lines denote the self-interference channels, and the dashed red lines denote the inter-node interference channels.

Figure 2 shows basic network set-ups related to the above mentioned full-duplex use cases and illustrates the full-duplex implementation challenges in these scenarios. The basic set-up (Figure 2 a) is the point-to-point connection between two nodes (either BS or UE types, or both). In this set-

up, the specific challenge with full-duplex transmission is the self-interference in each node. Depending on the link scenario, the transmit power level may range from roughly 80 dB to 120 dB stronger than the receiver noise floor, thus implying that the total self-interference reduction (isolation and cancellation) requirement should be on the same order [18].

Another potential usage scenario for full-duplex transmission is shown in Figure 2 b), where the same spectral resource is simultaneously used for two connections; i.e., the BS is transmitting a signal to one UE while receiving another signal from another UE. In this case only the BS needs to be full-duplex capable device, while the UEs can be legacy half-duplex devices. Additional challenge in this case is the inter-node interference (between the transmitting and receiving UE). This calls for novel radio resource management solutions (e.g., scheduling, power allocation) to use available radio resources efficiently.

In multiple cell case, full-duplex operation creates interference paths between all active nodes as illustrated in Figure 2 c). Thus, in network level, the full-duplex system implementation challenge is not only how to realize compact full-duplex device with high self-interference cancellation (SIC) capability, but also how to combat with additional inter-node interferences simultaneous transmission and reception causes to the system. Furthermore, in practice, the network level gain of full-duplex transmission depends on multiple aspects (traffic asymmetry, network architecture, propagation conditions, etc.).

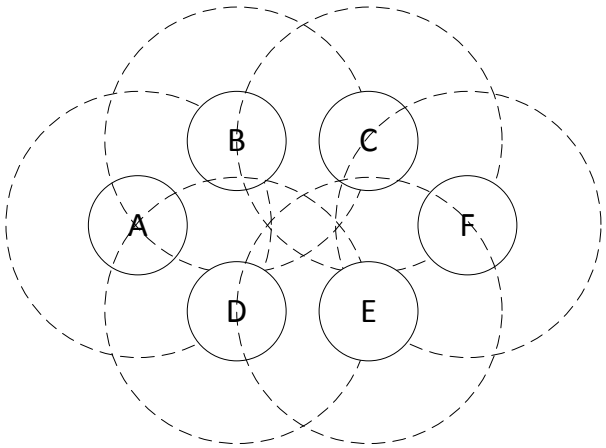

Figure 3. Mesh network topology with six nodes

Another network configuration covered in the DUPLO project is mesh network, as illustrated in Figure 3. DUPLO studies in this scenario are related to routing and protocol studies in IEEE802.11 technology based mobile ad-hoc networks deploying full-duplex nodes.

Finally, DUPLO full-duplex usage scenario in public safety networks consists of terminals operating in relaying mode forming UE relay connections and mobile ad-hoc network configurations.

2.3. Proof-of-concept

DUPLO has implemented a proof-of-concept hardware demonstrator to validate that the solutions developed in the project can be combined together as a complete and working full-duplex transceiver solution, operational on subset of system scenarios. The system set-up for the proof-of-

concept consists of short distance wireless point-to-point connection between two full-duplex transceivers, see Figure 4 .

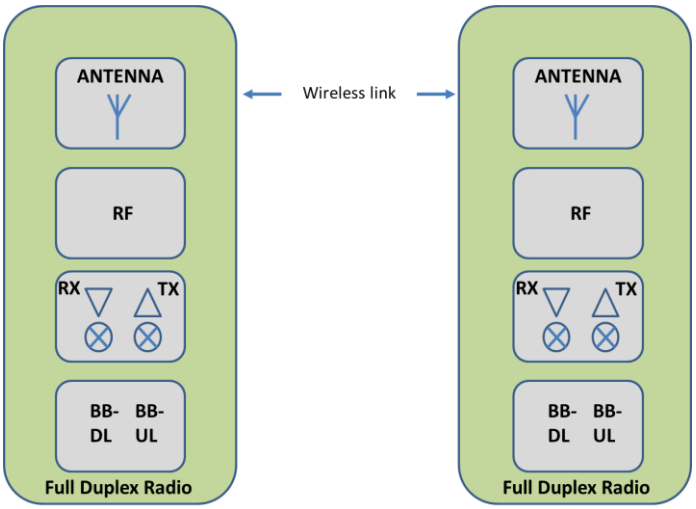

Figure 4. DUPLO Proof-of-concept system set-up

Two different demonstrators for the full-duplex transceiver hardware targeting at different form-factors are developed [25]. These demonstrators demonstrate different analog cancellation techniques while using the same digital baseband self-interference cancellation solution. The first analog solution, targeting to extremely compact radio devices, integrates a single port antenna with an electrical balance duplexing circuit. The second solution, targeting to compact radio devices such as small access point, consists of dual-polarized antenna and an active cancellation network. Both solutions use the WARP v3 [35] platform and WARPLab environment [36] for baseband processing. The proof-of-concept operates at 2.45 GHz carrier frequency.

3. FULL-DUPLEX TRANSCEIVER

Full-duplex is a promising scheme in wireless communications to increase the spectral efficiency and/or throughput while improving the network fairness and coordination. Full-duplex is considered as a promising candidate to support the mobile network evolution towards 5G. The implementation of the full-duplex concept is, however, hampered by the limited capability of the radio transceivers to prevent receiver sensitivity degradation due to self-interference. To overcome this, the transceiver radio should implement methods to prevent the RF-signal generated by the local transmitter from leaking onto its own receiver and to cancel any remaining self-interference from the receiver path using knowledge of the transmitter signal. This transceiver ability sets challenging requirements for the complete radio design, as these methods should be implemented along the complete transceiver chain, including digital, analog, RF and the antenna(s). These requirements are amplified as the DUPLO project targets small form-factor solutions which can be integrated in compact radio devices such as smartphones. Therefore, e.g. TX-RX physical separation/shielding and bulky antenna structures are not permitted in this project. The paper [27] derives the full-duplex transceiver requirements, and identifies the main bottlenecks in the design specifications. By trading-off the cancellation location in the transceiver and by providing the design requirement equations, the design specifications for analog/RF components and the digital baseband algorithms have been derived.

3.1. General

Figure 5 shows a full-duplex link with a local and remote transceiver node. Each node has one antenna for the transmitter and one for the receiver. In this link, three sources of SI limit the proper reception of the signal coming from the remote node by the local RX. First, leakage can occur on-chip or on-board (type A). Such direct cross-talk is likely to occur with dense integration. Second, line-of-sight leakage or spill-over between the two antennas may occur (type B). This SI is generally reduced by implementing antenna structures with specific radiation patterns or polarizations. Finally, TX signals may be reflected on nearby objects back into the receive antenna (type C). Such multipath refection typically result in frequency-dependent SI.

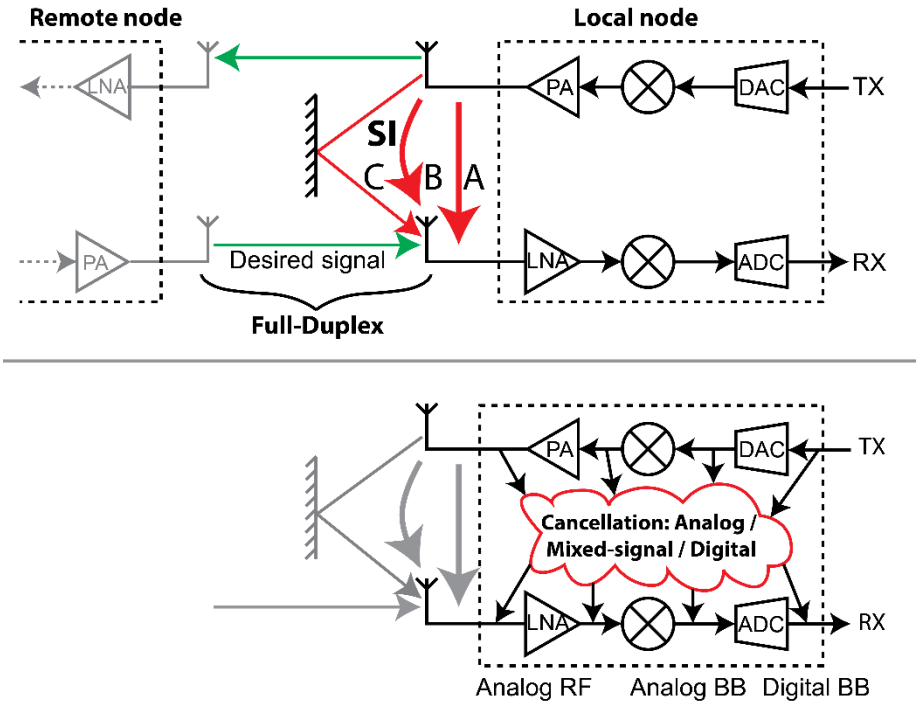

Figure 5. Full-duplex radio is subjected to different self-interference paths. Self-interference cancellation can be realized from various points in the transmitter chain to various points in the receiver chain.

The self-interference caused by the different paths can be cancelled by copying reference signal(s) from the TX chain and subtracting reference signal(s) after modification in the RX chain. This modification involves attenuation and phase shifting to cancel the frequency-independent SI and additional signal delaying to cancel the frequency-dependent SI. As shown in bottom figure of Figure 5, the SI cancellation can be realized from various points in the transmitter chain to various points in the receiver chain. Therefore, different architectural options exist.

The DUPLO project developed cancellation solutions both at RF/analog and antenna level, as well as at digital baseband. The RF/analog and antenna solutions mainly target to prevent and cancel the SI due to direct cross-talk and line-of-sight leakage (type A and B), while the digital solutions further cancel the SI towards a total of 70 to 100 dB, while covering also the SI due to multi-path reflection.

In the following sections, the main SI-cancellation techniques developed in the DUPLO project are briefly described. These techniques cover different solutions for the RF/antenna/analog part of the radio transceiver as well as different solutions for the digital part.

3.2. RF/analog and antenna solutions for full-duplex transceiver

One of the main objectives of the DUPLO project was to pave the way for the introduction of the full-duplex concept in short range wireless communication systems. Focussing on the RF/antenna/analog part of the full-duplex transceiver, different design requirements were targeted:

- compact in form-factor to support dense system integration
- implementable in low-cost scaled technology

- suitable for mass-production
- reconfigurable to support e.g. other operation frequencies or modes
- self-tuning with changing operation conditions or environmental conditions
- compatible with in-system and/or legacy components (e.g. commercial off-the-shelf components)

The implementation of SI-cancellation techniques close to the antenna (RF/analog) is essential mainly for two reasons. First, the power difference of the transmit and receive signal is maximal in RF, and causes a high risk for saturation of the receiver (with high gain). Second, using the TX signal close to the antenna as a reference is beneficial as it contains most information: the signal, any in-channel TX imperfections such as TX-generated noise and distortion, as well as any gain and phase imbalance across the channel that the signal has experienced through the TX chain. If, for example, the TX reference would be copied before the power amplifier (PA), the (dominant) PA-nonlinearities cannot cancelled.

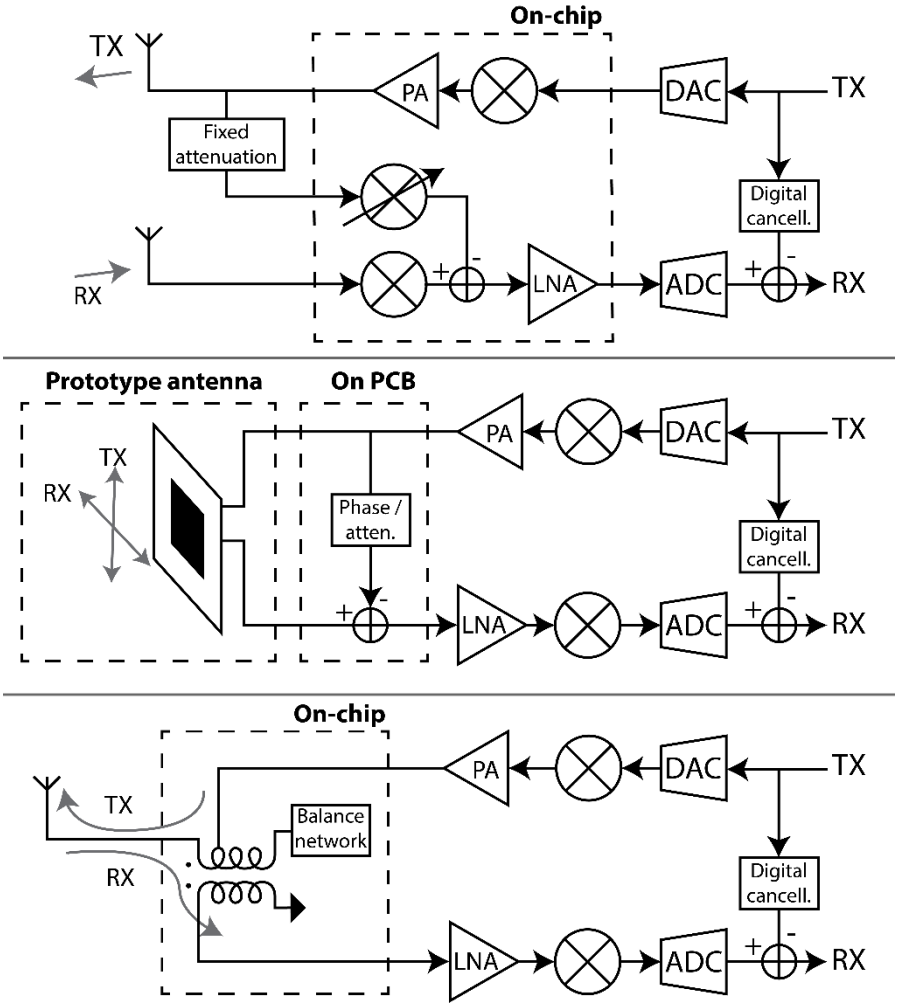

Figure 6. Three topologies developed in WP2 of the DUPLO project to reduce self-interference, applied in a generic full-duplex transceiver structure with digital cancellation. Top: front-end with SI-cancelling receiver, middle: dual-polarized antenna and active cancellation network, bottom: electrical balance duplexer

In DUPLO, different RF/antenna/analog solutions have been developed. These solutions cover 1) a SI-cancelling front-end, 2) a dual-polarized antenna structure and 3) an electrical balance duplexer as illustrated in Figure 6. Although all three solutions target integration in compact radio units, they offer specific benefits and can thus be applied in different applications. The SI-cancelling front-end targets dense on-chip implementation suitable for mass-production and digital/analog/RF co-integration, and uses a dual COTS antenna structure with a moderate isolation between the antenna elements. The dual-polarized antenna structure targets integration in larger radio units such pico-cell base stations. The electrical balance duplexer also targets dense on-chip implementation, but uses a single conventional antenna for simultaneous transmission and reception. Each of these solutions have been prototyped (even different prototype iterations) and measured. The main findings and design aspects have been published in top tier conference proceedings and journals as both collaborative and individual work. Although the different solutions are targeting different applications and are not fully complementary, the collaborative aspect within this work package was a key asset. This collaboration seeded cross-fertilisation and synergy which leaded to more innovation and better results. The three solutions are elaborated more in detail in the next sections.

3.2.1. SI-cancelling front-end

In compact FD radio devices, space may not permit sophisticated antenna solutions to provide high SI isolation. Also, a varying near-field environment (e.g. a person holding the device) constantly changes the magnitude and phase of type A and B self-interference (Figure 5), requiring an adaptive solution. Experiments using two crossed WLAN dipole antennas as a simple FD antenna showed that 20dB worst-case isolation is a reasonable assumption for a basic 2-port antenna solution in such situations. This leaves room for 20 to 40dB improvement in the analog domain before type C (Figure 5) SI becomes the bottleneck [27].

Given this scenario, different potential front-end architectures have been investigated and traded-off [18] based on the design requirements of the transceiver components calculated with the equations presented in [27]. Based on this analysis, a novel front-end architecture has been identified as illustrated in Figure 6(top). The main novelty is the cancellation path that taps the signal at TX RF and injects it at the RX analog baseband. This topology is mainly suitable to *actively boost the isolation of a moderate antenna solution*. E.g. when an antenna solution is used that provides a moderate 15-20 dB isolation, this topology can improve the isolation by 30-45 dB before reflections become the dominant self-interference. These reflections are then cancelled in the digital baseband by a second cancellation path that accounts for delay in the digital domain.

A strong point of this architecture is that *attenuation, phase shift and downconversion can be combined into one functional component: a vector modulator mixer.* However, since the cancellation point is located in analog baseband, the strong self-interferer is fully present in LNA, downconverter and vector modulator. To prevent drowning the weak underlying desired signal in distortion in these stages, *extreme linearity* is required. This can be accomplished by using a *mixer-first architecture* [37] for both the main mixer and the vector modulator. Circuit simulations confirmed the unique potential of this architecture and indicated that the drawbacks could be resolved by using appropriate circuit topologies.

3.2.1.1. Front-end design

As shown in Figure 6, the SI-cancelling path takes a copy of the transmitted signal at RF through a fixed attenuator. The attenuator value is chosen dependent on the worst-case isolation expected from the antenna solution. Subsequently, a variable phase shift and attenuation is applied, the signal is downmixed and the resulting signal is subtracted in the analog baseband. The advantage of this architecture is that phase shift, attenuation and downmixing can be efficiently combined in a *vector modulator (VM) downmixer*. Figure 7 shows a simplified implementation of the receiver with

such a VM downmixer. Essentially, both the VM and the main RX mixer are 4-phase switched resistor mixers which maintain high linearity under large SI powers. The VM is a sliced version of the main RX mixer, incorporating multiplexers in each slice that steer the 4-phase output current to the appropriate baseband phases.

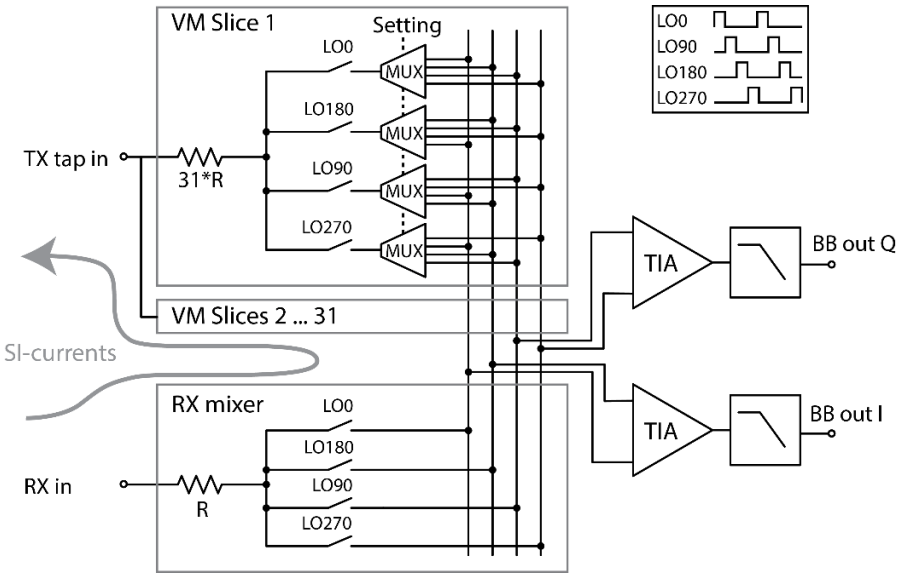

Figure 7. Simplified implementation of the SI-cancelling receiver. One slice of the 31-slice vector modulator (VM) downmixer is shown in detail. The depicted design is single-ended, the actual design is fully differential. Implementation details are shown in [38].

The amount of slices of the VM determines the number of phase / amplitude constellation points that can be covered and thus the amount of cancellation that can be achieved due to quantization effects. For 31 slices, this results in a 32x32 constellation of discrete phase/amplitude values, theoretically allowing 27.1 dB SI-cancellation.

For the transmitter, a four-phase sampling mixer architecture has been selected which samples its output on the gates of a class-A common source PA as depicted in as illustrated in Figure 8 [38][39]. This architecture has been selected for its high in-band accuracy (low 1/f noise and predictable distortion), which is important for full-duplex, as highly deterministic self-interference is more easily cancelled digitally. Moreover, this architecture can also be clocked with the same four-phase, non-overlapping full-swing clock signals readily available in the receiver.

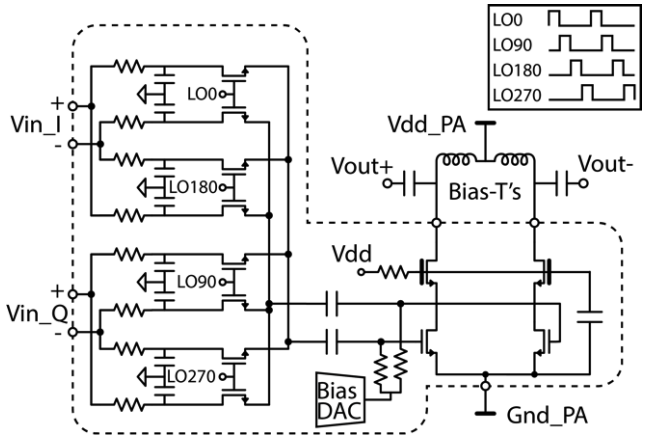

Figure 8. Transmitter topology: Four-phase sampling mixer and common source class-A PA. Dashed line indicates the chip boundary. The clocks are shared with the receiver.

This front-end has been implemented in 65nm CMOS and covers an area of 2mm^2 only; a die photo is shown in Figure 9.

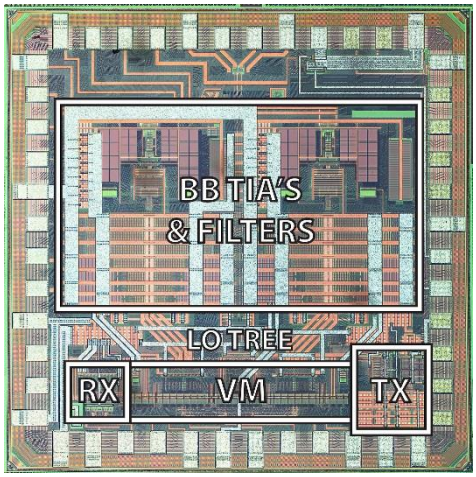

Figure 9. Chip photo of the 1.4 x 1.4mm SI-cancelling front-end prototype in 65nm CMOS

3.2.1.2. Experimentation results

The SI-cancellation performance of the SI-cancelling front-end was measured with the build-in transmitter and crossed WLAN dipole antennas as illustrated in Figure 10 (a) [40]. A test signal of 20 tones with random phases over a 16.25 MHz bandwidth are transmitted at 2.5GHz. The setup was located in an RF lab environment without taking any specific measures to induce or reduce reflections. The external attenuator is set to 20dB to mimic a worst-case antenna isolation of 23dB (including 3 dB VM attenuation). Figure 10 (b) shows measured spectra in the system: at the transmitter output, at the receiver input and after cancellation (referred to the receiver input). At a transmit power level of about 0dBm, the antenna isolation equals 28.9dB. Added with a VM cancellation of 16.8dB, the combined SI rejection equals 45.7dB. The residual SI becomes strongly frequency-selective, indicating the presence of reflected SI (type “C” in Figure 5) in the residue, since this type of SI is delayed and therefore not well approximated by a phase shift & attenuation. In conclusion, delayed SI, reflected by the environment comes in at 46dB below the transmitted power level, which is in the range of 40 to 50 dB as expected. Such reflections can be subsequently handled in the digital domain.

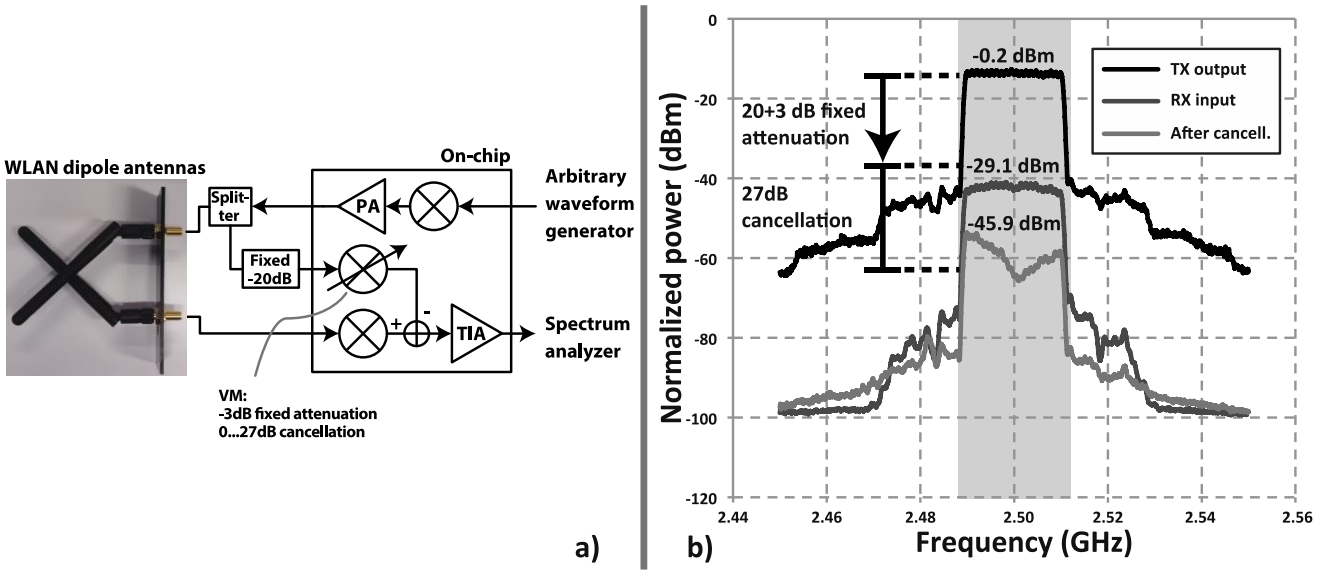

Figure 10. a) Simplified measurement setup using two crossed WLAN dipole antennas as a simple FD antenna, b) representative measured spectra at the output of the transmitter, input of the receiver and after analog cancellation (referred back to the RX input).

The main transmitter and receiver measured performance and cancellation performance are evaluated in [38][39]. Table 1 lists the main specifications of the transmitter and receiver. Note that for both the transmitter and the receiver are frequency agile, allowing operation of the entire SI-cancelling transceiver at carrier frequencies from 0.15 to 3.5 GHz.

Table 1. Main measured SI-cancelling front-end performance

Transmitter specifications @ 2.5 GHz carrier frequency		Mixer-first receiver + SI-cancelling VM-down-mixer	
	Technology	65 nm CMOS	
	Supply	1.2V	
	Operating frequency	0.15 – 3.5 GHz	
	Area	2 mm^2	
	TX/RX isolation	27 dB	
	Area	2 mm^2	
Output IP3	20.1 dBm	Maximum gain	24 dB
Image rejection ratio	38 dB	Noise figure	10.3 – 12.3 dB (6.3 in HD)
LO radiation	-49 dBm	Power consumption	23 – 56 mW (incl. LO tree)
Power consumption	108 mW from 2.0V (PA) 21 mW from 1.2V (LO)	Baseband bandwidth	24 MHz
Maximum single-tone output	12.4 dBm	In-band IIP3	+8 dBm
Efficiency at max. output	13%	Effective in-band IIP3 for SI	+19 dBm
EVM @ 0dBm 802.11a output	-40 dB	Out-of-band IIP3	+22 dBm

All mixers in the prototype are operating on the same frequency synthesizer, which contributes to the phase noise immunity in full-duplex mode [39]. Such immunity is required as experiments in [41] show that different synthesizers generating -38dBc *uncorrelated* phase noise in the band of interest induces a combined noise floor of -35dBc, limiting the cancellation. To verify the impact of the phase noise, experiments where done based with different local oscillator sources as illustrated in Figure 11 and a single-tone baseband signal at 1kHz. The results shown in Figure 12 illustrate

with shared/correlated clocks, the noise floor is hardly affected by phase noise. Experiments with an unshared clocks, however, resulted in a noise floor degradation of about 9.4 dB.

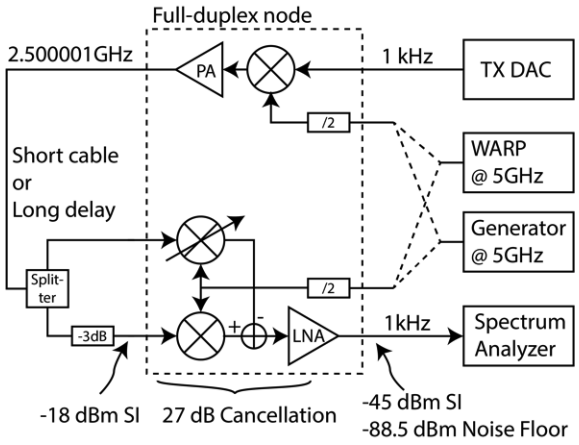

Figure 11. Simplified set-up used to measure the effect of correlated and non-correlated phase noise between TX and RX/VM, for short and long self-interference paths. The power levels are all referred to the RX input.

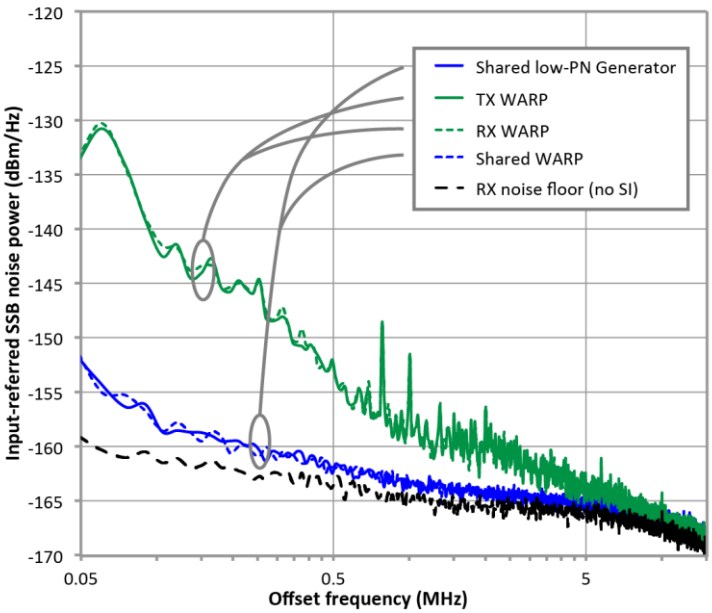

Figure 12. Measured input-referred noise spectra for the four clocking configurations with a short SI-path: A shared WARP clock shows comparable PN performance as a low-PN generator.

3.2.2. Dual-polarized antenna structure

The main goal of this task was the development of a compact antenna structure with a high isolation between its transmitter and receiver port. Different antenna structures have been considered and evaluated in [16], but to achieve such compact form factor and to maintain the radiation pattern, we opted for a dual-port single-aperture microstrip antenna structure with

orthogonal polarization to achieve an intrinsic isolation between the two antenna ports as illustrated in Figure 6 (middle).

The main objective for dual-polarization operation is to achieve high isolation and low cross-polarization simultaneously, especially in full-duplex application where high isolation between the antenna ports is crucial. Fulfilling both specifications simultaneously is very challenging, especially for compact antenna solutions, where both excitation ports are closely spaced and the parasitic coupling between them is high. In order to reach both conditions, a variety of feeding techniques have been considered [16]. Overall, the best performance is achieved by combining different excitation mechanism such as slot-coupled and multi-point excitation feeding networks in stacked-patch antenna structures offering attractive isolation values. In this DUPLO activity, a dual-polarized antenna with a stacked-patch antenna structure with two square patches and a symmetrical excitation network has been used. Also, a dual-linear polarization was used because linear polarization is generally not operation frequency dependent (in contrast to circularly polarized antennas).

The dual-polarized antenna has been implemented using microstrip technology, because of its properties to enable low profile, low cost and easy integration. For a microstrip patch antenna, dual linearly-polarized operation can be obtained by using a pair of probe feeds to respectively excite two orthogonal fundamental modes from a single radiating patch. The discrimination between the two polarizations could however be degraded by undesirable higher-order modes which can cause cross-polarization. To suppress the cross-polarization at each feeding port of the dual-polarized microstrip antenna, and thus improving the isolation level between ports, the antenna structure incorporates a symmetrical dual-feed excitation network with a phase difference of 180º and a pair of coupling slots.

Two different antenna prototypes have been evaluated based on experimental implementation. In the first prototype, the antenna is symmetrically excited in the horizontal plane by means of using a Wilkinson divider and the 180º phase shifted lines. Additionally, the antenna is excited in the vertical plane by a microstrip line with matching stubs

This first prototype has been analyzed in depth [16][27][28]; it provides >50dB isolation over a bandwidth of 10MHz, and covers an area of 90x90mm. This bandwidth is mainly limited by the impedance BW of the antenna. This gained knowledge was used for a redesign with more challenging requirements, targeting to further reduce the form factor, and to improve the matching bandwidth while maintaining the performance in terms of antenna isolation.

3.2.2.1. Final antenna prototype design and performance

Figure 13 illustrates the antenna geometry of the second dual-polarized antenna prototype. As in the first antenna prototype, the antenna consists of two square patches and three substrate layers with the same thickness and dielectric constant. In the horizontal plane (PORT 1), the Wilkinson divider has been replaced by a 1:2 divider. The vertical polarization (PORT 2) is excited by a 50Ω microstrip line and an internal via. Moreover, a rigid dielectric material with a dielectric constant of 2.5 has been included to separate the two square patches.

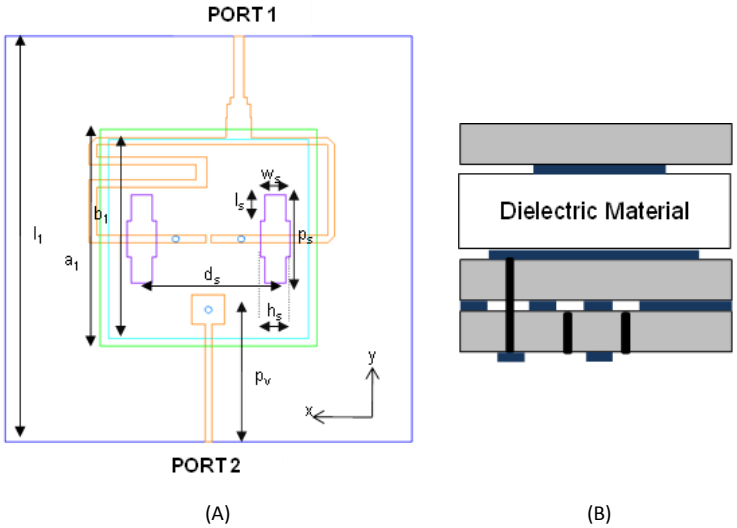

Figure 13. Geometry of the dual-polarized antenna. (A) Top view of the antenna, (B) multilayer antenna stack-up.

The optimum performance of the proposed antenna has been achieved by means of the parametric studies carried out on the full 3D electromagnetic model of the antenna. The antenna was simulated using a Rogers substrate with 3.55 dielectric constant and 0.508 thickness. The sensitivity analysis of the proposed antenna with respect to its resonance frequency, impedance matching and antenna isolation as a function of each geometrical parameter was performed with the 'Trust Region Framework' algorithm. The obtained optimal design parameters are given in Table 2 [40].

Table 2. Dual-polarized antenna design parameters.

Parameter	d	l_1	a_1	b_1	d_s	p_s	l_s	h_s	w_s	p_x
Dimension [mm]	7.0	60	33	30	20	13.7	4.0	2.5	3.3	20.2

The manufactured dual-polarized antenna prototype is shown in and measures 60x60x8mm [40].

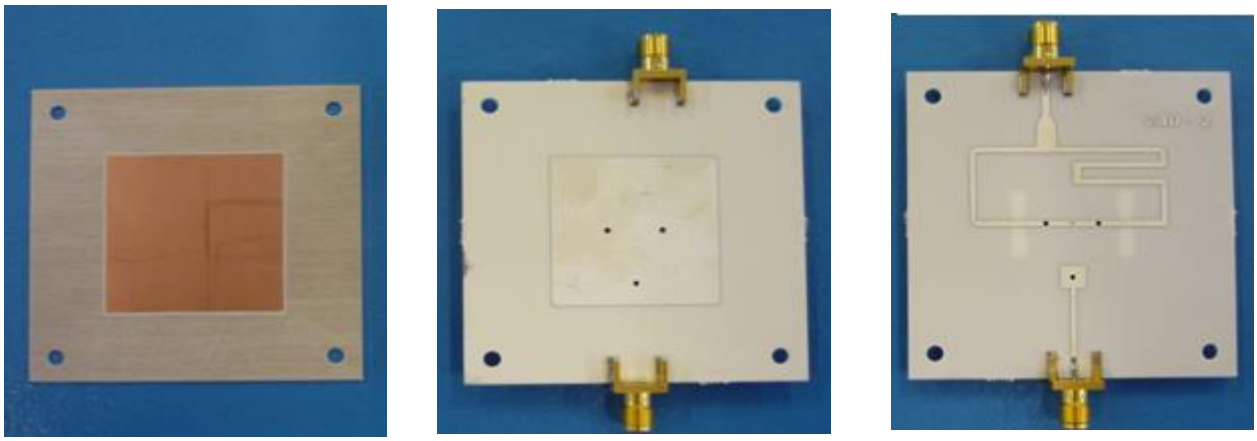

(A) (B) (C)

Figure 14. Dual-polarized antenna manufacturing. A) Upper patch. B) Lower patch C) Excitation networks for PORT1 and PORT2.

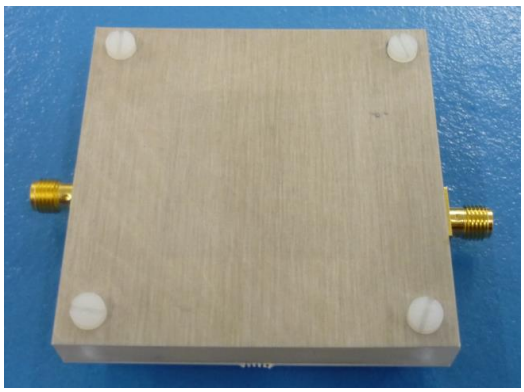

Figure 15. Final dual-polarized antenna with SMA connectors.

The measured antenna matching, isolation and radiation performance over different operation bandwidths are reported in Table 3. The measurement of the isolation and matching were performed in a normal lab environment, while the radiation patterns of the antenna were measured inside an anechoic chamber. This antenna prototype provides a 42dB SI-isolation over an 80MHz BW with an antenna efficiency of more than 70%.

Table 3. Measured specifications of the antenna prototype

BW [MHz]	10 (channel)	80 (band)
Antenna Return loss	< -15dB	< -9dB
Antenna Isolation	< -49dB	< -42dB
Antenna Gain	> 6.5dB	> 5.5dB
Antenna XPD	> 24dB	> 20dB
3dB BeamWidth	> 70 deg	> 75 deg
Antenna efficiency	> 75%	> 70%

3.2.2.2. Active RF cancellation

The changes in the environment close to the FD antenna may affect its performance in terms of passive suppression. To maintain a SI rejection of more than 50dB before the LNA, an active cancellation network operating in-between the antenna ports is used as indicated in Figure 6 (middle). This active RF cancellation network uses an attenuated and phase shifted copy of the transmitted RF signal to cancel the SI and implements a tunable attenuator and phase shifter. The remaining SI signal power automatically tunes these components based on a gradient descent algorithm. The active cancellation network has been implemented on PCB as illustrated in Figure 16.

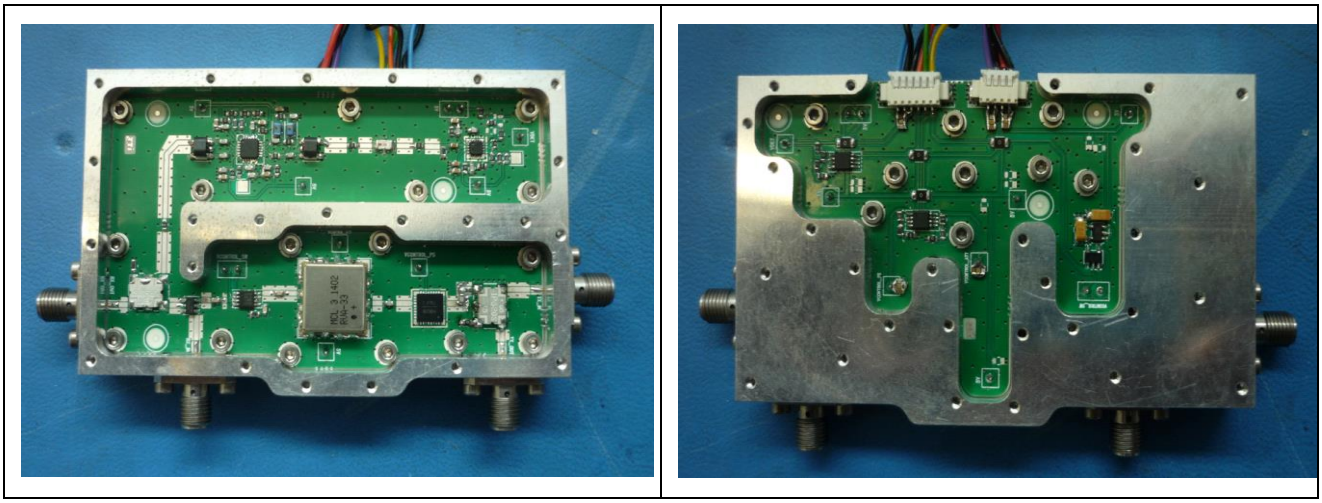

Figure 16. Active cancellation new board. (left) RF board with active cancellation loop and detection, (right) control board.

Figure 17 shows the measured SI-isolation and cancellation performance of the dual-polarized antenna with and without the active cancellation network. The experiment uses a 16QAM modulated 15MHz bandwidth signal which is transmitted around 2.46GHz with an RF power of 15dBm. The residual SI is measured with a spectrum analyzer. The obtained dual-polarized antenna isolation equals 50dB, whereas active cancellation further improves the isolation to 62dB over the signal BW of 15MHz.

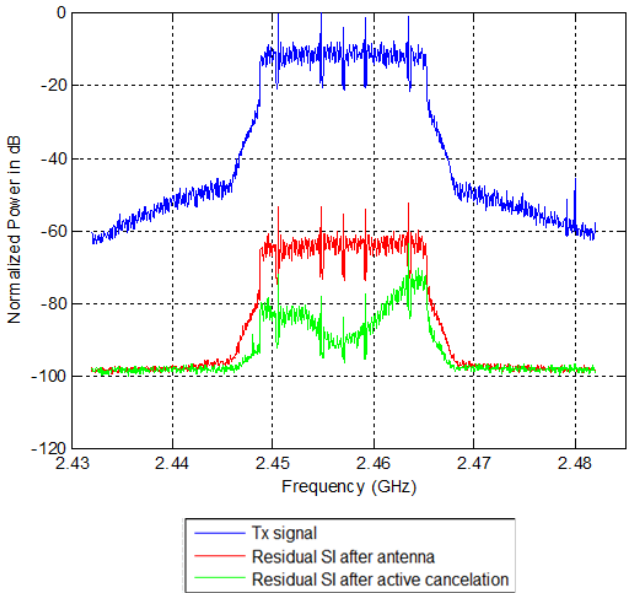

Figure 17. Lab-measured spectrum response of the dual-polarized antenna with and without active cancellation

3.2.3. Electrical balance duplexer

The antenna size is generally considered as one of the main bottlenecks for compact integration of FD radios. In the previous section, an antenna technique was described which combines transmission and reception in a compact form-factor antenna structure. When targeting even denser integration, it would be favourable to replace this special antenna structure with a conventional single port antenna, which are commercially available in extremely small size (e.g. SMD components). When using such COTS antenna, it could enable dense co-integration of FD and other transceivers while eventually sharing the same antenna.

Using a conventional single-port antenna for FD means that this antenna will be used for simultaneous transmission and reception. To enable such simultaneous operation, a duplexer is required in-between the antenna and the transceiver (as illustrated in Figure 6 (bottom)) to prevent the transmitter signal from coupling into its own receiver.

Traditionally, surface-acoustic wave (SAW)-type duplexers are commonly used in FDD systems to prevent the TX signal and TX-generated noise at the RX frequency from leaking into the RX. SAW-duplexers can, however, exploit the frequency difference between the two FDD-signals and use *filtering* to prevent leakage. Therefore, SAW duplexers are unable to support FD operation, when there is no frequency separation. Some FD designs propose a circulator to route the TX and RX signals over the common antenna. However, such circulators provide a moderate isolation (~20dB) and would require additional cancellation loops at RF [6]. Therefore, circulators are unattractive for implementation in compact radios such as smartphones.

In the DUPLO project, an electrical balance duplexer (EBD) concept has been developed instead of a circulator. This technique has been proposed to achieve tunable duplexer filters for FDD [42] and [43]. In DUPLO, this technique is applied in the context of full duplex, where it shows to provide RF self-interference cancellation for compact radio devices [27].

The electrical-balance duplexer operation principle is illustrated in Figure 18; the RF circuit comprises a hybrid transformer and a balance network which is essentially a tunable dummy load impedance. In case the dummy load impedance matches the antenna impedance, an “electrical balance condition” is achieved, virtually isolating the receiver from the transmitter. By virtue of this purely passive cancellation process, any noise and nonlinearity products generated in the transmitter are also cancelled in such electrical balance condition.

We have proposed [16][27] the usage of an EBD to enable self-interference cancellation in RF for FD operation, and its potential has been validated based on real measurements with on a prototype [28]. This prototype, of which the operation principle is illustrated in Figure 19, has been integrated in a test and validation radio platform, and an intelligent tuning algorithm has been developed. This work has been published [44] and is considered as part of the DUPLO WP5 activities. This first prototype showed a number of important limitations as discussed in [16][27][28]. Briefly, these limitation are:

- The 50dB isolation bandwidth of the prototype is limited to about 6 to 10MHz, which is limiting the applicability in high data-rate communication applications. This limitation mainly arises from the fact that the impedance variation across frequency of the antenna is much larger than the variation across frequency of the balance network impedance.
- The linearity of the balance network limits the TX path IIP3 of the prototype to 20 to 38dBm. This means that IM-products arising at the Rx input will exceed the level of the direct leakage from about >-5dBm TX power.

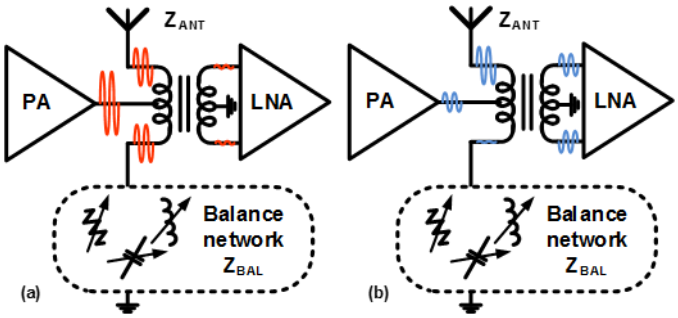

Figure 18. Electrical balance operating principle illustrated on the first prototype for (a) TX operation and (b) RX operation: in FD, (a) and (b) occur *at the same time and frequency.*

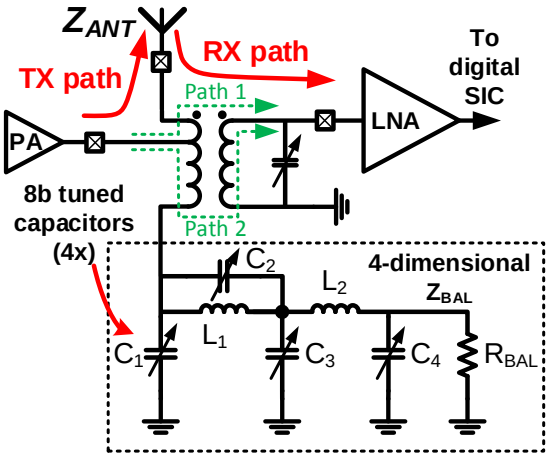

Figure 19. The antenna interface implemented in the second prototype using an electrical-balance duplexer.

As these limitations mainly originate from the balance network, this network has been redesigned and prototyped. This prototype has been implemented in 180nm Silicon-on-Insulator (SOI) CMOS as this technology provides several advantages compared to bulk CMOS. Moreover, alternative balance network topologies have been considered [17] to replace the R/C structure used in the first prototype. The topology offering a high linearity and tuning freedom while maintaining the implementation efficiency is illustrated in Figure 19. The design considerations and trade-offs are described in [17][45]. Note that as oppose to the first prototype, a single-ended topology at the receiver side of the hybrid transformer is preferred to avoid a common-mode SI and to enable high-power operation [45][46]. Then, in the “balance condition”, the magnitude and phase of two TX-RX transfer paths are made equal such that they destructively interfere at the single-ended RX port as illustrated in Figure 19.

The prototyped chip layout and micrograph of the chip bonded to the test PCB are shown in Figure 20. Measurements in this prototype indicate two breakthrough achievements namely the impedance tuning range and the linearity (IIP3). These breakthroughs tackle the main limitations observed in the first prototype.

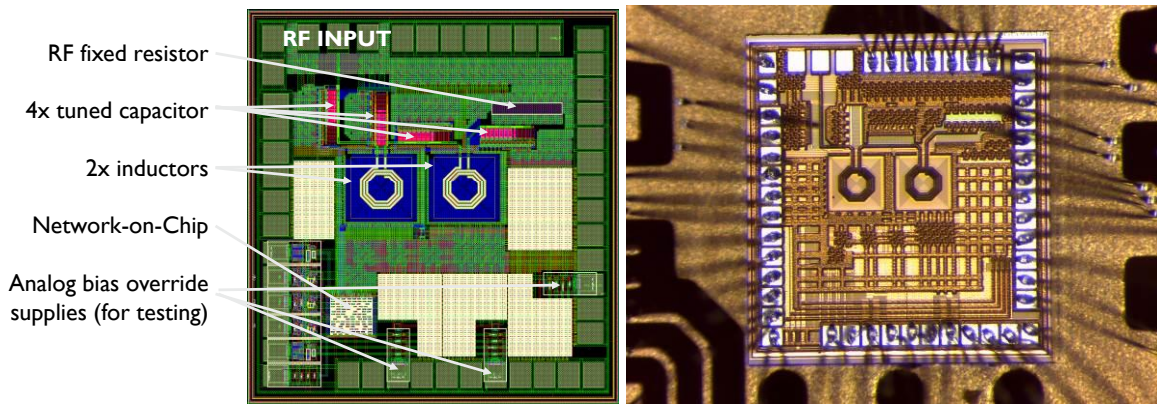

Figure 20. Implemented balance network, fabricated in 180nm SOI CMOS.

The 4-dimensional tuning capability enables to tune the real and imaginary impedance across the frequency and to trade-off the bandwidth with the average SIC, resulting e,g. an SIC of 55 dB over a 138 MHz bandwidth as illustrated in Figure 21. This issue is discussed in [46]. Note, however, that this SIC isolation was measured with a with a capacitive 50 Ohm test-termination; using a real antenna is considered as future work. Also linearity measurements on the balance network are performed; Figure 22 shows the resulting linearity in terms of IIP3. The measured IIP3 lies between 70-85dBm, which is extremely good. To our knowledge, this is the highest published IIP3 value in comparable circuits. This value exceeds the design requirement of 68dBm. This linearity is discussed in [46].

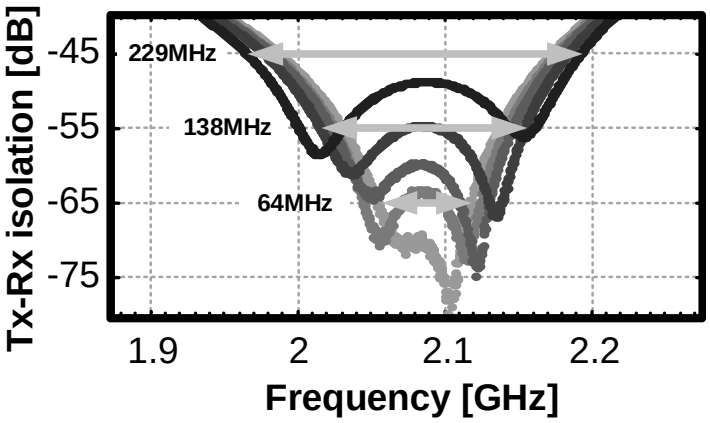

Figure 21. TX-RX isolation achieved when the balance network is used in a prototype duplexer for FDD around 2GHz

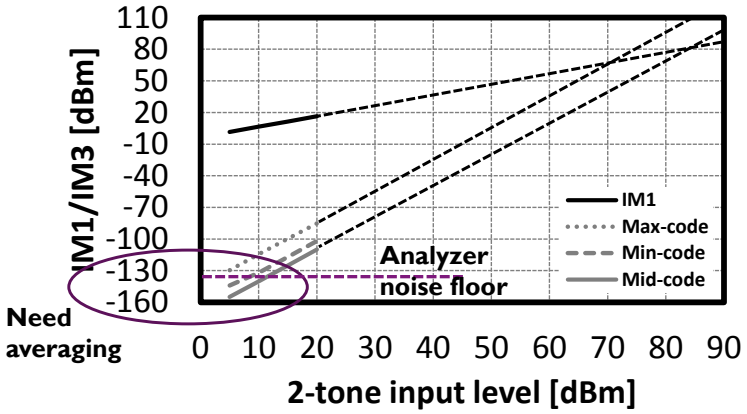

Figure 22. Balance network IIP3 measurement result across tuning settings

3.2.4. Application overview of the proposed solutions

All proposed RF/antenna/analog SI-cancellation techniques target integration in compact radios, but they offer specific benefits and can thus be applied in different applications. This diversity of applications is required [47] when targeting future networks like 5G. Table 4 highlights specific characteristics of the different techniques.

Table 4. Specific benefits of the three proposed RF-SI rejection techniques

SI-cancelling front-end:
• *Integration:* dense on-chip implementation (2mm^2 in 65nm CMOS); suitable for mass-production and digital/analog/RF co-integration • *Antennas:* any two-port antenna solution with moderate initial isolation (e.g. two conventional WLAN antennas) • *Flexibility:* broad flexibility in operation frequency (0.15–3.5GHz), tunable SI cancellation • *Isolation & bandwidth:* Moderate isolation over a broad bandwidth (45.7 dB in 16 MHz with WLAN antennas)
Dual-polarized antenna:
• *Integration:* patch structure for system integration (60x60x8mm), larger than 2 other techniques • *Antennas:* one radiation aperture with 2 ports (TX/RX) • *Flexibility:* frequency fixed, tunable SI cancellation • *Isolation & bandwidth:* High SI isolation over a broad bandwidth (49dB/10MHz stand-alone and 62dB/15MHz with added active cancellation) • *Note:* Polarization dependent performance over wireless link
Electrical balance duplexer:
• *Integration:* dense on-chip implementation (1.75mm^2 in 180nm SOI CMOS); suitable for mass-production and digital/analog/RF co-integration • *Antennas:* one conventional single antenna (for simultaneous TX/RX operation) • *Flexibility:* frequency flexible, tunable SI cancellation • *Isolation & bandwidth:* Isolation vs. bandwidth trade-off, high peak SI isolation • *Note:* Moderate loss (<3.9dB), high TX-power capable

3.2.5. Publication overview

The DUPLO work on RF/antenna/analog solutions for self-interference cancellation transceivers have gained a lot of attention outside the project, and was well received for top-tier publications. To guide the reader through the different publications, a brief logic is sketched.

Due to the cohesion and the synergy between the different WP2 partners and WP2 activities, a substantial amount of the publications are collaborative papers. The JSAC-2014 paper [27] describes the first direction in FD transceiver design based on the link budget and the circuit specifications. This paper gives the first design directions of the RF/antenna/antenna parts of the DUPLO system. The CrownCom-2014 paper [28] is presented at the first DUPLO workshop and presents the first WP2 designs and prototypes, including initial experiment results. The paper [40] presented during the second DUPLO workshop at the VTC-2015 presents the latest hardware prototypes of all the WP2 activities, including the main findings and results. Also, a paper [47] was accepted for the focussed session “5G: next generation wireless beyond 4G” at ESCCIRC-2015, where the WP2 solutions are presented in the frame of 5G. And finally, all the main WP2 findings

and validations have been bundled together with WP3 and WP4 tangible results in a paper [29] accepted on special session “duplexing techniques” at the CAMAD-2015 conference.

In addition to the collaborative papers, several papers have been published focussing on the specific designs. During the first international conference on 5G for Ubiquitous connectivity, an advanced tuning algorithm for the electrical balance duplexer is presented [44]. At the prestigious ISSCC, we published one paper on the second design of the electrical balance duplexer [45] and one paper on the design of the SI-cancelling front-end [38]. More advanced findings and continued work on these prototypes will be published at ESCCIRC-2015 (as an individual paper, different from the common paper) [46] and has been published [39] at RF-IC respectively. The published work on the SI-cancelling front-end has been bundled and submitted to address the invitation from the JSSC journal.

In addition to the paper publications, WP2 had several poster presentations (e.g. RF-IC, ESSCIRC) and participated to different discussion groups.

3.3. Digital baseband solutions for full-duplex transceiver

The total self-interference cancellation requirement in the full-duplex transceiver can be more than 100 dB to get full gain out of full-duplex transmission. To achieve this challenging requirement, the self-interference cancellation is implemented constructively in multiple stages across the full-duplex transceiver chain (antenna, RF, and baseband). Self-interference cancellation is done mainly at the antenna (isolation), RF and analog circuits to keep the LNA and ADC from saturation and to minimize the noise elevation. Full-duplex transceiver at digital baseband is required to remove the residual self-interference which could not be removed by previous cancellations. The received signal at the digital baseband of the full-duplex transceiver includes residual of the linear self-interference, after analog/RF cancellation, and nonlinear components which are added to the signal in the transmitter and the receiver by nonlinear elements, e.g. power amplifier, mixers, LNA, etc. Therefore two main tasks expected from the full-duplex digital baseband are cancelling the residual self-interference and compensating nonlinear components. It is observed that digital cancellation in a full-duplex transceiver has the same structure as a general echo canceller.

3.3.1. Digital baseband self-interference cancellation

A general block diagram for the digital cancellation is displayed in Figure 23. Known transmitted data is used for SI channel estimation, the accuracy of which is relied on the self-interference-to-noise ratio. In a real scenario, self-interference channel includes multipath and it can change dynamically. Using the estimated linear and nonlinear components, an estimate of total self-interference is subtracted from the received signal. Maximum achievable self-interference cancellation depends on the channel estimation accuracy and goodness of nonlinear models. Training signals transmitted in half-duplex mode can provide a higher self-interference-to-noise ratio to increase self-interference channel estimation accuracy. In addition, an adaptive algorithm can be considered to follow dynamic changes in the multipath channel. To improve the estimation performance, coefficients for nonlinear models are estimated jointly with self-interference channel impulse response. Finally, by joint RF and digital cancellation, the overall performance can be enhanced while feedback between RF self-interference cancellation circuits and digital self-interference cancellations can be used to enhance the overall performance. These schemes will be discussed separately in the following sections.

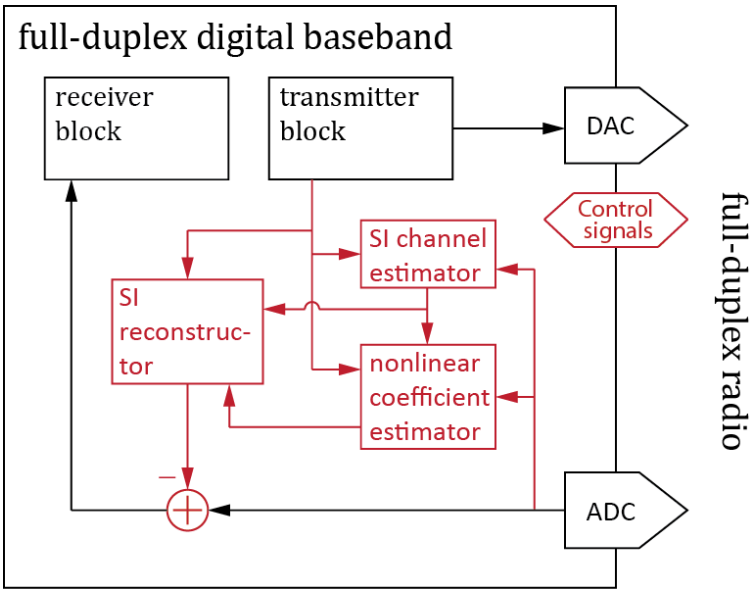

Figure 23. Block diagram of the digital baseband self-interference cancellation.

3.3.1.1. System model

In an in-band full-duplex link the local node is communicating to a full-duplex, or two half-duplex, remote node(s). The local node transmit digital baseband signal, $x(t)$, includes modulated data in the data-transmit period and pilot symbols during the training period used for channel estimation. After passing through analog circuits and RF chain, the transmit signal is contaminated with the transmitter noise, $v_t(t)$. Thus the signal at the transmit antenna could be expressed as $s(t) = x(t)_t + v_t(t)$, where $x_t(t)$ is the upconverted transmit signal at the transmit antenna port. At the local node receive antenna port, the received signal is composed of self-interference plus received signal from the remote node, i.e. the desired signal. Assuming the desired signal is $d(t)$, and desired signal channel response and self-interference channel response at the receive antenna port indicated by $h_{des}(t)$ and $h_{si}(t)$, then the total received signal at the receive antenna port, $r(t)$, can be expressed as

$$r(t) = h_{des}(t) * d(t) + h_{si}(t) * s(t) + v_r(t) \quad (3.1)$$

where * indicates convolution and $v_r(t)$ is the white Gaussian noise. For the narrowband signal this can be presented in the frequency domain as

$$R(f) = H_{des}(f)D(f) + H_{si}(f)S(f) + V_r(f) \quad (3.2)$$

where $H_{des}(f)$ and $H_{si}(f)$ indicate the desired signal channel and self-interference channel frequency responses up to the antenna port, and by $D(f)$, $S(f)$ and $R(f)$ are Fourier transforms of the desired signal, self-interference and the received signal up to the antenna port, and $V_r(f)$ is the narrowband receiver noise.

It is observed that the self-interference channel, $h_{si}(t)$, includes the propagation channel as well as the response of antenna(s) and RF transmit and receive RF chains including the isolation circuits and RF cancellation circuits. Hence the self-interference channel is frequency selective, i.e. the

response is not uniform over the system bandwidth, and it includes nonlinear components due to circuit elements such as power-amplifier on the signal path.

After self-interference cancellation at the digital baseband, the received signal can be represented as

$$Y(f) = H_{\text{des}}(f)D(f) + H_{\text{si}}(f)S(f) - \hat{H}_{\text{si}}(f)X(f) + V_{\text{r}}(f) \quad (3.3)$$

Where $Y(f)$ is the Fourier transform of the received signal after baseband self-interference cancellation, $y(t)$, the $X(f)$ is the transmitted signal $x(t)$ in frequency domain, and $\hat{H}_{\text{si}}(f)$ is an estimate of the self-interference channel $H_{\text{si}}(f)$. From Eq. (3.3) it is observed that the performance of a full-duplex system is affected by three factors: a) the transmitter noise in $S(f)$ multiplied by the self-interference channel $H_{\text{si}}(f)$, b) any enhancement of the receiver noise $V_{\text{r}}(f)$ (compared to half-duplex) due to self-interference cancellation at RF, c) any self-interference channel estimation error, $H_{\text{si}}(f) - \hat{H}_{\text{si}}(f)$. It is observed that factors a) and b) above can be minimized by enhancing the RF self-interference cancellation, i.e. a better RF self-interference cancellation makes a smaller $H_{\text{si}}(f)$, and less enhancement in the noise factor $V_{\text{r}}(f)$. To reduce the factor c) a better self-interference channel estimate is required. This can be done by enhancement in the SNR for the channel estimation process, e.g. by using half-duplex training signal for the self-interference channel estimation.

3.3.1.2. Bidirectional channel estimation

In a full-duplex transceiver, to estimate the $H_{\text{si}}(f)$ and $H_{\text{des}}(f)$, training signal is required. Assuming a full-duplex OFDM based system, a channel estimation scheme similar to those used for MIMO-OFDM systems can be employed. The basic channel estimation scheme for such a system is based on the embedded pilot subcarriers at each OFDM symbol. Vast literature on the channel estimation for OFDM systems exist which usually exploit the time and frequency domain coherence of the channel on top of this basic approach. Moreover a time domain interpolation may be used to improve the channel estimates in a continuous time domain frame.

To cover the full bandwidth, scattered pilots on each frame are designed whose distances are based on the channel coherence over the frequency band and time. Figure 24 displays two alternative solutions for the proposed scattered pilot arrangement. In this figure, the two OFDM symbols transmitted by the two communicating nodes are overlapped in time, although they are depicted separately.

Arranging pilot symbols for estimation of both self-interference channel and desired signal channel causes overhead when compared to pilot arrangements with conventional half-duplex system. However, the amount of overhead can be kept small compared with the overall radio resources needed for the data transmission [20].

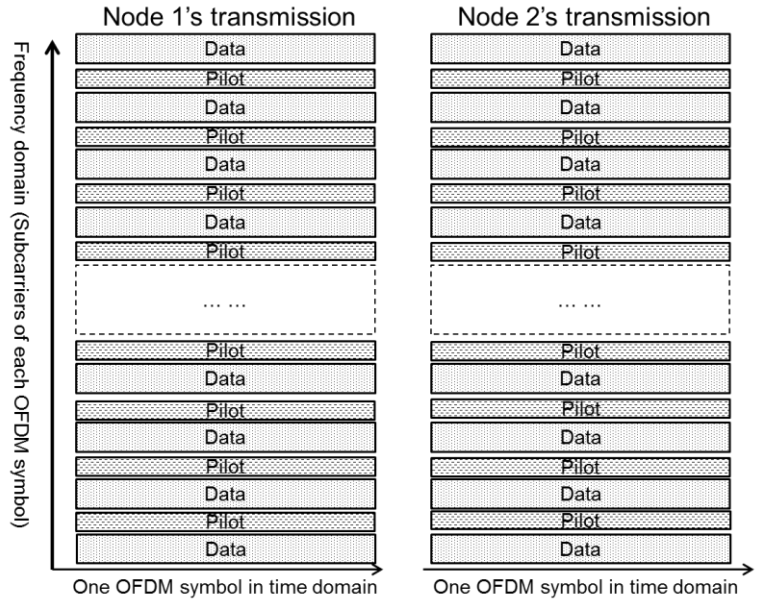

(a) common pilot subcarriers for both full-duplex link ends

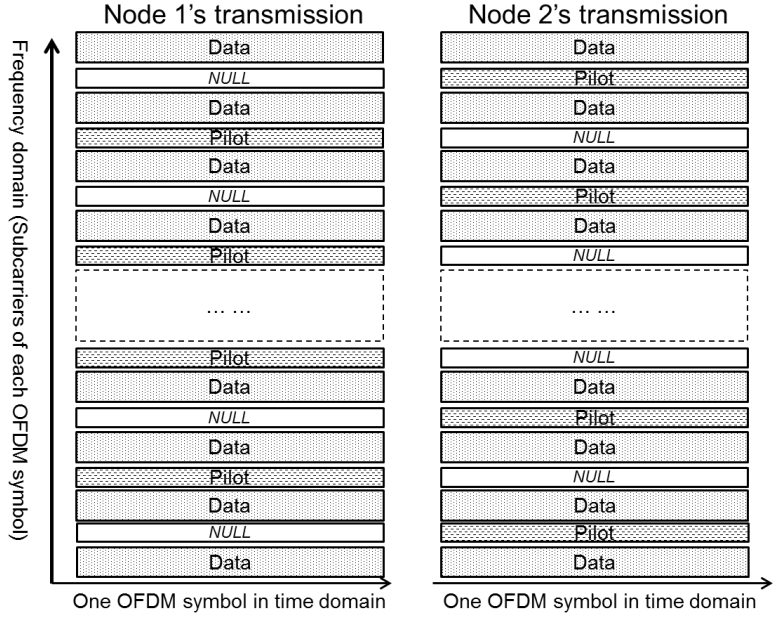

(b) orthogonal basis for pilot subcarriers (each pilot subcarrier is used only at one link end)

Figure 24. Scattered pilot design for bidirectional channel estimation in a full-duplex link

3.3.1.3. Subband approach for joint baseband-RF self-interference cancellation in full-duplex wideband transceiver

The performance of the full-duplex system can be degraded by the frequency selective transmit-receive path isolation in the full-duplex transceiver and also due to multipath in the SI channel.

One solution to overcome this problem is an uneven SI cancellation over the received signal band, i.e. the frequency band is divided into several subbands and then SI cancellation is performed at each subband independent from other subbands. One realization for this solution is presented in Figure 25, where the received signal is filtered to N_{sub} subbands, and then SI cancellation is performed at each subband independently.

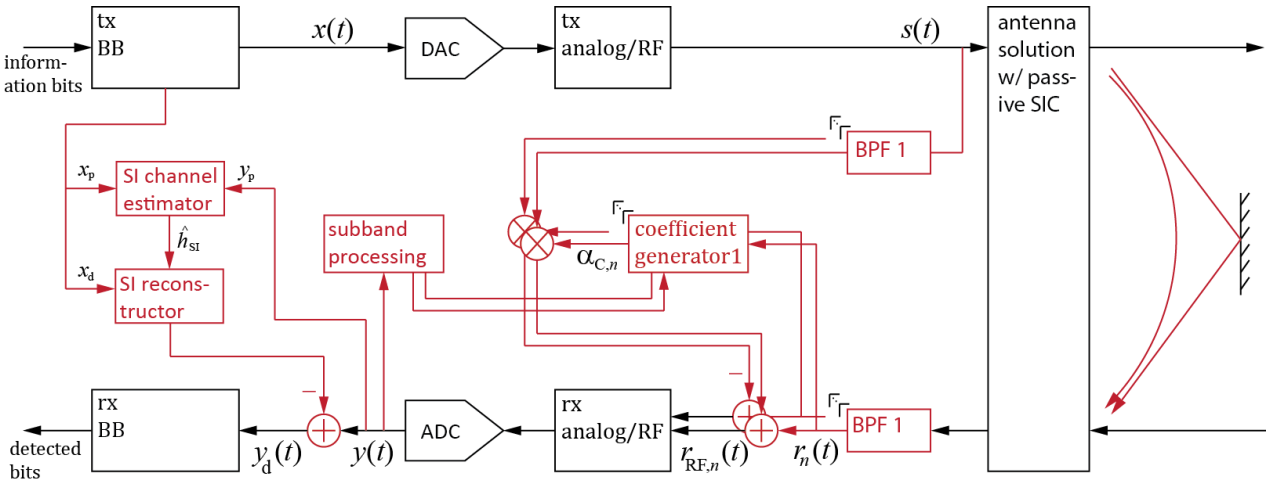

Figure 25. Block diagram for joint analog/RF and digital baseband SI cancellation.

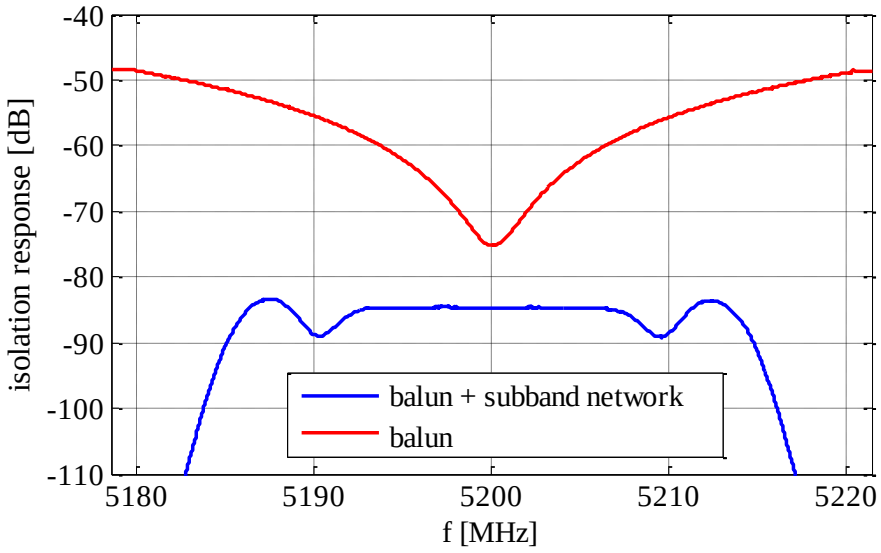

Figure 26. Balun and subband approaches isolation performance

Figure 26 shows the frequency response of self-interference cancellation performance of the full-duplex transceiver using an isolation circuit, e.g., balun, with and without the subband cancellation circuit. It is observed that by using the subband approach in active self-interference cancellation the frequency response is more flat over the full signal bandwidth. Moreover the self-interference signal is attenuated around 8 dB compared to its weakest value before subband network. It is

noted that since an identical network is used on the desired signal path, this loss is incurred on the desired signal as well [60].

Figure 27 present the BER performance of the full-duplex system using the isolator (Balun), and isolator plus subband cancellation. It is observed that, in the study case, the BER performance is poor when subband circuit is not used; this is due to strong self-interference at parts of the frequency band. By employing the subband circuit self-interference is uniformly reduced across the bandwidth so that the BER performance shows significant improvement.

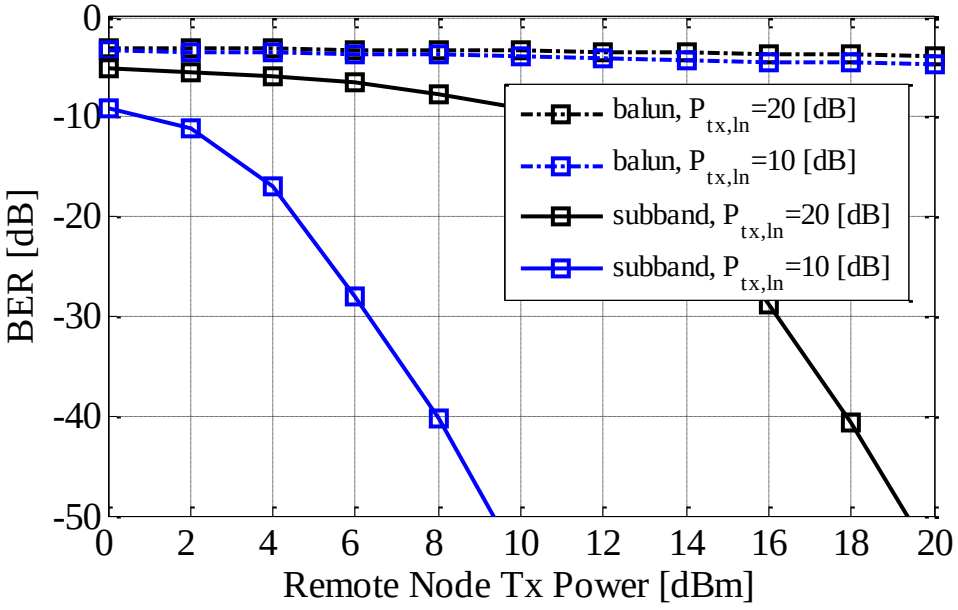

Figure 27. BER improvement in subband approach.

3.3.1.4. Nonlinear self-interference cancellation

Due to nonlinear effects in the in the SI path plain linear cancellation is not enough to cancel the self-interference fully. Advanced SI modelling and processing, taking into account the existing analog impairments, is required in order to produce a sufficiently accurate cancellation signal. The full-duplex transceiver nonlinear effects on the self-interference cancellation, specifically effects due to PA, IQ imbalance and phase-noise, were analysed in this project. Moreover two approaches to baseband SI cancellation taking into account the nonlinear effect due to PA are investigated.

The estimated SI channel and known transmitted signal are used to form the emulated self-interference signal which is then subtracted from the received signal in order to cancel the SI. The nonlinear power amplifier is modelled using the Modified Saleh - I (MS-I) model, which models amplitude (AM-AM) and phase (AM-PM) distortions of a memoryless solid state power amplifier [61]. In the first approach initially the linear estimate of the SI channel is used to remove the linear SI from the received signal and then the remaining signal is used to estimate the nonlinear component by an LS estimator. In the second approach nonlinear amplifier model and linear SI model are used simultaneously as a Hammerstein model, as illustrated in Figure 28. The parameters are then estimated using the LS estimator.

The performance of the SI cancellation using the Hammerstein model is presented in Figure 29 and Figure 30 for a frequency selective SI channel. In the case of Figure 29, the estimation is done

using a data signal. In this approach the SI channel is estimated while transmitting data to the distant node in the half-duplex mode, and the full-duplex mode is started after both nodes have estimated their nonlinear SI channels. Figure 30 shows the performance when a preselected preamble is used. The fixed preamble is found with a computer search by testing different signals and selecting the one that gives the best performance with the fifth order nonlinearity model. Solid and dashed lines in Figure 29 and Figure 30 show the performance when the nonlinearity order of the Hammerstein model equals to three and five, respectively. Parameter INR is the self-interference-power-to-noise power ratio before the baseband cancellation. As can be seen the fifth order model gives significantly better performance than the third order model. A more detailed analysis is given in [21].

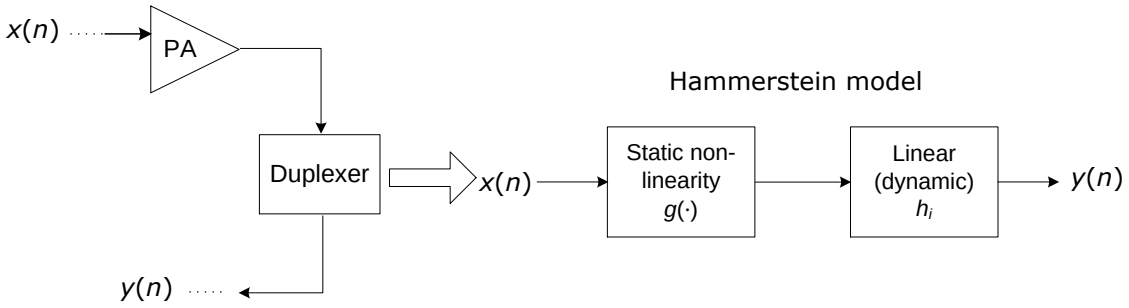

Figure 28. Hammerstein model.

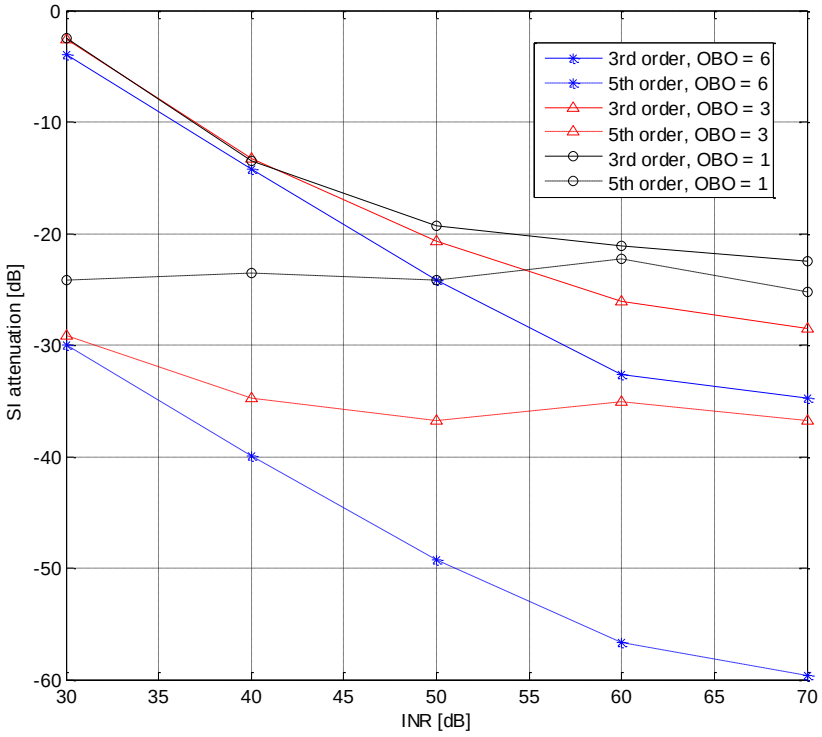

Figure 29. Hammerstein model based self-interference cancellation with random preamble.

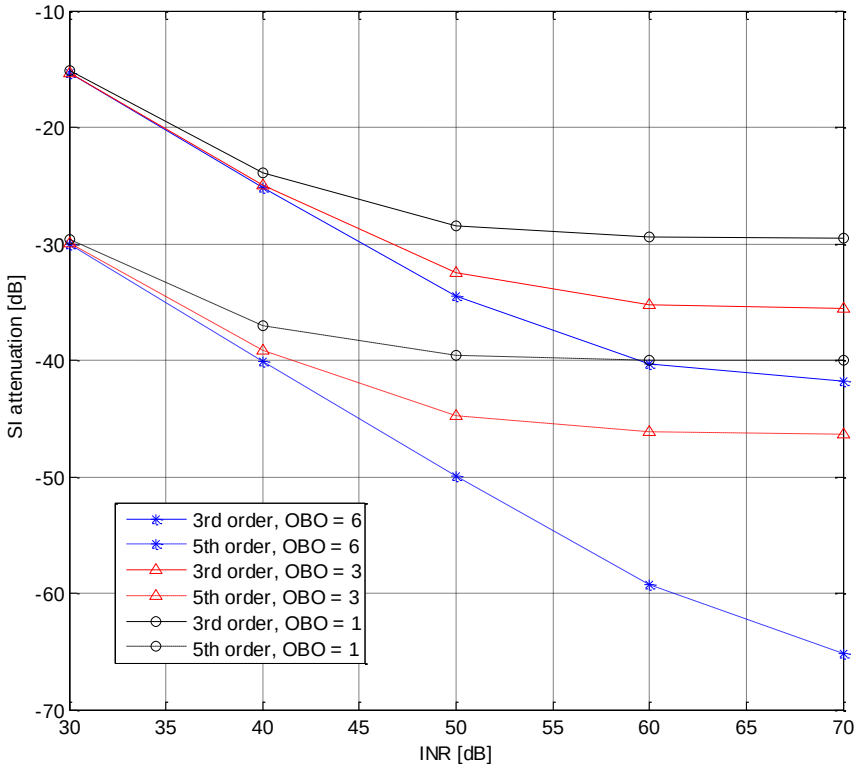

Figure 30. Hammerstein model based self-interference cancellation with preselected preamble

3.3.2. Multiple antenna full-duplex systems

The SI cancellation with full-duplex MIMO system is a challenging task. This section describes robust signal processing techniques to mitigate the residual SI in the digital baseband of the full-duplex MIMO system. A straightforward method in the SI cancellation is to estimate the MIMO SI channel, and subtract the emulated SI, using the SI channel estimate, from the received signal. The performance of this scheme depends on the SI channel estimate accuracy. In case there is an error in the channel estimation, or there are nonlinear components which are not included in the cancellation, a residual SI is remained. To cancel the SI further, low complexity precoding methods are introduced, analysed and simulated.

The block diagram of the full-duplex MIMO system with two identical transceivers is shown in Figure 31. Each transceiver equipped with *M* transmit antennas and *N* receive antennas. Perfect synchronization is also assumed. As depicted in Figure 31, the desired channel between the transmitter node $j \in (1,2)$ and the receiver node $i \in (1,2)$ is denoted as $H_{ji} \in \mathbb{C}^{N_i \times M_j}$, while the MIMO self-interference channel from the transmitter node $i \in (1,2)$ to itself is denoted as $H_{ii} \in \mathbb{C}^{N_i \times M_i}$. The elements of the MIMO SI channel matrix are assumed random variables with Rayleigh distribution. This makes sense assuming multipath in the self-interference channel and considering that main component is cancelled in the SI cancellation process. Thus the received

signal at the receiver node *i* is expressed as:

$$\mathbf{y}_i = \sqrt{\rho_i}\mathbf{H}_{ji}\mathbf{x}_j + \sqrt{\eta_i}\mathbf{H}_{ii}\mathbf{x}_i + \mathbf{n}_i \,, \tag{3.4}$$

where $\rho_i > 0$ indicates the average gain of the desired channel while $\eta_i > 0$ denotes the average gain in the residual self-interference channel at node i after RF cancellation and achieved isolation in the full duplex transmit-receive path. $\mathbf{n}_i \in \mathbf{C}^{N_i \times 1}$ represents the complex AWGN with zero mean and covariance matrix $\sigma_n^2 I_N$.

The design of transmission strategies for a full-duplex MIMO system is even more challenging because of the SI in the system. Clearly, the desired transmit technique must provide a trade-off between system performance and algorithm complexity. The aim of any precoding introduced for full-duplex MIMO system is to reduce/cancel any remaining residual SI. Assuming the data symbol vector is denoted as $\mathbf{s}_i \in \mathbf{C}^{L \times 1}$ at node i, where L is the number of parallel transmitted data symbols which is precoded using the precoding matrix $\mathbf{T}_i \in \mathbf{C}^{M_i \times L}$, the transmitted symbol vector is given by

$$\mathbf{x}_i = \mathbf{T}_i \mathbf{s}_i \,. \tag{3.5}$$

Then, the received signal in Eq. (3.4) can be rewritten as:

$$\mathbf{y}_i = \sqrt{\rho_i}\mathbf{H}_{ji}\mathbf{T}_j\mathbf{s}_j + \sqrt{\eta_i}\mathbf{H}_{ii}\mathbf{T}_i\mathbf{s}_i + \mathbf{n}_i \,. \tag{3.6}$$

The zero-forcing (ZF) precoding scheme can cancel the residual SI perfectly. To guarantee the existence of a nonzero precoding matrix, a sufficient condition is that the number of the transmit antennas M_i is larger than the sum of the number of receiver antennas N_j and the SI receiver antennas N_i, that is

$$M_i \geq N_i + N_j \,. \tag{3.7}$$

After the SI is perfectly removed by the ZF, the received signal at node i could be expressed as:

$$\mathbf{y}_i = \sqrt{\rho_i}\mathbf{H}_{ji}\mathbf{T}_j\mathbf{s}_j + \mathbf{n}_i \,. \tag{3.8}$$

The precoding matrix may be chosen as

$$\mathbf{T}_i = \mathbf{V}_{ii}\mathbf{A}_{ii} \,, \tag{3.9}$$

where $\boldsymbol{A}_{ii}$ is a nonzero ZF precoding matrix with dimensions $n_u \times L$, where $n_u > M_i - N_i$ is the order of the channel null-space, i.e. $\mathbf{V}_{ii} \in \mathbf{C}^{M_i \times n_u}$ is the null-space of $\mathbf{H}_{ii}$, which can be derived by SVD as [62]:

$$\mathbf{H}_{ii} = \left[\tilde{\mathbf{U}}_{ii}\ \mathbf{U}_{ii}\right] \cdot \begin{bmatrix} \sum & \mathbf{0} \\ \mathbf{0} & \mathbf{0} \end{bmatrix} \cdot \begin{bmatrix} \tilde{\mathbf{V}}_{ii}^H \\ \mathbf{V}_{ii}^H \end{bmatrix}, \tag{3.10}$$

where columns of $\mathbf{V}_{ii}$ and $\tilde{\mathbf{V}}_{ii}$ form an orthonormal basis for the channel, with $\tilde{\mathbf{V}}_{ii} \in \mathbf{C}^{M_i \times n_s}$ signal space of the channel and rich-scattering is assumed with $M_i > N_i$.

To relax the requirement Eq. (3.7) and mitigate the effect of noise enhancement observed in the ZF method an alternative method based on the signal-to-leakage-plus-noise (SLNR) can be used.

The SLNR-based precoding avoids the joint design of the precoders between two transceiver devices and can lead to a closed form characterization of the optimal $\mathbf{T}_i$ in terms of generalized eigenvalue problems.

$$SLNR_i = \frac{\left\| \sqrt{\rho_i} \mathbf{H}_{ij} \mathbf{T}_i^2 \right\|^2}{N_i \sigma_n^2 + \left\| \sqrt{\eta_i} \mathbf{H}_{ii} \mathbf{T}_i^2 \right\|^2} \tag{3.11}$$

Figure 32 presents the BER performance versus SNR of both the precoding schemes and the digital SI cancellation for full-duplex MIMO systems, with different channel estimation errors, at SNR = 10 dB in the case of the residual SI channel gain $\sqrt{\eta_i}$ = 20 dB. It is observed that when the channel estimation errors are lower than -17 dB, the digital SI cancellation alone outperforms both precoding techniques, but with the increase of the self-interference channel estimation errors, the precoding schemes present a better performance. It is observed that the precoding schemes can be used after the digital SI cancellation is achieved. Figure 33 shows the BER performance when using both digital SI cancellation and then precoding with $\sqrt{\eta_i}$ = 20 dB. It is observed that, with the joint SLNR-bases precoding and digital self-interference cancellation, there is 8 dB improvement at a BER= 10^{-3} compared to precoding alone. This outperforms the joint ZF precoding and digital SI cancellation by around 2 dB at BER = 10^{-3}.

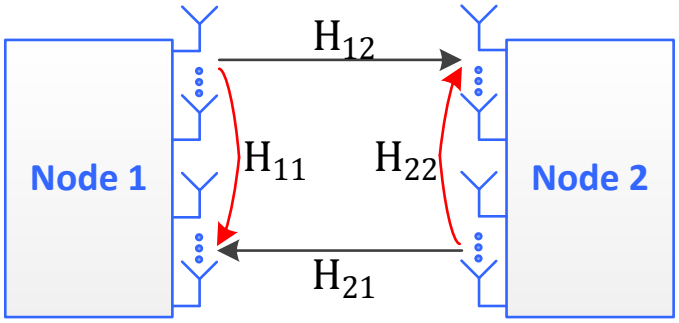

Figure 31. Block diagram of a full-duplex MIMO system.

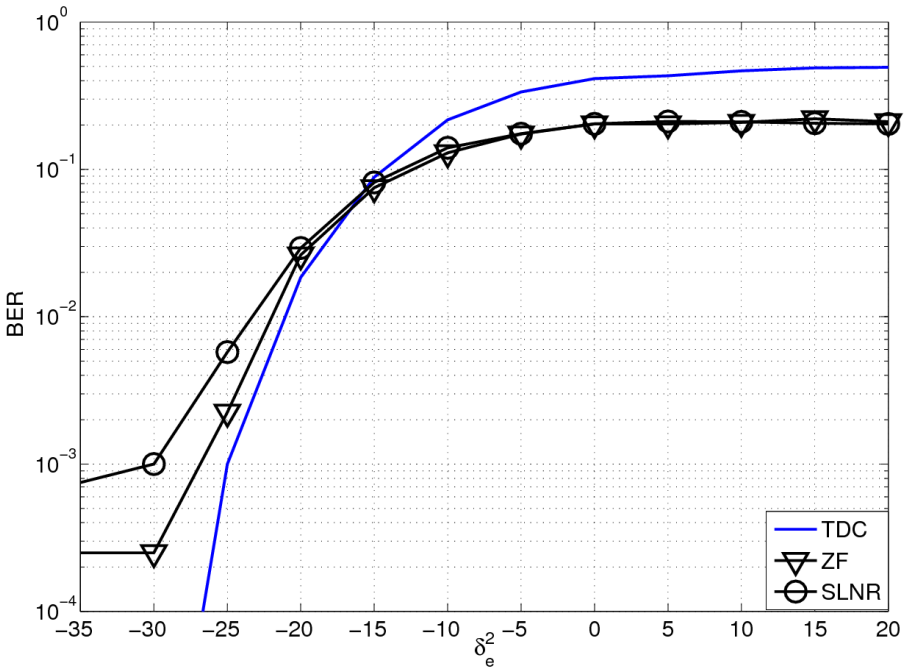

Figure 32. Impact of the SI channel estimation error on the BER performance of the full-duplex MIMO system using digital SI cancellation, ZF or SLNR-based precoding, where $M_i = 4$, $N_i = 2$, $N_j = 2$, $\sqrt{\eta_i}$ = 20 dB, SNR = 10 dB.

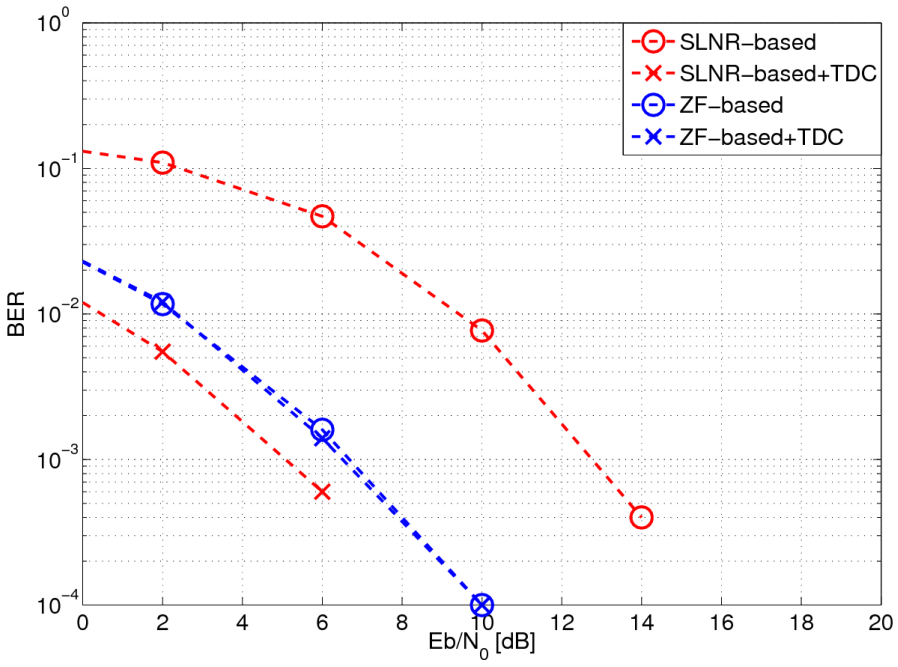

Figure 33. The BER performance for both precoding schemes, with and without digital SI cancellation, $M_i = 4, N_i = 2, N_j = 2$, (TDC indicates digital SI cancellation).

4. FULL-DUPLEX TRANSMISSION IN WIRELESS NETWORK

This chapter outlines key results and observations from system level performance studies and radio resource management and protocol related studies conducted in DUPLO WP4. Section 4.1 focuses on achievable system level performance with full-duplex transmission under different operation assumptions, having conventional half-duplex transmission system (either FDD or TDD) as the reference system and comparison point. Section 4.2 discusses radio resource management and protocol solutions for full duplex transmission. Section 4.3 gives brief summary on main system level results. The considered system scenarios were defined in DUPLO D1.1 [15] and introduced in section 2.2.

4.1. Full-duplex system performance

This section summarizes full-duplex system performance investigations conducted in DUPLO WP4, and documented in D4.1.2 [23]. The reference scenarios are listed here first. It is worth noticing that the algorithms and protocols related to the assessed study cases are described in detail in another DUPLO WP4 deliverable, D4.2 [24] and treated in summary fashion in next section.

1) A point-to-point link is an essential unit and basic building block of many wireless networks. For example, in a wireless local area network (WLAN), every transmission between user devices and their access point (AP) can be regarded as a point-to-point link during the transmission period. Yet another example would be wireless backhauling in small cell deployments on mobile platforms such as trains, cars or airplanes.
2) Standalone small cell with a full-duplex base station serving multiple UEs which operate a) in half duplex mode or b) in full duplex mode. A typical realization of this use case could be a small cell deployed at home in e.g. residential area.
3) Multiple small cells with a full-duplex base station serving multiple UEs which operate a) in half duplex mode or b) in full duplex mode. A typical realization of this use case could be a small cell deployment in an office space, sports arena or shopping centre to name a few.
4) One considers relaying schemes, where a FD BS helps the communication between two UEs, as depicted in Figure 48. In this scenario, the FD BS implements cooperative protocols in order to help the communication between two UEs. This scenario may be used in coverage extension of networks.
5) Finally, scenarios IEEE 802.11 FD Mobile Ad-hoc NETworks (MANET) are investigated and the scenarios are typical for instance in future public protection and disaster relief (PPDR) systems.

4.1.1. A point-to-point link

The first theoretical analysis on the full-duplex link performance is based on comparison of achievable rate region and sum power efficiency for bi-directional full-duplex or half-duplex point-to-point connection utilizing cyclic prefix (CP) assisted OFDM waveform for the signal transmission [48][49]. The impact of the transceiver imperfection on the full-duplex link performance has been evaluated.

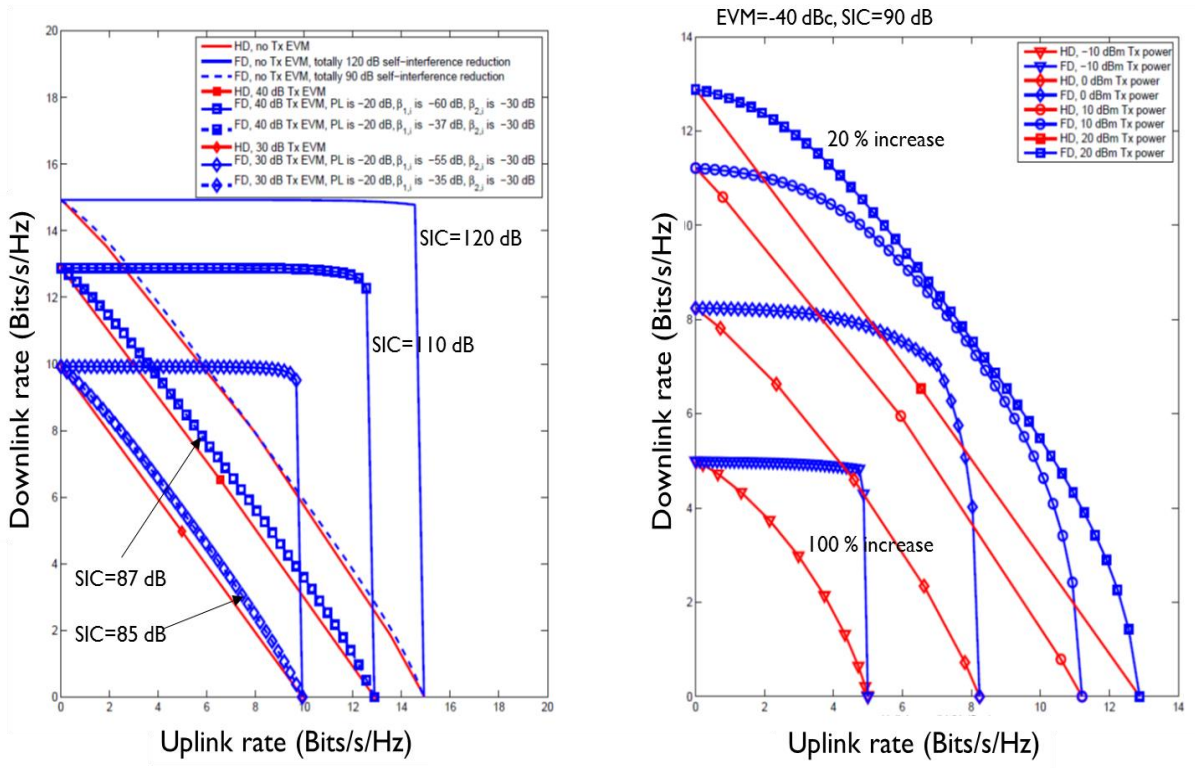

Figure 34. Full-duplex and half-duplex rate regions: a) with different EVM noise levels, b) with different maximum transmission powers. Blue lines denote the rate regions with full-duplex transmission mode and red lines with the half-duplex transmission mode.

As a conclusion of the rate region study we can state that in the comparison of uniform and non-uniform power allocation the latter allows for higher full-duplex throughput gain over half-duplex in frequency selective fading environment. In the presence of -30 or -40 dBc EVM noise and having respective total SI cancellation 85 or 87 dB ensures comparable FD and HD rate regions as seen in Figure 34.

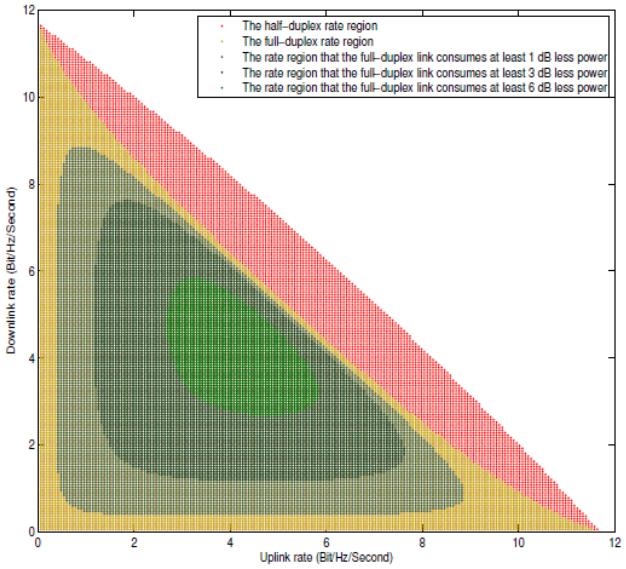

Figure 35. Sum transmission powers of using full- and half-duplex technologies

At low transmission powers the maximum FD rate can be twice the HD rate but by increasing Tx power the gap between them decreases. FD link distances should be short enough. Finally, FD has also good energy saving properties when achieving the maximum link rate is not the primary target which is indicated by Figure 35. It can be concluded that FD link can achieve over 75% of its rate region with 1 dB less power consumption than that of the HD link. Furthermore, in the area around downlink-uplink rate pair {4.5, 4.5} bit/Hz/s the power efficiency advantage is larger than 6 dB.

As for power allocation policies in a single link, it can be seen that with the proposed scheme [50], the downlink rate can be increased with the degradation in uplink while satisfying the SINR and QoS constraints. When we consider both the physical layer and the MAC layer, the low SINR region suffers from the low packet transmission rate and the high SINR region suffers from the increased interference. At the optimal SINR the physical layer and the MAC layer are balanced to achieve the maximum throughput [50].

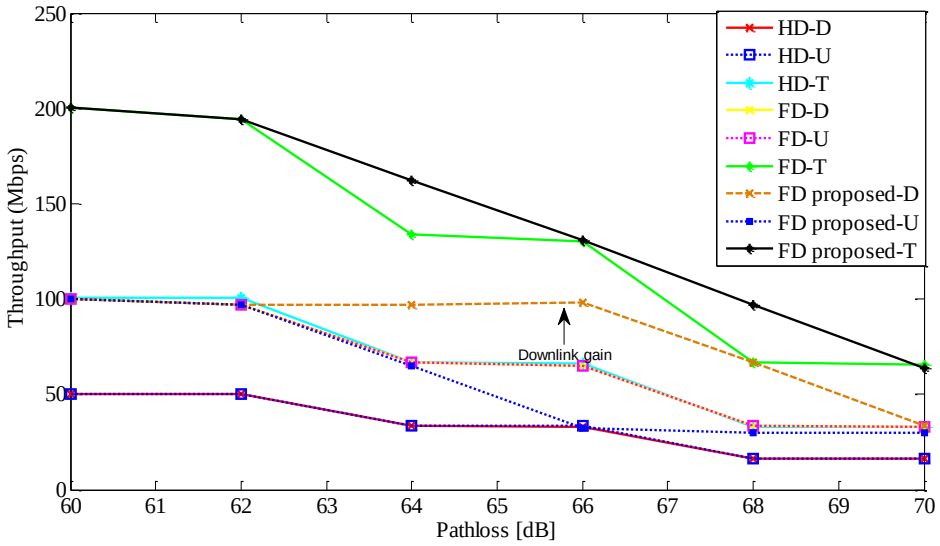

Figure 36. Throughput performance comparison of FD and HD users with power allocation

4.1.2. Single standalone full duplex small cell

In this study a single-cell with 200 m radius is considered, where the users' locations are randomly generated and uniformly distributed within the cell. The full-duplex base-station has 30 dBm maximum transmit power, and the users each has 23 dBm maximum transmit power. The total number of users is 20, with 10 downlink users and 10 uplink users [33].

.

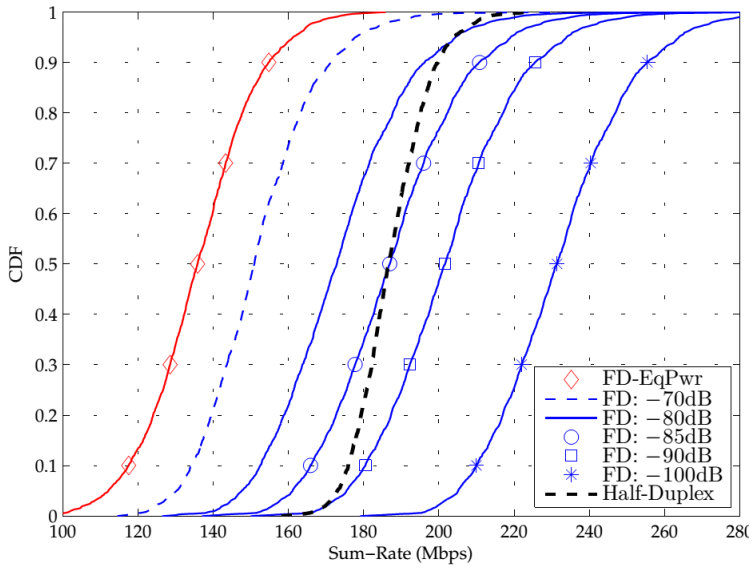

Figure 37. Sum-rate comparison in single standalone full duplex small cell for full-duplex and half-duplex systems with BS transmit power of 30 dBm and UE transmit power of 23 dBm as a function of SIC capability.

Figure 37 shows the cumulative distribution function (CDF) of the sum-rate for full-duplex system, with different self-interference cancellation values. As benchmarks for comparison, we used full-duplex with equal power allocation and time-division duplex (TDD), i.e. half-duplex system, with optimal subcarrier and power allocation. In this case it can be concluded that with 85 dB SIC, the FD system is at par with HD system but with SIC of 110 dB 40 % increase in performance is observed.

What happens if smart scheduling and power allocation will be used? Next in this section, the performance of three resource allocation algorithms is discussed which consider both the subcarrier and power allocation for an OFDMA system having a full-duplex base-station with randomly distributed half-duplex uplink and downlink users.

A simple three-step algorithm was proposed to maximize the sum-rate of the system full-duplex system subject to predefined target rate constraints at the uplink and downlink users, and transmit power constraints at the base-station and uplink users [32]. In Figure 38 a), the distribution of average full-duplex (FD), half-duplex uplink (HD-UL), and half-duplex downlink (HD-DL) rates over 500 drops are shown under various self-interference cancellation levels. It is seen that the self-interference needs to cancel at least 80dB so that full-duplex system achieves higher sum-rate than half-duplex system. Since self-interference cancellation level, i.e. C_{SI} affects only the uplink rate in the considered case, in Table 5 we show the average gain of full-duplex uplink channel over half-duplex uplink channel. Note that we also observe 23% average gain in the downlink channel.

Depending on the locations of the mobile users, propagation channels, the self-interference cancellation capability of the base-station, transmission power of the mobile users and base-station, etc, it might be better to switch to half-duplex mode. Therefore, a dynamic hybrid scheduler that can switch between half-duplex uplink, half-duplex downlink and full-duplex mode opportunistically to maximize the sum-rate has been designed [31]. In Figure 38b), it is seen that at high self-interference cancellation values, FD scheduling outperforms HD-TDD scheduling, and hybrid scheduling switches to the FD scheduling, so it is beneficial to allocate each time slot to simultaneous uplink and downlink transmission. On the other hand, at low self-interference cancellation values, HD-TDD scheduling outperforms FD scheduling, and hybrid scheduling starts

switching to HD-TDD scheduling, so it is beneficial to allocate time slots either uplink or downlink transmission.

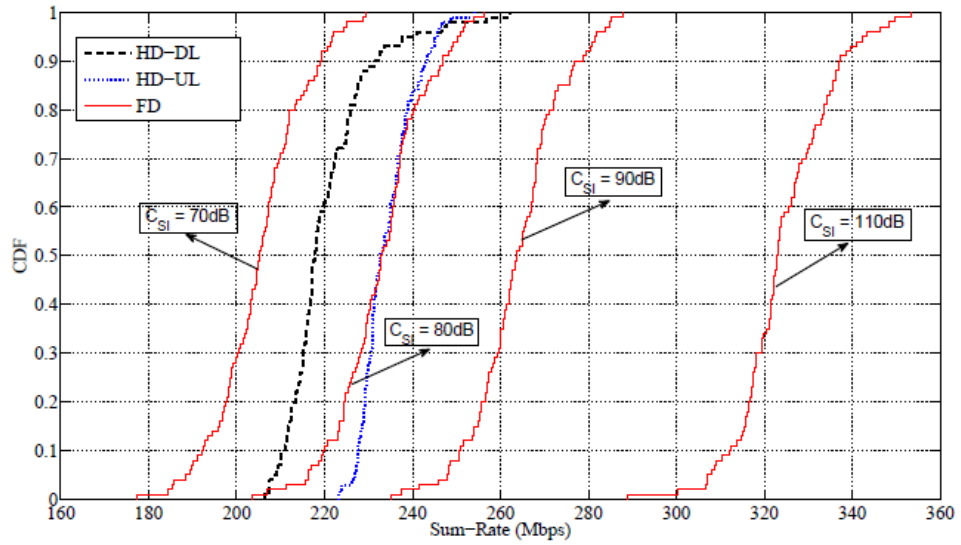

a)

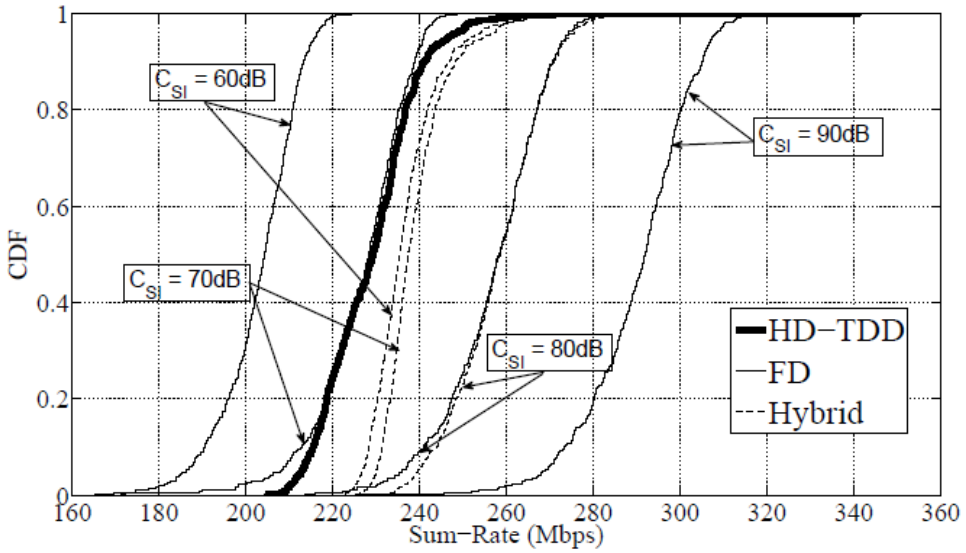

b)

Figure 38. a) Average sum-rate comparison of FD and HD systems under iterative water-filling, b) Average sum-rate comparison of hybrid, FD and HD-TDD systems under different self-interference cancellation values

Table 5. Average Rate Gain of Full-duplex Uplink System over Half-duplex system

C_{SI}	85dB	90dB	100dB	110dB	120dB	130dB
	0.86%	11%	39%	61%	75%	78%

Conducted studies on the average goodput performance of the full-duplex system (uplink plus downlink) under different channel estimation errors indicate that the performance degrades as the estimation error increases. There can easily be a 10-20% system performance decrease with moderate channel estimation errors thus highlighting the importance of high quality channel estimators with FD operation.

4.1.3. Multiple full-duplex small cells

This section provides system simulation results for full-duplex operation in multiple LTE small cells environment, assuming that there is only single full-duplex user equipment (UE) per cell. Therefore, the focus is on investigating the impact of inter-cell interference due to full-duplex transmission. As a result, we provide throughput comparisons under indoor and outdoor environment. Half-duplex TDD operation mode is used as the reference scheme in comparisons. User scheduling and power control is not considered in current simulations. Two types of multiple cell deployment scenarios are considered, namely indoor and outdoor scenarios. For both the indoor and outdoor scenarios, this section presents the average UE throughput results in the DL and UL directions.

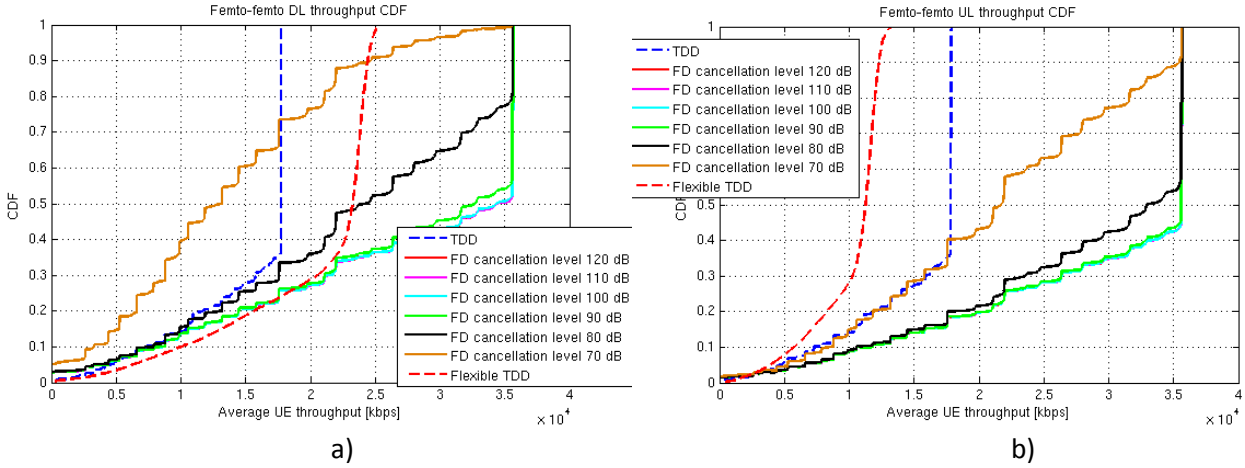

Figure 39. Indoor a) DL and b) UL average UE throughput.

Figure 39 a) and b) present the CDF of the average UE throughput in the DL and UL of the indoor scenarios, respectively. From these figures, the maximum throughput in the FD deployment becomes twice as much the one achieved in TDD mode, as expected. It is worth noting that the FD scheme not only outperforms the TDD in the low SINR regime, but also guarantees the maximum achievable throughput for about 50% of the FD UEs if the self-interference cancellation level is at least 80 dB. By comparing the FD and TDD coverage in this particular scenario, the former is only slightly worse than the latter in the DL, while both are equal in the UL. While the flexible TDD scheme outperforms the standard TDD in the DL, it performs poorer in the UL. In all cases, excluding FD with 70 dB self-interference cancellation, the used MCS limits the achievable maximum throughput.

Figure 40 a) and b) illustrate the average UE throughput in the DL and UL of the outdoor scenarios, respectively. In the DL of these scenarios, the FD scheme with self-interference cancelation of at least 80 dB achieves higher throughput than the standard TDD while providing almost similar coverage (low values of CDF). Moreover, about 40% of the FD UEs achieve the maximum throughput in the DL direction. In the UL, while nearly 30% of the FD UEs with self-interference cancellation of at least 90 dB achieve throughput higher than that of the TDD users, only about 20% of them perform as good when the cancellation level is 80 dB. The coverage is actually the main limitation of this scenario: only 5% of the TDD UEs are in outage in contrast with

nearly 50% of FD ones. The reason is the additional inter-cell-interference in FD deployments, more specifically the DL to UL cross interference and poor isolation between outdoor BSs.
Based on the results, it is evident that in indoor scenarios with good isolation between BSs, the full duplex configuration can outperform the TDD schemes in terms of average UE throughput while providing similar coverage as long as the self-interference cancellation level is at least 80 dB. In addition, whenever the isolation between the BSs is poor, both the coverage and the achievable data rates of FD-enabled UEs decrease due to high DL to UL cross interference. However, these results are limited to scenarios with a single UE per cell site and further studies are needed to confirm if they still hold in multiuser deployments (more than one UE per cell). From these investigations, we also identified the need to devise interference mitigation techniques so as to reduce the DL to UL cross interference and, as a result, to enable full duplex communications in scenarios with poor isolation between nodes, especially BSs with high transmission power. For instance, power control and inter-cell-interference cancellation or coordination schemes are envisaged as promising for interference management solutions.

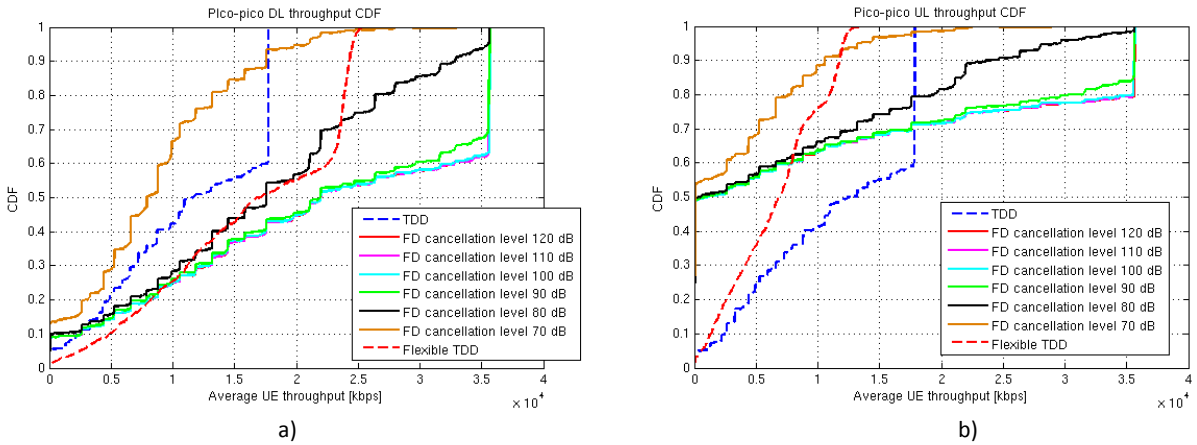

Figure 40. Outdoor a) DL and b) UL average UE throughput.

Without coordination - in multi-cell environment with multiple FD users - consider an interference-limited network where all nodes operate in FD fashion. The DL of a traditional HD network constitutes our benchmark scenario wherein the user of interest is interfered by surrounding small cells. BSs independently schedule a random user in every transmission interval. All communicating nodes are equipped with omni-directional antennas. BSs and UEs are also assumed to have full buffer and symmetric traffic patterns. We resort to an analytical framework defined in .

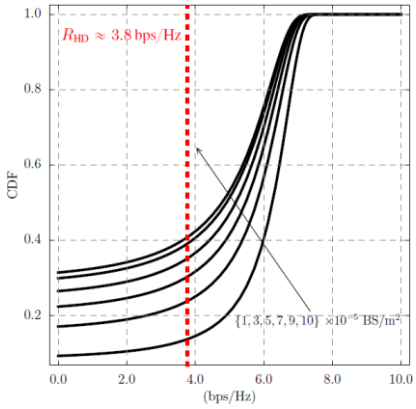

Figure 41. Shows the outage probability of the tagged receiver in FD mode as function of increasing density of interfering nodes and self-interference cancellation of δ = -100dB.

Now Figure 41 shows the outage probability of the tagged receiver in FD mode as function of increasing density of interfering nodes and self-interference cancellation of δ=-100dB. In this configuration, the FD communications can effectively achieve much higher rates when compared to the traditional HD networks, even though suffering additional interference from neighboring UEs as well as self-interference. Actually, the FD network only becomes viable if the self-interference is cancelled by about -90 dB when the maximum rate nearly doubles the one achieved in HD mode. But as mentioned earlier, simulation studies need to be performed to verify the results in real environments.

4.1.4. MANET and relaying results with FD transceivers

In MANET study with FD enabled IEEE802.11 network, we now focus on the large scale network results displayed in Figure 42. The results were obtained using UDP as a transport protocol and selecting 5 sources and 5 destinations over the 30 node network. Each simulation set is defined as a list of sources and destinations over a given topology. When changing sets, the topology is randomly redefined and the sources and destinations are again randomly chosen. Once the parameters for a given set are chosen, we start multiple runs of simulations. The results obtained here show the average results over multiple simulation sets [23].

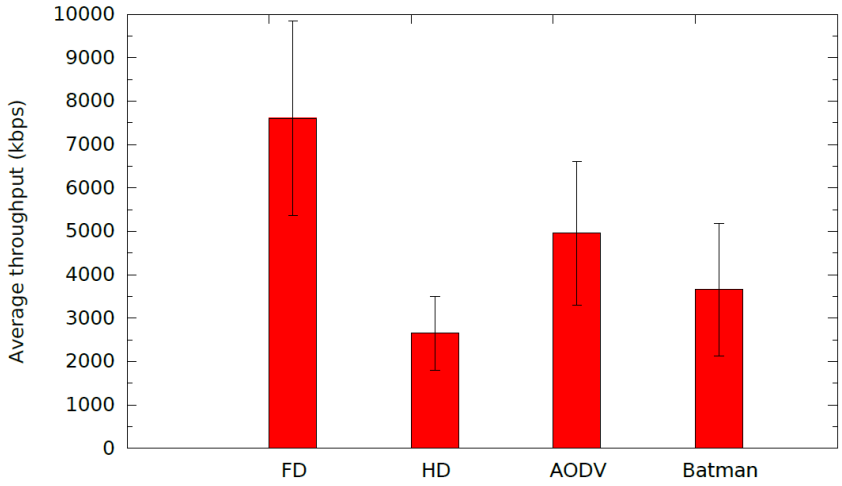

Figure 42. Large scale simulation results (with 95% confidence intervals)

The results in Figure 42 show the average throughput at both destinations and sources (bidirectional UDP traffic from source to destination and from destination to source). What we observe at first glance is the net improvement of using full duplex when compared to half duplex in the static routing case. On average, we observe an increase of 187% in average throughput which is higher than the 100% increase expected from full duplex technology. We also observe better performance by using static routing in FD mode than by using readily available ad-hoc routing protocols. Indeed, we observe that on average, static routing performs 53% better than AODV and 107% better than Batman. While these results can, in part, be accounted for by the overhead of signalling of both those ad-hoc routing protocols, they also show that having bidirectional routing paths in FD networks increases the overall throughput.

DUPLO addresses full-duplex relaying as well as MAC protocol for MANETs. FD relaying overcomes the spectral inefficiency of its HD counterpart, and additionally enhances performance. In what regards to the design of cooperative networks with FD relays, DUPLO provides theoretical benchmark and guidelines. Therefore, practical protocols and implementation need to be

assessed. However, based on the analysis steady-state throughput efficiency for decreasing relay loop interference attenuation with FD configuration is shown in Figure 43.

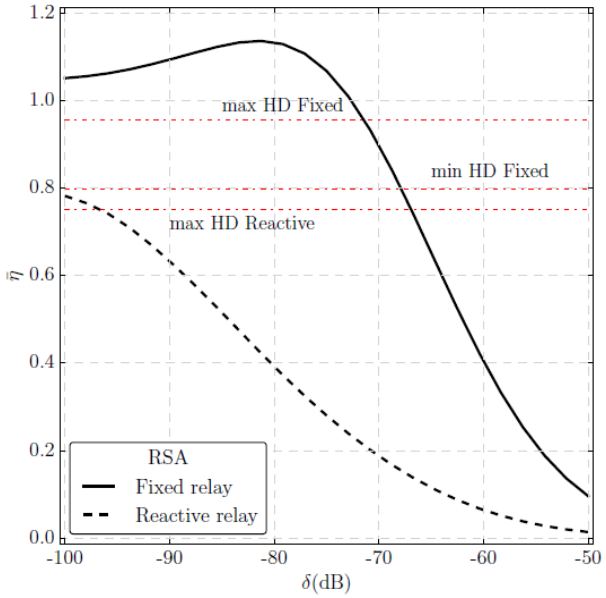

Figure 43. Steady-State Throughput as a function of the residual-self-interference cancellation at the FD relay

The separation distance between source-destination is set to 50m. As previously observed in the HD configuration [23], the steady-state throughput with reactive relay is severely degraded by the relay selection procedure and barely outperforms the HD scenario with 100dB loop interference attenuation. Regarding the fixed relay scheme, the FD configuration with loop interference attenuation ranging from -100 to nearly -70dB shows much better performance than HD mode, whereas the performance degrades faster with low attenuation values.

4.2. Radio resource management and protocols

In this section we focus on protocols and algorithms developed in DUPLO for full duplex. We first discuss radio resource management in small cells (single and multi-cell deployments), then we introduce relaying in full duplex and finish with protocols for MANETs. All protocols and algorithms depicted here are detailed in D4.2 [24].

4.2.1. Radio resource management in small cells

Radio resource management is a crucial point to consider in order to exploit full duplex as efficiently as possible. In DUPLO, we have considered several aspects of radio resource management in both single cell and multi cell deployments. Several algorithms have been devised in order to tackle problems such as spectral efficiency maximization, scheduling, co-channel interference, power allocation etc.

4.2.1.1. Single cell deployments

Here, we consider a single cell with a full duplex base station. Therefore, we do not consider inter-cell interference. In this context, we have developed several algorithms which are presented in this section.

Spectral efficiency and beamformer design

The assumed system model is illustrated in Figure 44. The number of transmit and receive antennas at the BS are N_T and N_R, respectively. The full-duplex capable base station is assumed to operate with multiple half-duplex users on the same system resources. The main challenges in the design are the self-interference due to FD and co-channel interference (CCI) due to multiple users transmitting at the same time. In FD systems SI and CCI problem between up- and downlink is coupled. Therefore, the best solution is to optimize both link directions jointly. Thus, the main objective here is to propose a joint beamformer design approach, which accounts for the downlink and link simultaneously. The problem of interest is to maximize total system spectral efficiency (SE) under some power constraints. We adopt a linear beamforming technique for downlink design. For the uplink we adopt minimum mean square error and successive interference cancellation (MMSE-SIC) that is optimal nonlinear multi-user scheme.

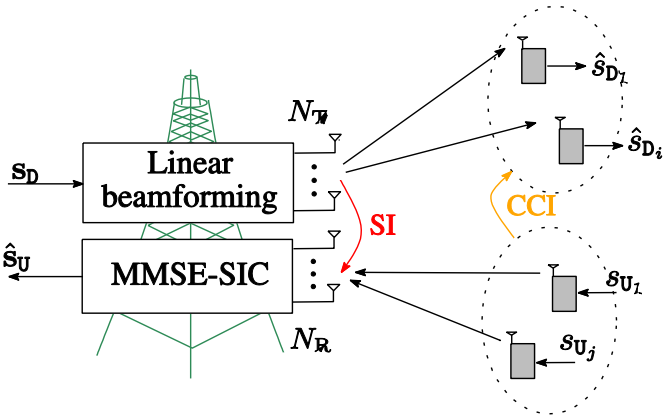

Figure 44: Illustration of the multi-user small cell scenario in full-duplex wireless systems.

In this context, we have proposed two algorithms to solve the spectral efficiency maximization problem. The first algorithm is based on iterative determinant maximization (MAXDET) but due to the scarcity of solvers, an iterative semidefinite program (SDP) based algorithm was also proposed [30].

Scheduling and power allocation strategies

Advanced wireless communication systems dynamically schedule users, and allocate subcarriers and power among them in order to meet the quality of service (QoS) requirements of each user, and to utilize the limited resources efficiently. In DUPLO, we have studied scheduling and power allocation strategies for FD operation in SISO and MIMO cases having the deployment scenario fundamentally similar to the previous case, i.e., full-duplex base station communicating with half-duplex UEs.

Three resource allocation algorithms which consider both the subcarrier and power allocation for OFDMA system having a full-duplex base station with randomly distributed half-duplex uplink and downlink users have been defined and analysed in [31][32][53]. A simple three-step algorithm is proposed in [32] to maximize the sum-rate of full-duplex system subject to predefined target rate constraints at the uplink and downlink users, and transmit power constraints at the base station and uplink users. Dynamic hybrid scheduler that can switch between half-duplex uplink, half-duplex downlink and full-duplex mode opportunistically to maximize the sum-rate has been designed in [31]. These algorithms in [31] and [32] assume perfect channel state information (CSI) at the transmitting nodes which may be unrealistic because of user mobility, feedback/processing delay and small channel coherence time. Therefore, a subcarrier and rate allocation for full-duplex OFDMA systems under imperfect CSI has been studied in [53]. Figure 45 illustrates the operation principle of the hybrid scheduler. Some performance results for the discussed schemes are shown in Figure 38, while more detailed description of the schemes and their performance is given in the DUPLO deliverables D4.1.2 [23] and D4.2 [24].

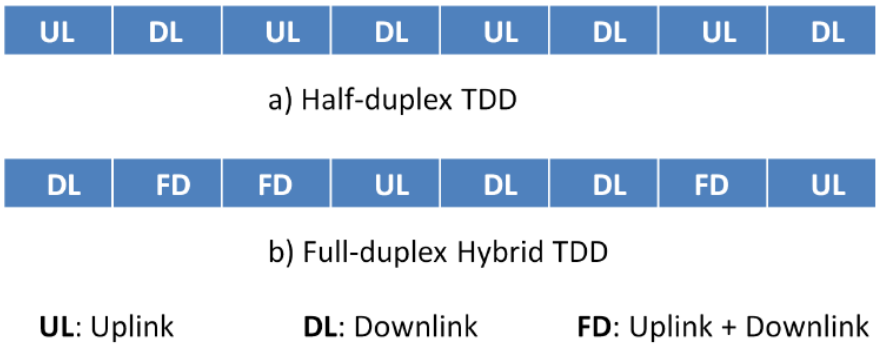

Figure 45. a) Half-duplex TDD scheduling, b) Hybrid scheduling

In [33], we give analysis on power allocation strategies for single cell deployments. The conclusions outlined are valid for both cells with half duplex or full duplex UEs. Our studies highlight the necessity for a joint downlink and uplink power allocation in order to optimize the system performance in both transmission directions. This is due to the coupling of the downlink and the uplink because of the self-interference and the co-channel interference between UEs. Unfortunately, the subcarrier and power allocation problem that maximizes the system spectral efficiency cannot be expressed as a convex optimization because of interference terms. Therefore, finding the optimal solution is computationally difficult and intractable for systems with large number of users and subcarriers. Instead of seeking the global optimal, we solved the problem for competitively optimal power allocation by modelling the problem as a non-cooperative game. We also proposed algorithms to reach equilibrium by performing iterative water-filling on the uplink and the downlink alternatively. These studies provided some insight for the required self-interference cancellation and showed that the greater the distance between UEs and base station, the greater the self-interference cancelation required was. The greater the distance in between UEs, the smaller was the required self-interference cancelation.

Correlated co-channel interference from UL to DL

Co-channel interference was also studied in DUPLO. More specifically, we have focused on co-channel interference from uplink UEs to downlink UEs connected to a same base station and have taken into account the effect of correlated shadowing. We have considered multiple half duplex UEs randomly scattered around a full duplex base station and have devised a procedure to derive the approximated distribution parameters of the received power from the desired transmitter as well as the co-channel interference at the user of interest thus making it possible to derive the distribution of the signal to interference ratio (SIR) which lead to an expression for the outage probability [54].

4.2.1.2. Multi cell deployments

DUPLO system level work has also consisted of multi cell deployment studies. In these setups, inter-cell interference is now another factor to take into account on top of the co-channel interference and self-interference (to name a few).

In Figure 46, we show a multi cell deployment scenario with multiple base stations and multiple UEs. A given user receives interference not only from neighbouring users but also from neighbouring base stations.

We derived formulations for the spectral efficiency of a given user and the outage probability in such circumstances [51].

We have also considered the MIMO case in multi cell deployments. In this case, multiple antennas are used to serve multiple full duplex users from a full duplex base station as shown in Figure 47. In order to solve the weighted sum-rate maximization problem to compute the optimum precoding vectors and the receiving vectors, we proposed a low complexity alternating algorithm which converges to a local optimum point [24].

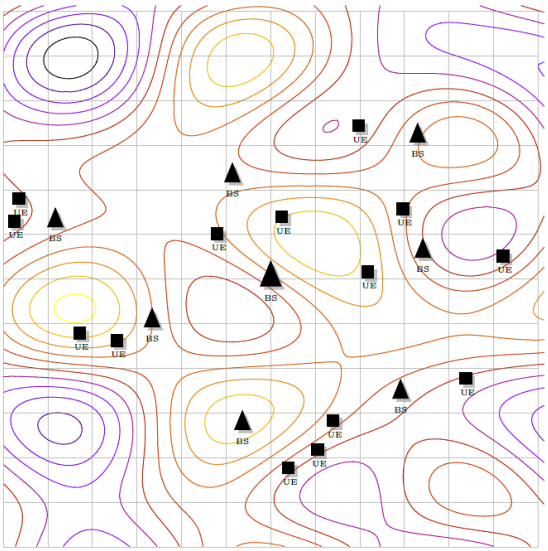

Figure 46. Illustration of a random deployment of small cells and user terminals over an arbitrary network area. Shaded squares represent user terminals, while shaded up-triangles depict small cell base stations. A heat map represents the corresponding random composite fading channel where the fading intensity varies from red/strong to dark blue/weak.

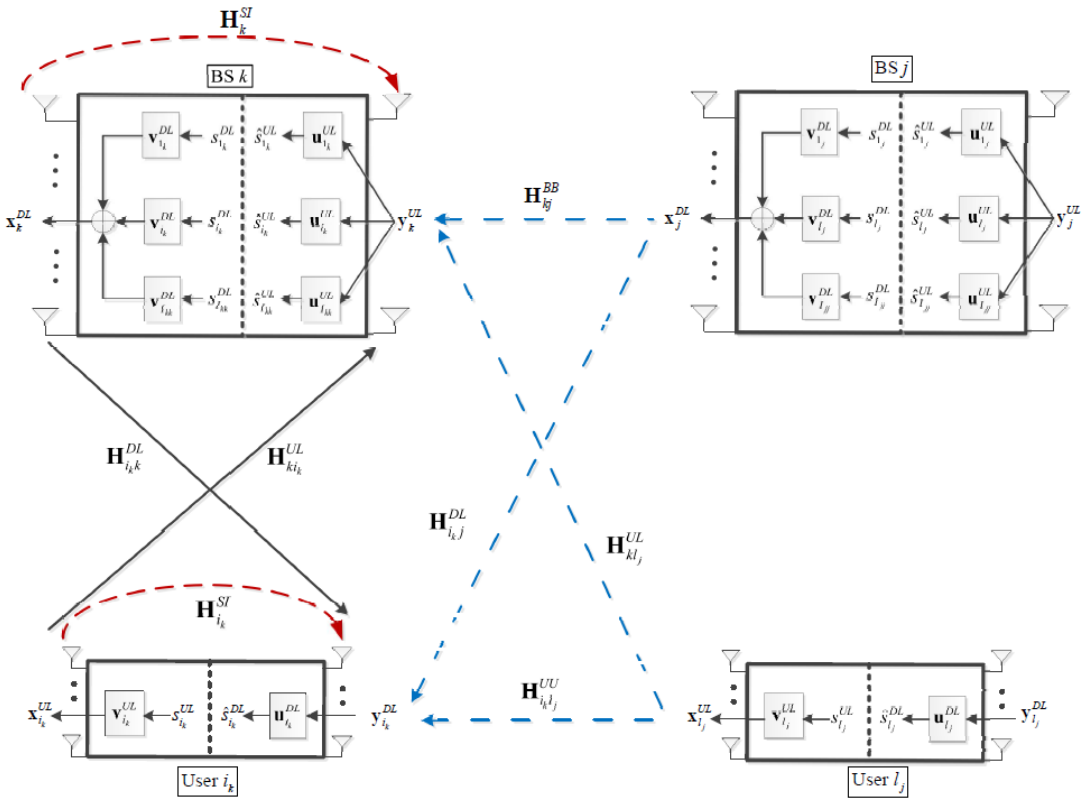

Figure 47. Full-duplex MIMO multi-cell system

4.2.2. Relaying

In this section, we highlight DUPLO results with respect to full duplex relaying schemes. Indeed, full duplex relays can help overcome the shortcomings of traditional half duplex relaying schemes which are quite inefficient. All studies in this section were done under Nakagami-m fading and taking into account the co-channel interference.

The topology in Figure 48 shows a full duplex base station assisting in relaying data from one user to another user. In this context, we have studied two full duplex relaying schemes: full duplex dual hop (FDHD) and full duplex joint decoding (FDJD). In the first case, the direct link (source to destination) is seen as interference for the destination while in the second case, the direct link is seen as useful information and an iterative block decoding process is employed at the destination. We derived outage probability formulations in both cases [55].

We also performed network level studies where we specified a relay selection algorithm based on a RTS/CTS mechanism and modelled the relay selection procedure with a Semi-Markov process. We then derived the steady state throughput accounting for the cost of the relay selection procedure.

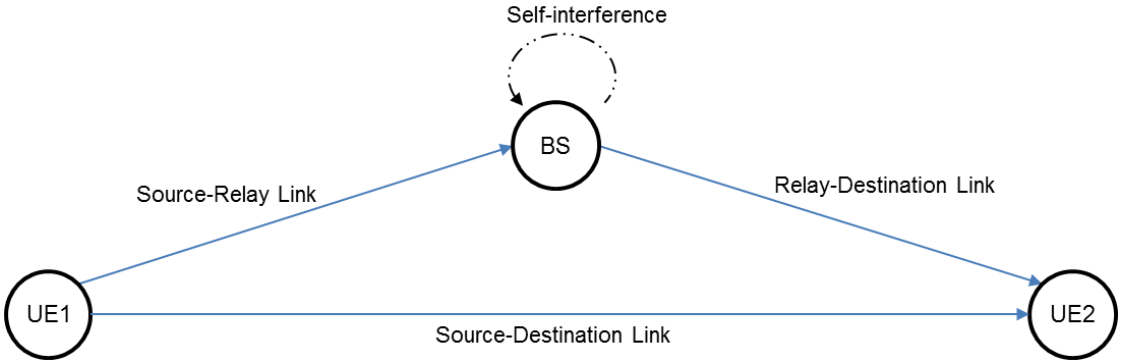

Figure 48. 3-node relaying setup: UE1 acts as a source and communicates to the destination, UE2, with help of a FD BS, which acts as a relay node.

4.2.3. MANET protocols

DUPLO system level studies have also focused on Mobile Ad-hoc Networks. In these types of networks, there is no central decision system (such as a base station or an access point) and information is usually relayed through several nodes before reaching the destination. Figure 49 shows an example of such a network with multiple multi-hop transfers occurring.

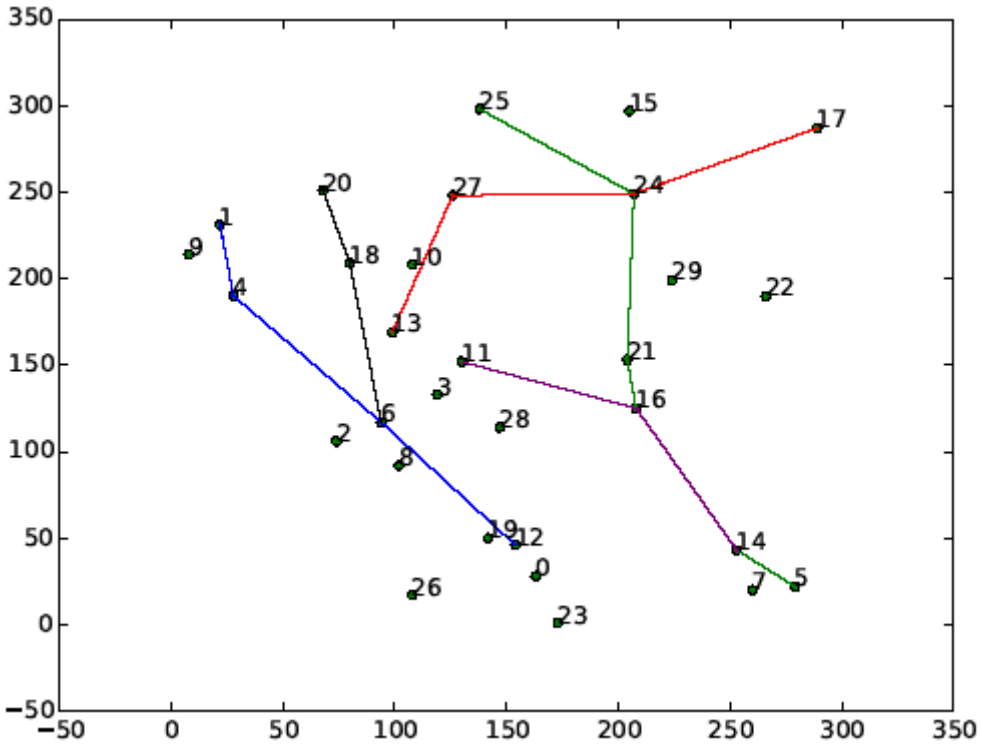

Figure 49. Example MANET topology with multiple multi-hop transfers

We have first developed a MAC protocol for full duplex MANETs [34]. This protocol is based on the IEEE 802.11g protocol and enhances it with bidirectional full duplex capabilities. A modified RTS/CTS mechanism is used in order to perform channel reservation and agree on the full duplex nature of the transfer. Backwards compatibility has been kept in mind and only minor modifications to available half duplex equipment are necessary in order to make them communicate with their full

duplex counterparts. This MAC protocol isn't restricted to ad-hoc mode and can be used in more traditional managed mode (with an access point).

Based on simulation results, we have seen that routing can also be optimized for full duplex MANETs but a substantial amount of control information would need to be exchanged between the different nodes in the network. This is why we have also proposed a control plane design that takes a cross-layer approach in order to merge network and MAC layer information and aggregates control messages in order to have a better view of the topology whilst limiting the amount of control messages flowing through the network.

4.3. Summary on key results

Chapter 4 outlines key findings and numerical results of the DUPLO WP4 work and by no means all the results. The focus was on studying point-to-point full-duplex links, standalone single or multi-user small cells with single/multiple full- and/or half-duplex links, full-duplex relaying, mobile ad-hoc networks and their performance. The WP4 results are documented in full depth in DUPLO deliverables D4.1.2 [23] and D4.2 [24].

Numerical results from link level performance studies show that self-interference cancellation of about 80-90 dB is needed to outperform HD links. It is also demonstrated that short distance links with low transmission power (such as 5G indoor small cells) are the most suitable use case for full-duplex communication. Energy efficiency of FD links proves also to be promising.

Numerical results from conducted performance studies in network level indicate that in small area systems full-duplex transmission can provide system level performance gains over half-duplex even with moderate self-interference cancellation levels (70 dB … 90 dB). However, better self-interference cancellation capability in the full-duplex transceiver is beneficial in expanding the competitive operation range of full-duplex transmission. Maximum observed system level capacity gain of full-duplex transmission over half-duplex transmission in small cell networks varies from 40% to 80% depending on the study assumptions.

Conducted system studies with full-duplex MAC protocols in IEEE 802.11 MANET kind of network environment demonstrate that full-duplex transmission can provide substantial throughput gains even with non-symmetrical traffic, for instance when using TCP as a transport protocol.

Radio resource management is a crucial point to consider in order to utilize full-duplex transmission efficiently in wireless networks. In DUPLO, we have considered several aspects of radio resource management in both single cell and multi cell deployments. Several algorithms have been devised in order to tackle problems such as spectral efficiency maximization, scheduling, co-channel interference, power allocation etc. Advanced relaying schemes, protocol solutions for mobile ad-hoc networks and network level management solutions are also covered.

Results of this work have been published in four journal papers [30][49][56][57] and more than ten conference papers, including (but not limited to) the following [29],[31-34], [48], [50-55].

All in all, the results from system level studies are encouraging, and pave path for introducing full-duplex transmission as an air interface technology for future 5G systems.

5. PROOF-OF-CONCEPT VALIDATION AND TESTING

This chapter reports the DUPLO proof-of-concept hardware demonstrator implemented in the framework of DUPLO WP5. Furthermore, the validation and testing of this DUPLO full-duplex transceiver, as well as its main performance results are also introduced in this chapter.

5.1. Proof-of-concept demonstrator

DUPLO project has identified small cells as one of the main areas of interest for the project, due to their relevance for future 5G networks, as well as because small areas with short link distances and low transmission powers forms feasible deployment scenario for full-duplex technology. Due to these reasons, a small cell indoor scenario has been selected for the DUPLO proof-of-concept.

DUPLO WP5 showcases two DUPLO demonstrators which embed different DUPLO solutions. These DUPLO demonstrators are:

- Single-port antenna radio node demonstrator: This demonstrator comprises the electrical balance duplexer developed in DUPLO WP2 and the digital SIC algorithm developed in DUPLO WP3.
- Dual-port antenna radio node demonstrator: This demonstrator comprises the dual-polarized antenna and the active cancellation network developed in DUPLO WP2 and the digital SIC algorithm developed in DUPLO WP3.

Both demonstrators are able of adapting to the environmental changes close to the antenna by means of implementing automatic tuning algorithms over the analog circuitries. The radio nodes are completed with WARP version three radio boards [35] and WARPLab framework [36].

5.1.1. Single-port antenna radio node

Figure 50 illustrates the architecture of the single-port antenna radio node. This transceiver integrates a tunable RF circuit which comprises a hybrid transformer in combination with an electrical balance network. Note that the first EDB prototype developed in WP2 has been considered in WP5 to respect the project timeline. The tunable RF circuitry is directly connected to the RF ports of the WARP v3, and it isolates the received signals from transmitted signals. The single-port antenna radio node also comprises digital SIC algorithms to further cancel the remaining SI.

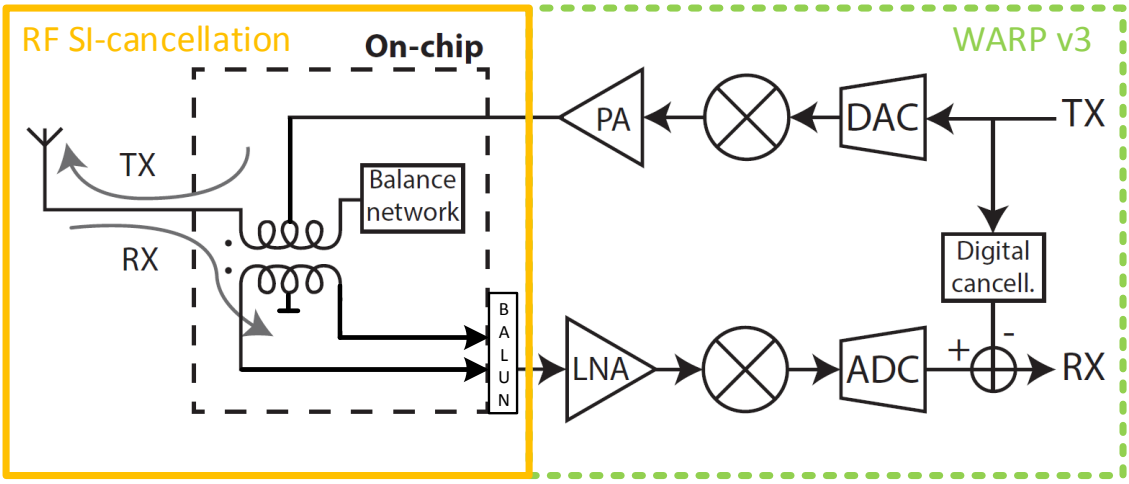

Figure 50. Architecture of the single-port antenna radio node comprising the first electrical balance duplexer prototype developed in DUPLO WP2 [16].

Figure 51 shows a picture of the single-port antenna radio node:

1) WARPv3: WARP v3 has been used as the integration platform. WARP v3 is controlled by MATLAB via the Ethernet connection, as will be described later in this section.

2) Tunable electrical balance duplexer module: The tunable electrical balance duplexer is mounted on this module via direct chip bonding.

3) Power supply board: This power supply board has the ability to route and distribute different supply voltages by manual setting of the jumpers. Redistribution of the supply voltages is not needed. External power supply sources are connected to the power supply board.

4) Serial control module: The serial control module is a custom-designed PCB which enables communication from MATLAB to the shift register via USB. The serial control module performs the necessary data translation and takes care of the USB protocol.

5) Antenna: An antenna from a commercial USB WiFi module has been used. This WiFi module has been hacked to connect directly to the antenna itself, bypassing all the hardware on this WiFi module. The antenna has a planar inverted-F patch structure, and has only one radiation element and one connector port.

The self-interference isolation performance of the tunable duplexer is determined by how accurate the balance network impedance equals the antenna impedance. With this regard, an automatic tuning algorithm has been implemented in MATLAB to tune the EBD impedance over different operating conditions [26].

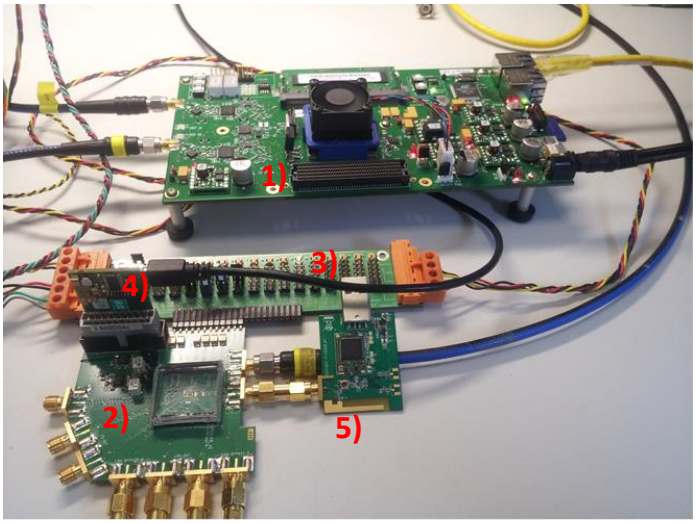

Figure 51. Picture of the full-duplex single-port antenna radio node.

The automatic tuning algorithm implemented for the electrical balance duplexer is executed in two main phases. The first phase is the training and modelling phase which gathers a data-set that describes the relation between the SIC and R/C codes during constant antenna impedance conditions. Figure 52 (a) shows an example of the data-set gained from the training phase. Based on the obtained data-set a mathematical model is derived by fitting the theoretical equations that describe the circuit. During the second phase, the tuning is performed during system operation, when the balance network is tuned by estimating the difference between antenna and EBD impedance from applying the measured SIC in the model derived in the previous phase. But as the antenna impedance is a complex value, an angular search algorithm is required to determine also the phase of the difference between impedances to be able to use the model to find the required R/C codes. Figure 52 (b) shows an example of the angular search implemented in the second phase of the tuning algorithm.

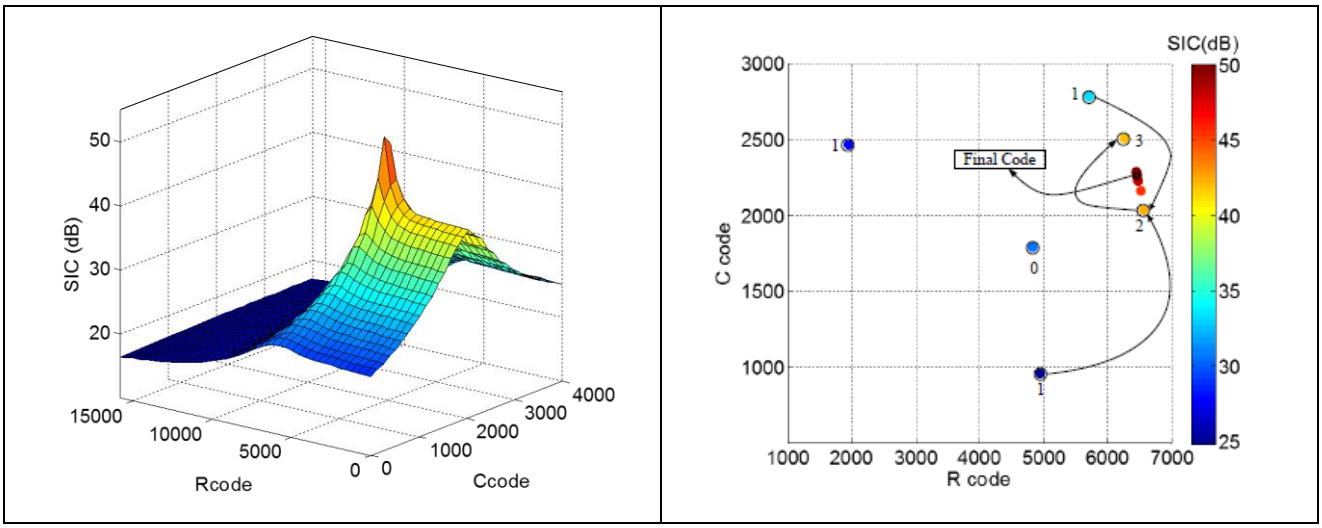

(a) (b)

Figure 52. (a) An example of the training data-set for the SIC versus R/C codes, (b) an example of the development of the angular search in terms of R and C codes.

5.1.2. Dual-port antenna radio node

Figure 53 illustrates the different key building blocks which integrate the dual-port antenna radio transceiver. As can be seen from this figure, the radio node consists of:

- Dual-polarized antenna: As reported in section 3.2.2, the dual-port planar microstrip antenna (second implemented prototype) provides more than 50 dB of SI suppression. The antenna has two ports which are connected respectively to the transmission and reception paths by means of using SMA connectors.

- Active Cancellation Network: As already described in section 3.2.2, the active cancellation (second implemented prototype) network improves in 10-12 dB the isolation provided by the antenna. The objective of the cancellation network is to compensate the environmental effects that can degrade the antenna SI suppression, maintain the analog SIC always above 50 dB. Furthermore, the active cancellation network includes a self-interference power detector which monitors the power of the SI signal after the active cancellation network. This power is used as the input of a gradient descent algorithm which finds the settings which minimize the residual self-interference signal after the active cancellation. The active cancellation board is controlled from an external control unit, i.e. the STM32F4 microcontroller.

- Digital Cancellation block: As in the case of the single-port antenna radio node, the digital cancellation block cancels the remaining self-interference up to the receiver noise floor.

- WARP v3 radio board: Again, the WARP v3 radio board has been also used for the integration of the dual-port antenna transceiver.

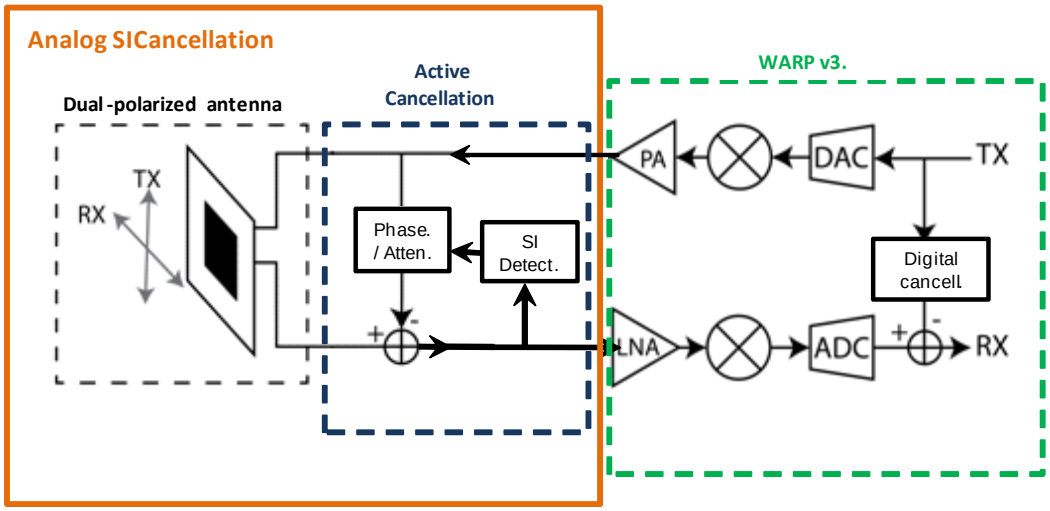

Figure 53. Architecture of the dual-port antenna radio node

Figure 54 shows a picture of the dual-polarized antenna radio node. The different abovementioned key building blocks can be shown is this figure as well as the external control unit used to control the settings of the active cancellation network. The transmission and reception RF paths are connected via SMA connectors and RF cables, and external power supply is used to power the active cancellation network.

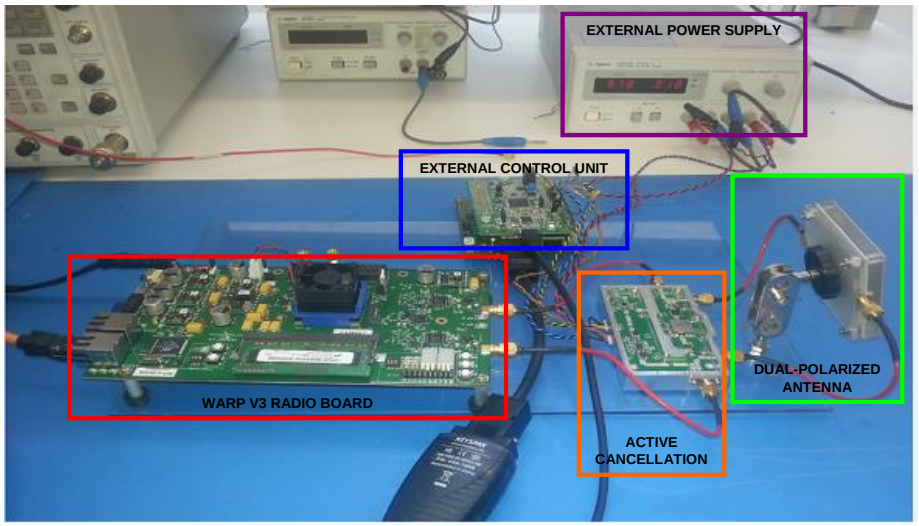

Figure 54. Picture of the dual-port antenna radio transceiver.

The active cancellation network uses variable amplitude and phase coefficients to cancel the self-interference leaking from the antenna. These coefficients must be dynamically tuned in order to adapt the cancellation signal to the wireless channel response, therefore, an automatic tuning algorithm is necessary to find the attenuator and phase shifter values which minimize the level of detected self-interference in an efficient way. Figure 55 (a) shows the remaining self-interference signal power when variable attenuator and phase shifter are swept over their respectively attenuation and phase-shift range. The obtained results indicate a deep null at the optimal point which corresponds to the optimal attenuation/phase code combination. An efficient search algorithm with a reduced number of iterations can be implemented by means of using a gradient descent algorithm. Figure 55 (b) illustrates the convergence rate of the developed auto-tuned algorithm. As can be seen, the optimal point is found in around 12-15 iterations. The external STM32F4 microcontroller has been also used for the implementation of the gradient descent algorithm.

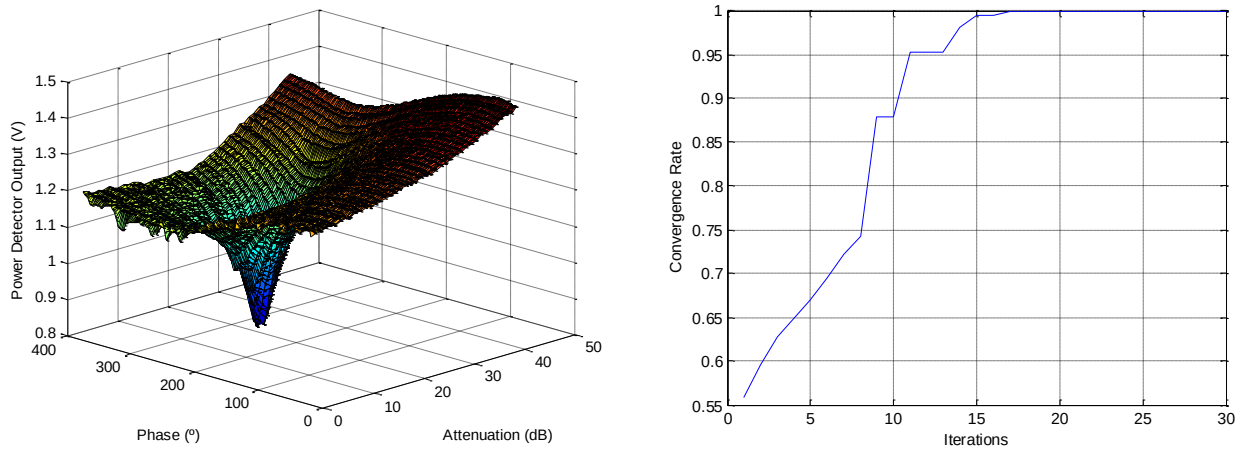

(a) (b)

Figure 55. (a)The RSSI output sweeping attenuator and phase shifter values, (b) converge rate of the developed auto-tuning algorithm.

5.1.1. Full-duplex baseband and Digital Cancellation Block

As already mentioned, WARP version three hardware platform [35] is being used for both DUPLO demonstrators. This radio board integrates a high performance FPGA, two flexible RF interfaces (one is configured as transmitter and the other RF chain is configured as receptor) and multiple peripherals to facilitate rapid prototyping of custom wireless designs. The reference design used for the demonstrator is WARPLab framework [36]. This WARPLab framework enables PHY prototyping using WARP hardware for waveform transmission/reception and MATLAB for signal processing. By doing so, the arbitrary I/Q signals samples generated in MATLAB are sent to the WARP board via the Ethernet cable to their up-conversion and transmission. Likewise, the signals received by the WARP board are down-converted and transferred to MATLAB for post-processing. Additionally, WARPLab framework allows to control various hardware blocks of the WARP radio board like transmit and receive amplifiers, AGC, etc. by using MATLAB.

The full-duplex baseband developed for DUPLO demonstrator is based on an OFDM waveform and it has been implemented in MATLAB. Figure 56 shows the transmitted frame structure in time domain for the two node link setup, i.e. two full-duplex nodes separated a certain distance operating both in FD mode. The long training sequence (LTS) is used for detecting the symbol boundary and calculating the frequency offset. The short training sequence (STS) purpose is to train the automatic gain controller (AGC) of the WARP. For Node 0 transmission, zeros are inserted in between the preamble (STS, LTS and Training sequence) and the data part. The number of zero samples is denoted by D, whose value is equal to length of the preamble and a fixed delay of 200. One sample delay is equal to 25ns because the sampling frequency is equal to 40 MHz. In case of Node 1, zeros are transmitted first followed by preamble and data. The zeros are used in order to transmit the preambles in a time orthogonal manner.

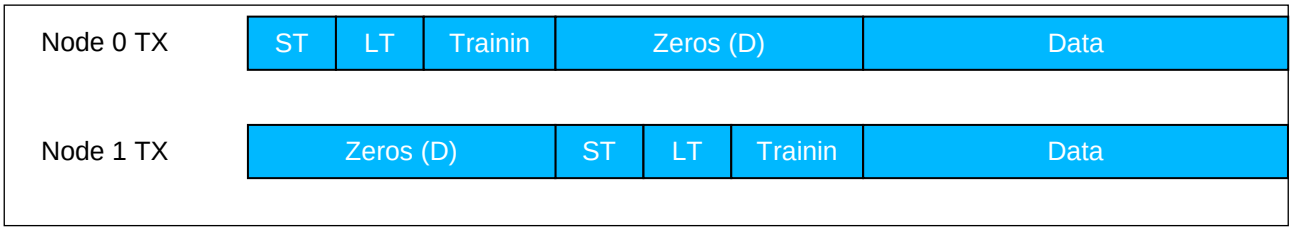

Figure 56. Time domain representation of the full-duplex frame.

In order to decode the received data and to do self-interference cancellation, an estimate of the channel is needed. The training sequence is used for calculating the channel estimate. It consists of two OFDM symbols, each sub-carrier of which is modulated with a pseudo random BPSK symbol. The training symbol differs from the normal OFDM symbol in the sense that it has a DC component and its bandwidth is larger than the normal OFDM symbol. This modification helps in the case of time domain cancellation of the self-interference.

Digital cancellation block forms a part of the digital baseband and it has been implemented as a feed forward filter using MATLAB. Considering a linear system model in time domain,

$$y_t = h_{t,SI} * x_{t,SI} + h_{t,Des} * x_{t,Des} + n, \quad (5.1)$$

Where $h_{t,SI}$ and $h_{t,Des}$ are the self-interference and desired channel respectively, $x_{t,SI}$ and $x_{t,Des}$ represents the transmitted self-interference and desired symbols, $(*)$ represents the convolution operation and n represents the noise. The previous equation can be written in frequency domain as,

$$y_f = h_{f,SI}x_{f,SI} + h_{f,Des}x_{f,Des} + n_f. \quad (5.2)$$

Therefore digital cancellation can be defined as

$$SIC_{t,D} = y_t - \bar{h}_{t,SI} * x_{t,SI}, \quad (5.3)$$

$$SIC_{f,D} = y_f - \bar{h}_{f,SI}\bar{x}_{f,SI}. \quad (5.4)$$

Furthermore, as OFDM is used as the modulation technique, each sub-carrier can be treated independently in the frequency domain, thus leading to a sub-carrier based cancellation

$$SIC_{k,f,D} = y_{k,f} - \bar{h}_{k,f,SI}\bar{x}_{k,f,SI}. \quad (5.5)$$

These linear models lead to two different implementations of digital cancellation, which are time domain cancellation and frequency domain cancellation. The symbol boundaries in the received signal are derived from the LTS sequence. Due to propagation delay and trigger delay, there can be a mismatch between the symbol boundaries of the two nodes in the received signal. Since OFDM can only be demodulated at the correct symbol boundary, this makes it necessary to include implementations of both frequency domain and time domain interference cancellation algorithms in the demonstrator. Figure 57 shows the spectrum of the self-interference signal at the digital baseband and the spectrum of the residual self-interference after doing frequency domain cancellation. As the cancellation is performed only for the data sub-carriers, there is higher residual at the pilot frequencies.

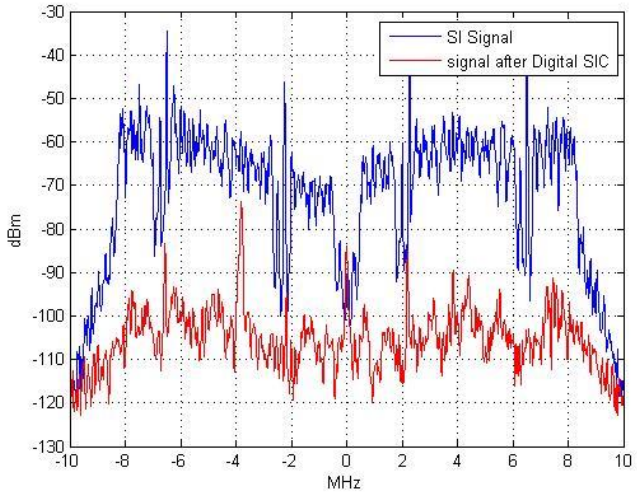

Figure 57. Frequency domain self-interference cancellation.

5.2. Validation and performance measurements

The DUPLO demonstrator has been evaluated in a wireless indoor environment with people and objects moving around the full-duplex radio transceiver. By doing so, the adaptability of the analog and digital cancellation blocks to the time varying wireless channel is demonstrated. Table 6 depicts the main features and technical details of the scenario used for DUPLO proof-of-concept validation.

Table 6. Specifications for DUPLO proof-of-concept.

Feature	Specification
Scenario	Wireless point-to-point connection between two full-duplex transceivers Objects and people moving around the full-duplex radio node
Distance	Distance between nodes up to 16 meters
Carrier frequency	2.45 GHz
Signal BW	20 MHz
Transmit power	Up to 20 dBm
Type of Signal	OFDM based Waveform
Modulation Schemes	Up to 64QAM

5.2.1. Single-port antenna radio node

Figure 58 illustrates the measurement setup for the evaluation of the full-duplex wireless link with two single-port antenna radio nodes. As can be seen, both WARP boards are connected to a control PC which comprises full-duplex baseband and digital cancellation block. Moreover, the EBD tuning is also implemented in this PC. The total self-interference cancellation provided by the single-port antenna radio node is 66 dB in 20 MHz of bandwidth. Figure 59 shows a picture of the system setup including the wireless link. A detailed description of this setup is given in [26].

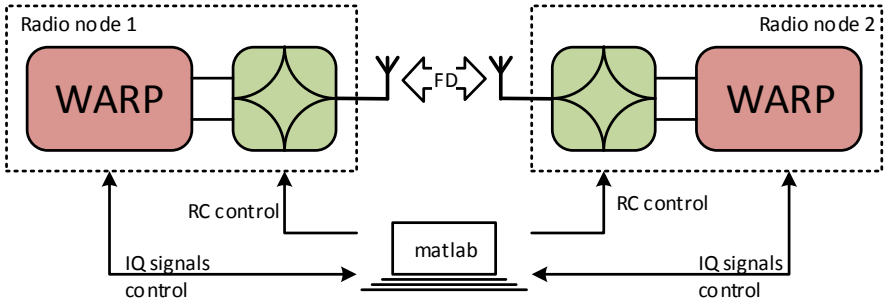

Figure 58. Measurement setup for the evaluation of the full-duplex wireless link.

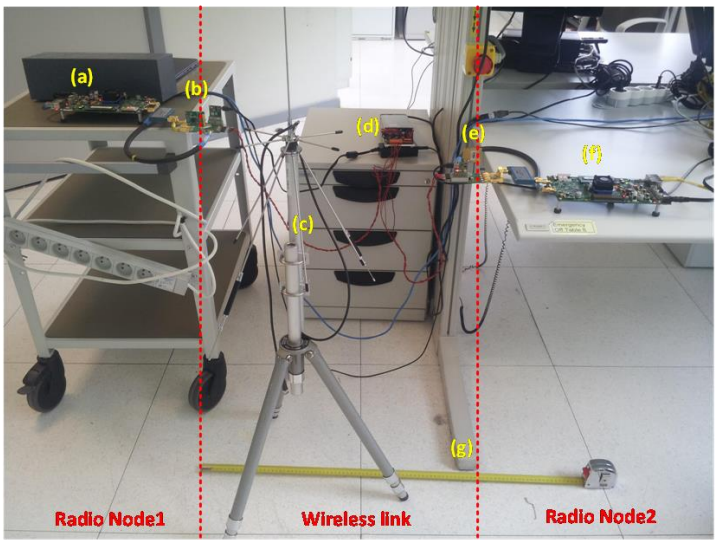

Figure 59. Full-duplex evaluation platform building on two full-duplex single-port antenna radio nodes [26].

Figure 60 illustrates the system performance over different link distances (for a BPSK digital modulated signal with 0 dBm of WARP transmit power). These results show the EVM performance measured at both radio nodes when the nodes are operating in full-duplex or in half-duplex (noSI). It can be observed that the EVM performance during full-duplex closely matches with the half-duplex performance. This means that the SI is sufficiently reduced (i.e. below the receive noise floor) by the SIC solutions to maintain the SNR at the receiver. With a link distance less than 40 cm, the EVM equals about -25 dB while an EVM of more -15 dB is obtained with a link distance between 40 – 80 cm. Beyond a link distance of 100 cm, the EVM floors at -7 dB both for half- and full-duplex operation. Note that the achieved performance is bounded by the sub-optimal structure of the experimentation setup; the measurements are performed in a realistic (unshielded) environment and are subjected to interconnection losses (e.g. cables, BALUN, ...), unidirectional antennas, multi-path distortion, etc. The performance limitations caused by the first EBD prototype have been identified in [16] and have been addressed in the second prototype presented in [17]. This second prototype offers the ability to increase the bandwidth and offers a strongly improved linearity. This improved linearity enables higher transmit powers which would result in larger link distances. Due to the project timeline, only the first EBD prototype is considered in WP5.

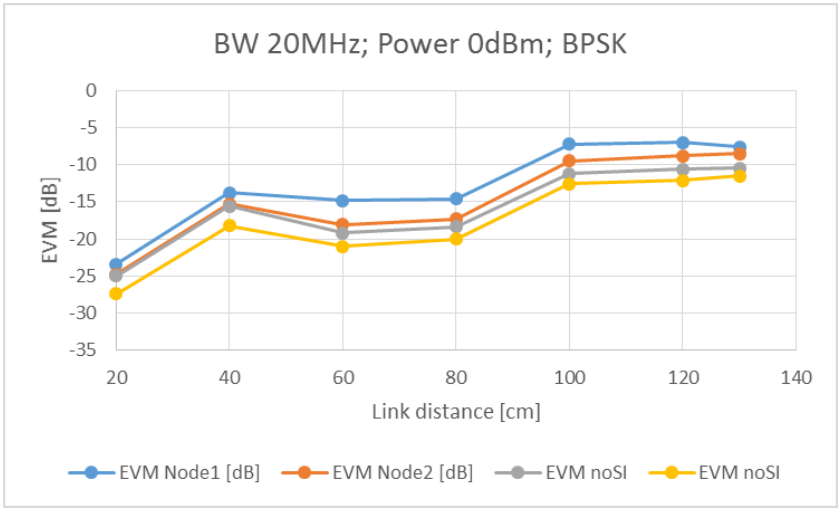

Figure 60. Measurement setup for the evaluation of the full-duplex wireless link.

The impact of the EBD linearity is illustrated in Figure 61, where the relation between the EVM performance is illustrated in function of the WARP transmit power at a link distance of 60 cm. As in half duplex operation the EVM scales linearly with the transmit power, the communication link is not subjected to any nonlinear distortion. In full-duplex operation, this linear trend is also observed at low WARP transmit powers. However, when the WAPR transmit power exceeds 0 dBm, the full-duplex EVM performance degrades because the balance network starts to generate nonlinear distortion which directly couples to its own receive [16], and degrades the FD EVM performance. Given the expected losses in the EBD and the inter-connections, the difference between WARP transmit power and the power provided to the antenna equals about 6 dB. This limits the link distance obtained with this EBD prototype and with this experimental setup.

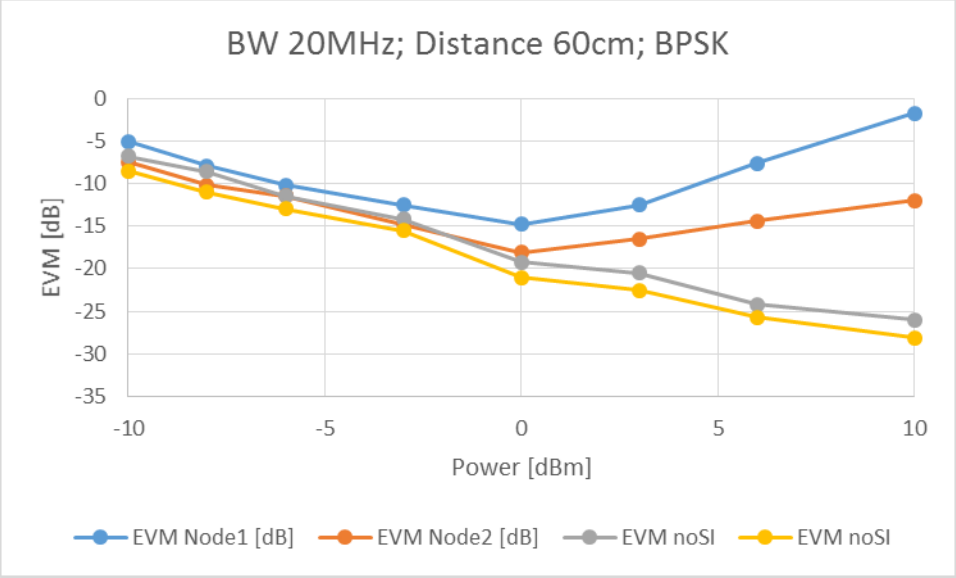

Figure 61. Relation between the measured EVM performance and the WARP transmit power.

5.2.2. Dual-port antenna radio node

This section reports the performance evaluation of the dual-port antenna demonstrator. As in the evaluation of the single-port antenna radio node, two full-duplex radio nodes were separated different distances, while both transceivers were connected to a control PC as Figure 62 illustrates. The full-duplex baseband and digital cancellation block runs on the control PC, while it also sends

the activation command via the serial port to the microcontroller when it is necessary to tune the active cancellation network, i.e. when analog SIC drops below 50 dB. Figure 63 shows a picture of the evaluation setup for the dual-port antenna demonstrator.

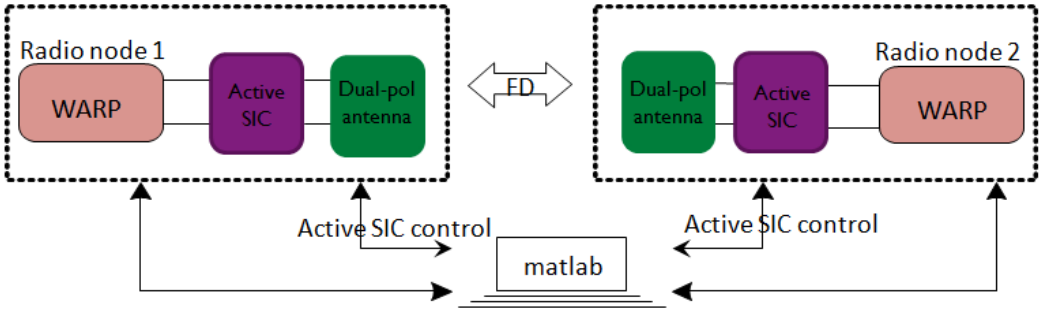

Figure 62. Measurement setup for the evaluation of the full-duplex wireless link.

Figure 63. Picture of the evaluation setup for the dual-port antenna demonstrator.

Firstly, the total self-interference cancellation provided by the dual-port antenna radio node has been evaluated. Figure 64 (a) illustrates the self-interference cancellation for different transmit powers (we conduct 30 runs for each transmit power and we calculated the mean SIC over the signal bandwidth, i.e. 20 MHz). As can be seen from the obtained results, the digital cancellation improves in 30 dB the cancellation at analog level which increases up to 85-90 dB the total amount of SIC provided by the overall radio transceiver. Figure 64 (b) shows the spectrum of the self-interference signal after analog (ASIC) and after digital (ADSIC) cancellation blocks when a BPSK modulated signal of 0 dBm is transmitted. As can be seen, digital cancellation achieves to cancel the remaining self-interference signal till the receiver noise floor which is around -85 dBm (when the transmit power is 0 dBm).

Secondly, the performance of a full-duplex wireless link has also been evaluated by means of measuring the error vector magnitude (EVM) of the constellation after demodulation and the symbol error rate for different distances and modulation schemes. Figure 65 shows the EVM for different modulation schemes up to 64QAM and different distances between nodes. FDAC represents the EVM when only analog cancellation is applied to SI (in this case analog SIC is around 60 dB), while FDADC represents the EVM when both analog and digital cancellations are applied. Finally HD is the EVM performance of the half-duplex link. As can be seen from the obtained results, the full-duplex link is slightly degraded compared to the half-duplex link, there is about 2% difference between the EVM of these two links at a maximum distance of 16 meters.

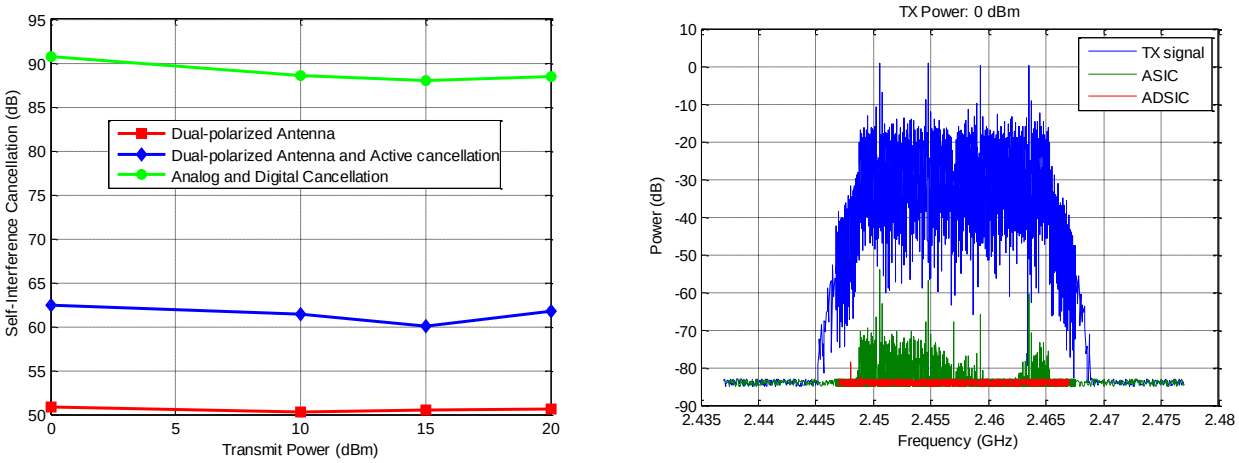

(a) (b)

Figure 64. Cancellation capabilities of the dual-port antenna radio node, (a) SIC at different stages of the transceiver for different transmit powers, (b) spectrum of the residual self-interference signal after analog and digital cancellation stages.

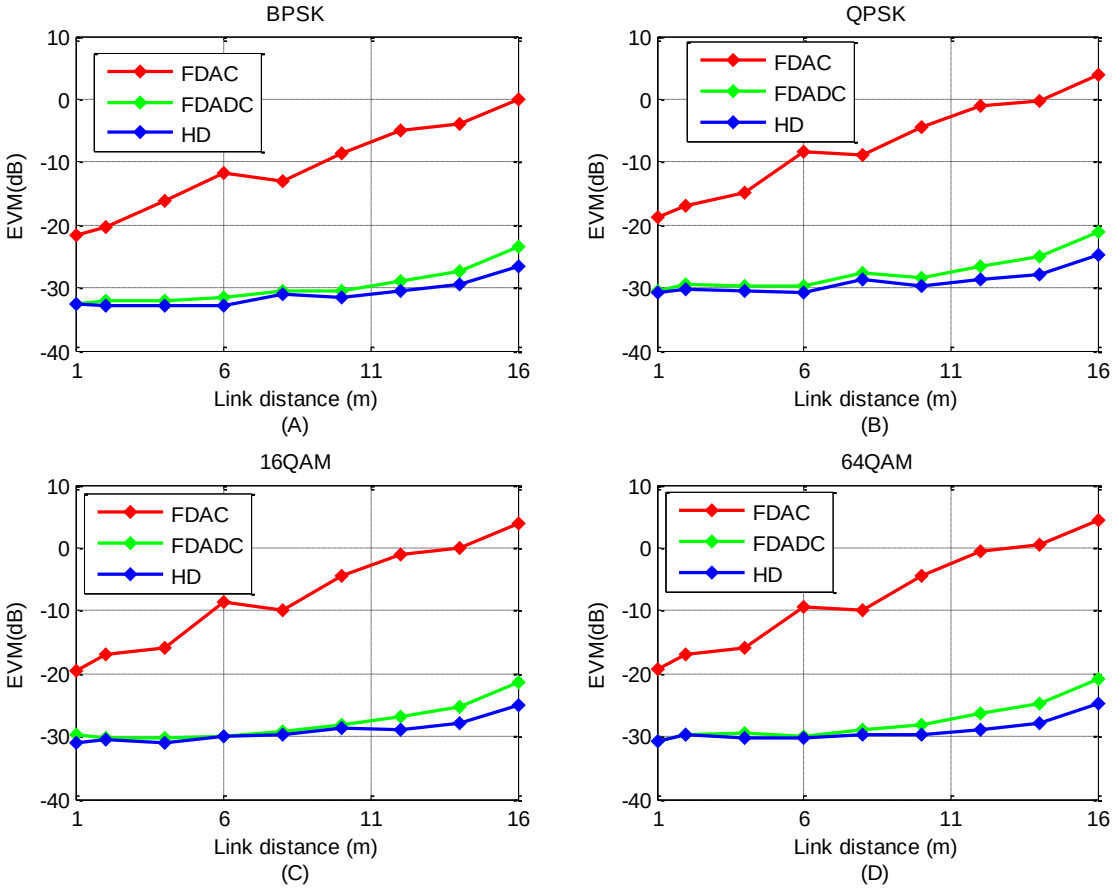

Figure 65. Full-duplex reception performance over distance between nodes. (A) BPSK modulated signal, (B) QPSK modulated signal, (C) 16QAM modulated signal, (D) 64QAM modulated signal.

The symbol error rate has been also evaluated when the dual-port antenna demonstrator operates in full-duplex.

Figure 66 shows the symbol error rate of the full-duplex link when the self-interference is cancelled below the receiver noise floor. As can be seen from the obtained results, error-free digital data reception over a link distance of 10 meters is achieved tor BPSK, QPSK, 16QAM and 64QAM modulation schemes. At the maximum distance of 16 meters, the symbol error rate is below 10^{-2} for the 64 QAM modulation scheme. Deliverable D5.2 includes further analysis and performance metrics of the DUPLO proof-of-concept.

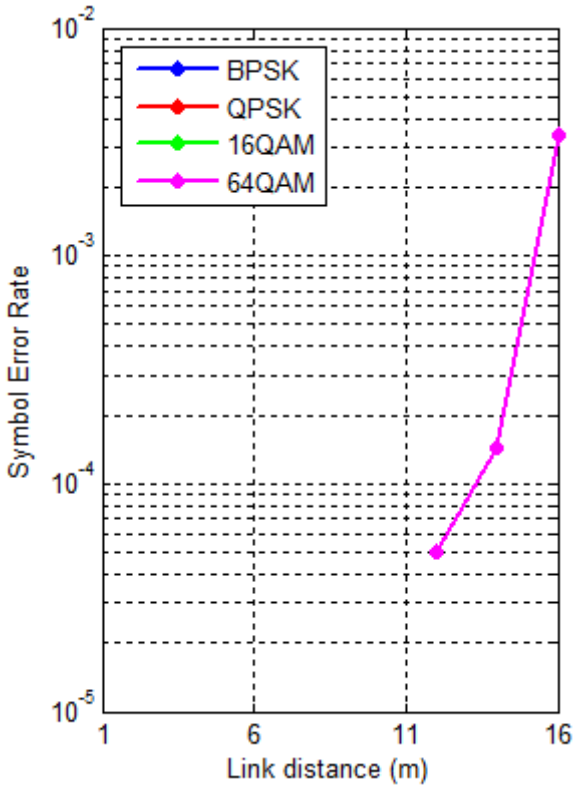

Figure 66. Symbol error rate versus the link distance

6. FUTURE OPPORTUNITIES

Full-duplex has gained lot of attention over the last couple of years. The attention has been accelerated because novel and interesting techniques are being developed which attempt to solve one of the main problems of full-duplex communications: the self-interference in the radio nodes. Apart from the DUPLO project, also other research groups are proposing new techniques to reduce the self-interference. The most promising techniques come from research groups which consider a system approach where the self-interference is rejected and cancelled at different locations in the radio, i.e., at the antenna and in the RF and digital domain. Also interest in applying full-duplex to future evolution of wireless systems has risen significantly. Full-duplex wireless transmission is considered as a promising air interface technique for 5G wireless systems as it tackles key areas where system improvements are needed, such as spectral efficiency, link level capacity and network latency [1].

DUPLO has studied potential full-duplex transceiver techniques for radio devices, aiming to solutions which are attractive in terms of form-factor, system integration, process technology and operation flexibility. Three RF/antenna/analog solutions have been developed. These solutions cover a SI-cancelling front-end, a dual-polarized antenna structure and an electrical balance duplexer. Digital baseband solutions have been studied with the focus in search for novel algorithms to improve self-interference cancellation performance in the presence of transceiver non-linearity, and in performance improvements with joint RF and digital cancellation. Compared to the state-of-the-art, the developed designs differ mainly in terms of form-factor and integration potential in compact or portable radio system devices. This is significant advance for the DUPLO solutions, since the previously published techniques mainly rely on physical dimensions (i.e. antenna spacing) and/or require bulky component. The DUPLO proof-of-concept hardware demonstrator integrates sub-set of the designs into a complete full-duplex transceiver solution enabling performance measurements in realistic dynamic indoor operation environment.

Conducted performance measurements indicate that the achievable self-interference cancellation capability is around 65 dB and 90 dB in 20 MHz bandwidth, with single port antenna solution and dual port antenna solution, respectively. This amount of self-interference cancellation can provide system level performance gains for full-duplex over half-duplex in some cases (i.e., short transmission distances), as DUPLO system performance studies indicate. However, better self-interference cancellation capability would be beneficial in expanding the competitive operation range of full-duplex transmission. Other limitations with the implemented DUPLO solutions are related with the limited linearity and the narrow bandwidth of the analog solutions. Thus future opportunities and development needs with the full-duplex transceiver techniques for compact radio devices are related to performance improvements (self-interference cancellation capability and bandwidth) and design improvements (improved linearity, architectural solutions to reduce phase noise, improved baseband algorithms).

Smart phones and other radio devices support multiple radio protocols and frequency bands. Therefore, from practical wireless transceiver design point of view it is important that in the full-duplex transceiver design also the integration with other radio protocols in the same radio device is considered. Transceiver design supporting flexible duplexing is also potential further research direction. The opportunity for full-duplex in larger form-factors should also be considered in relation with future 5G, for instance with connected cars. Furthermore, development of full-duplex techniques for multi-antenna systems is another potential research direction.

DUPLO system level studies have focused on full-duplex transmission in small cell radio system operation environment. Potential use cases are full-duplex BS serving half-duplex UEs, full-duplex UE, device-to-device connections, relaying, transmission in mesh networks and (self-)backhauling. Conducted system level studies indicate that in small area systems full-duplex transmission can provide performance gains over half-duplex even with moderate self-interference cancellation levels in the full-duplex transceiver. Thus it is not necessary to design full-duplex operation based on worst case link budget in order to benefit in system level. The system level solution could be adaptive change of operation mode between half-duplex and full-duplex transmission. Naturally, high self-interference cancellation capability in the full-duplex transceiver is beneficial in maximizing the system level gains of full-duplex transmission.

Radio resource management is a crucial point to consider when aiming to utilize full-duplex transmission efficiently in wireless networks. DUPLO has mainly focused on single cell scenario as the first step in study and development of network level solutions. In the next years, there will be significant increase on the number of small cells, thus coordination, self-organization, flexible and efficient use of spectral resources, scheduling and radio resource management in general as aspects that will be fundamental for the next generation of wireless communications. DUPLO has put some light into this matter, by providing benchmarks, guidelines and algorithms that deal with densification; however, those topics still need further investigation. For example, the impact of signalling limitations and imperfect channel state information (e.g., in scheduling algorithms) on the system performance, solutions to combat with inter-cell interference, and co-existence with half-duplex systems require further studies to get more comprehensive view on how full-duplex could be best deployed to future 5G systems. Also the developed MAC protocol and routing solutions can be optimized further to improve their performance in practical mobile ad-hoc networks.

Potential standardization opportunities to introduce full-duplex in to future wireless systems are identified as 3GPP ‘Study Item on 5G’ [58], and IEEE802.11ax ‘High Efficiency WLAN’ [59].

7. SUMMARY AND CONCLUSIONS

This document provides summary on main results from research on full-duplex transceiver techniques and system level solutions conducted in the DUPLO project.

The Full-Duplex Radios for Local Access – DUPLO project is a concerted effort with partners from industry and academia that addresses the challenge of developing transceiver techniques and system level solutions for full-duplex operation in small area radio systems. The project started in November 2012, and concludes in May 2015.

DUPLO has studied potential full-duplex transceiver techniques for radio devices, aiming to solutions which are attractive in terms of form-factor, system integration, process technology and operation flexibility. Three RF/antenna/analog solutions have been developed. These solutions cover a SI-cancelling front-end, a dual-polarized antenna structure and an electrical balance duplexer. Compared to the state-of-the-art, the developed designs differ mainly in terms of form-factor and integration potential in compact or portable radio system devices. This is significant advance for the DUPLO solutions, since the previously published techniques mainly rely on physical dimensions (i.e. antenna spacing) and/or require bulky component.

Main emphasis in the digital baseband solutions related studies has been in search for novel algorithms to improve self-interference cancellation capability in the presence of transceiver non-linearity, and in performance improvements with joint RF and digital cancellation. Furthermore, precoding techniques and baseband algorithms for full-duplex MIMO systems have been analysed and developed.

The DUPLO proof-of-concept hardware demonstrator integrates sub-set of the designs into a complete full-duplex transceiver solution enabling performance measurements in realistic dynamic indoor operation environment. Conducted performance measurements indicate that the achievable self-interference cancellation capability is around 65 dB and 90 dB in 20 MHz bandwidth, with single port antenna solution and dual port antenna solution, respectively. As proof-of-concept for the functional operation, the two integrated demonstrators illustrating a short distance point-to-point link based on DUPLO hardware technology has been successfully demonstrated in VTC-2015 Spring DUPLO Workshop.

DUPLO system level studies have focused on full-duplex transmission in small cell radio system operation environment. Potential use cases are full-duplex BS serving half-duplex UEs, full-duplex UE, device-to-device connections, relaying, and transmission in mesh networks. Numerical results from conducted performance studies in network level indicate that in small area systems full-duplex transmission can provide system level performance gains over half-duplex even with moderate self-interference cancellation levels (70 dB…90 dB). However, better self-interference cancellation capability in the full-duplex transceiver is beneficial in expanding the competitive operation range of full-duplex transmission. Maximum observed system level capacity gain of full-duplex over half-duplex in small cell networks varies from 40% to 80% depending on the study assumptions.

Radio resource management is crucial when aiming to utilize full-duplex transmission efficiently in wireless networks. Several algorithms have been devised to tackle issues such as spectral efficiency maximization, scheduling, co-channel interference, power allocation etc. Advanced relaying schemes, protocol solutions for mobile ad-hoc networks and network level management solutions are also covered.

The DUPLO work on full-duplex technology development has gained lot of attention outside the project, and has been well received for multiple top-tier publications and conferences in various domains. DUPLO has organized two workshops on full-duplex technology, the first in conjunction

with Crowncom 2014 and the second with VTC-2015 Spring conference. Both workshops were attended by around 40 people from academia and industry.

All in all, the results from conducted studies on full-duplex transceiver techniques and system level solutions are encouraging, and pave path for introducing full-duplex transmission as an air interface technology for future 5G systems. Obviously there are several further research opportunities and development needs remaining after the DUPLO project. For example, improving the performance of full-duplex transceiver designs for compact radio devices, integration of full-duplex with other protocols in the radio transceiver, full-duplex MIMO, and enhancements to radio resource management and protocols to improve system performance in multi-cell environments and in co-existence with half-duplex systems.

8. REFERENCES

[1] Next Generation Mobile Networks (NGMN) Alliance, “5G White Paper”, Feb. 2015.

[2] Ericsson, “5G Wireless Access”, *White Paper*, Feb. 2015.

[3] A. Sabharwal, P. Schniter, D. Guo, D. Bliss, S. Rangarajan, and R. Wichman, “In-band Full-duplex Wireless: Challenges and Opportunities”, *IEEE Journal on Selected Areas in Communications (JSAC)*, vol. 32, no. 9, Sept. 2014.

[4] J.F. O’Hara, G.M. Moore, “A high performance CW receiver using feedthru nulling”, Microwave Journal, vol. 6, no. 9, pp. 63-71, 1963.

[5] W.T. Slingsby, J. McGeehan, “A high-gain cell enhancer”, in IEEE 42nd Vehicular Technology Conference, pp. 756-758, vol. 2, 1992.

[6] D. Bharadia, E. McMilin, and S. Katti, “Full duplex radios”, in *Proc. SIGCOMM’13*, Hong Kong, China, Aug. 2013.

[7] S. Hong, J. Brand, J. Choi, M. Jain, J. Mehlman, S. Katti, P. Levis, “Applications of Self-Interference Cancellation in 5G and Beyond”, *IEEE Communications Magazine*, Feb. 2014, pp. 114-121.

[8] D. Kim, H. Lee, D. Hong, “A Survey of In-band Full-duplex Transmission: From the Perspective of PHY and MAC Layers”, in *IEEE Communications Surveys & Tutorials*, Issue 99, 2015.

[9] M. Khojastepour, E. Aryafar, K. Sundaresan, R Mahindra, S. Rangarajan, “Exploring the Potential for Full-Duplex in Legacy LTE Systems”, in *Proc. SECON 2014*, Singapore, Jun. 2014.

[10] J. Heo, H. Ju, S. Park, E. Kim, D. Hong, “Simultaneous Sensing and Transmission in Cognitive Radio”, *IEEE Transactions on Wireless Communications*, vol. 13, no. 4, Apr. 2014, pp. 1948-1959.

[11] EU funded research project DUPLO (Full-Duplex Radios for Local Access, FP7-ICT-316369, Nov. 2012 to May 2015), **http://www.fp7-duplo.eu/** .

[12] E. Everett, A. Sahai, A. Sabharwal, “Passive Self-Interference Suppression for Full-Duplex Infrastructure Nodes,” *IEEE Transactions on Wireless Communication*, Feb. 2014, pp. 680-694.

[13] B. Nauta, “Report from Technical Workshop”, INFSO-ICT- 316369 DUPLO - Report D6.2, June 2014.

[14] D.J. van den Broek, “Dissemination report”, INFSO-ICT- 316369 DUPLO - Report D6.4, May 2015.

[15] V. Tapio, “System scenarios and technical requirements for full-duplex concept”, INFSO-ICT-316369 DUPLO - Report D1.1, April 2013.

[16] B. Debaillie, “Design and Measurement report for RF and antenna solutions for self-interference cancellation”, INFSO-ICT- 316369 DUPLO - Report D2.1, April 2014.

[17] B. Debaillie, “Integration report of RF and antenna self-interference cancellation techniques”, INFSO-ICT- 316369 DUPLO - Report D2.2, October 2014.

[18] D.J. van den Broek, “Transceiver circuits simulation, implementation and measurement report”, INFSO-ICT- 316369 DUPLO - Report D2.3.1, April 2014.

[19] D.J. van den Broek, “Transceiver circuits simulation, implementation and measurement report”, INFSO-ICT- 316369 DUPLO - Report D2.3.2, April 2015.

[20] M. Ghoraishi, “ Digital baseband solutions for full-duplex transceiver”, INFSO-ICT- 316369 DUPLO - Report D3.1, May 2014.

[21] M. Ghoraishi, “Enhanced solutions for full-duplex transceivers and systems”, INFSO-ICT-316369 DUPLO - Report D3.2, June 2015.

[22] P. Pirinen, “Performance of full-duplex systems”, INFSO-ICT- 316369 DUPLO - Report D4.1.1, January 2014.

[23] A. Pouttu, “Performance of full-duplex systems”, INFSO-ICT- 316369 DUPLO - Report D4.1.2, April 2015.

[24] J. Seddar, “Radio resource management and protocol solutions for full-duplex systems”, INFSO-ICT- 316369 DUPLO - Report D4.2, May 2015.

[25] C. Palacios, “Early integration and test”, INFSO-ICT- 316369 DUPLO - Report D5.1, June 2014.

[26] C. Lavin, “Final proof-of-concept validation, results and analysisEarly integration and test”, INFSO-ICT- 316369 DUPLO - Report D5.2, May 2015.

[27] B. Debaillie, D.J. van den Broek, C. Lavin, B. van Liempd, E.A.M. Klumperink, C. Palacios, J. Craninckx, B. Nauta, and A. Parssinen, “Analog/RF solutions enabling compact full-duplex radios,” *IEEE Journal on Selected Areas in Communications (JSAC)*, vol. 32, no. 9, pp. 1662–1673, Sep. 2014.

[28] B. van Liempd, C. Lavin, S. Malotaux, D.J. van den Broek, B. Debaillie, C. Palacios, J.R. Long, E. Klumperink, and J. Craninckx, “RF self-interference cancellation for full-duplex,” in *Proc. International Conference on Cognitive Radio Oriented Wireless Networks (CrownCom)*, pp. 526-531, July 2014.

[29] K. Rikkinen, V. Tapio, H. Alves, M. Al-Imari, A.C. Cirik, J. Seddar, A. Sethi, B. Debaillie, C. Lavin, “Full-duplex transmission in small area radio communication systems,” *International Workshop on Computer-Aided Modeling Analysis and Design of Communication Links and Networks (CAMAD)* - Special Session on Duplexing Techniques for 5G Networks, Sept. 2015.

[30] D. Nguyen, L.-N. Tran, P. Pirinen, and M. Latva-aho, “On the spectral efficiency of full-duplex small cell wireless systems,” *IEEE Transactions on Wireless Communications*, Vol. 13 , No. 9, pp. 4896 – 4910, Sept. 2014

[31] A. Cirik, K. Rikkinen, M. Latva-aho, ”Joint Subcarrier and Power Allocation for Sum-Rate Maximization in OFDMA Full-Duplex Systems”, *IEEE Vehicular Technology Conference (VTC2015-Spring)*, May 2015.

[32] A. Cirik, K. Rikkinen, Y. Rong, “A Subcarrier and Power Allocation Algorithm for OFDMA Full-Duplex Systems”, *EuCNC2015 conference*, July 2015.

[33] M. Al-Imari, M. Ghoraishi, P. Xiao, R. Tafazolli, “Game Theory Based Radio Resource Allocation for Full-Duplex Systems”, *IEEE Vehicular Technology Conference (VTC2015-Spring)*, May 2015.

[34] J. Seddar, H. Khalife, W. Alsafwi, V. Conan, “A full duplex MAC protocol for wireless networks”, accepted to *The International Wireless Communications & Mobile Computing Conference (IWCMC 2015)*, Aug. 2015.

[35] **http://mangocomm.com/products/kits/warp-v3-kit** .

[36] **https://warpproject.org/trac** .

[37] D.H. Mahrof, E.A.M. Klumperink, M.S. Oude Alink, B. Nauta, "A Receiver with in-band IIP3>20dBm, exploiting Cancelling of OpAmp Finite-Gain-induced Distortion via Negative Conductance," *IEEE Radio Frequency Integrated Circuits Symposium*, June 2013.

[38] D.J. van den Broek, E.A.M. Klumperink, B. Nauta, "A self-interference-cancelling receiver for in-band full-duplex wireless with low distortion under cancellation of strong TX leakage," *IEEE Solid-State Circuits Conference (ISSCC)*, Feb. 2015.

[39] D.J. van den Broek, E.A.M. Klumperink, B. Nauta, "A self-interference-cancelling Front-End for In-Band full-duplex wireless and its Phase Noise Performance," *IEEE Radio Frequency Integrated Circuits Symposium (RFIC)*, May 2015.

[40] B. Debaillie, D.J. van den Broek, C. Lavín, B. van Liempd, E.A.M. Klumperink, C. Palacios, J. Craninckx, B. Nauta, "RF Self-Interference Reduction Techniques for Compact Full-Duplex Radios", *IEEE Vehicular Technology Conference (VTC2015-Spring),* May 2015.

[41] Sahai, A., et al., "On the Impact of Phase Noise on Active Cancelation in Wireless Full-Duplex", *IEEE Transactions on Vehicular Technology*, 2013. 62(9): p. 4494-4510.

[42] M. Mikhemar, H. Darabi, and A.A. Abidi, "A multiband RF antenna duplexer on CMOS: Design and performance," *IEEE Journal of Solid-State Circuits*, vol. 48, no. 9, pp. 2067–2077, Sept. 2013.

[43] S.H Abdelhalem, P.S. Gudem, and L.E. Larson, "Hybrid transformer-based tunable differential duplexer in a 90-nm CMOS process*," IEEE Transactions on Microwave Theory and Techniques*, March 2013

[44] M. Mikhael, B. van Liempd, J. Craninckx, R. Guindi, B. Debaillie, "A Full-Duplex Transceiver Prototype with In-System Automated Tuning of the RF Self-Interference Cancellation", *International Conference on 5G for Ubiquitous Connectivity (5GU)*, Nov. 2014.

[45] B. van Liempd, B. Hershberg, K. Raczkowski, S. Ariumi, U. Karthaus, K.F. Bink, J. Craninckx, "A +70dBm IIP3 single-ended electrical-balance duplexer in 0.18um SOI CMOS," *IEEE International Solid- State Circuits Conference (ISSCC)*, Feb. 2015.

[46] B. van Liempd, B. Hershberg, B. Debaillie, P. Wambacq, J. Craninckx, "An Electrical-Balance Duplexer for In-Band Full-Duplex with <-85dBm In-Band Distortion at +10dBm TX-power," *European Solid State Circuits Conference (ESSCIRC),* Sept. 2015.

[47] B. Debaillie, B. van Liempd, B. Hershberg, J. Craninckx, K. Rikkinen, D.J. van den Broek, E.A.M. Klumperink, B. Nauta, "In-Band Full-Duplex Transceiver Technology for 5G Mobile Networks*," European Solid State Circuits Conference (ESSCIRC)*, Sept. 2015.

[48] W. Li, J. Lilleberg, "Full-Duplex Link Performance Under Consideration of Error Vector Magnitude", In Proc. on *IEEE Wireless Communications and Networking Conference WCNC 2014*, pp. 654 – 659,Istanbul, Turkey, April 2014.

[49] W. Li, J. Lilleberg, K. Rikkinen, " On Rate Region Analysis Of Half- and Full-Duplex OFDM Communication Links*", IEEE Journal on Selected Areas in Communications (JSAC)*, Vol. 32, No. 9, pp.1688 - 1698, Sept. 2014.

[50] H. Malik, M. Ghoraishi, R. Tafazolli, "Cross-Layer Approach for Asymmetric Traffic Accommodation in Full-Duplex Wireless Network", *European Conference on Networks and Communications (EUCNC) 2015*, Paris, France, July 2015.

[51] C. H. M. de Lima, P. H. J. Nardelli, H. Alves, M. Latva-aho, "Full-duplex communications in interference networks under composite fading channel", in *2014 European Conference on Networks and Communications (EUCNC)*, June 2014.

[52] H. Alves, C. H. M. De Lima, P. H. J. Nardelli, R. D. Souza, and M. Latva-aho, On the Average Spectral Efficiency of Interference-Limited Full-Duplex Networks, in *9th International Conference on Cognitive Radio Oriented Wireless Networks (Crowncom),* June 2014.

[53] A. C. Cirik, K. Rikkinen, R. Wang, and Y. Hua, "Resource allocation in full-duplex OFDMA systems with partial channel state information," accepted to *IEEE China Summit and Int. Conf. Signal and Inf. Process. (ChinaSIP)*, July 2015.

[54] C. H. M. de Lima, H. Alves, P. H. J. Nardelli, M. Latva-aho, "Hybrid Half- and Full-Duplex Communications Under Correlated Lognormal Shadowing," IEEE Vehicular Technology Conference (VTC2015-Spring), May 2015.

[55] H. Alves, R. D. Souza, and M. Latva-aho, "Full-Duplex Relaying Systems Subject to Co-channel Interference and Noise in Nakagami-m", *IEEE Vehicular Technology Conference (VTC2015-Spring),* May 2015.

[56] A. C. Cirik, R. Wang, Y. Hua, and M. Latva-aho, "Weighted sum-rate maximization for full-duplex MIMO interference channels," *IEEE Transactions on Communications*, vol. 63, no. 3, pp. 801-815, March 2015.

[57] A. C. Cirik, "Fairness Considerations for Full Duplex Multi-user MIMO Systems", *IEEE Wireless Communication Letters*, accepted for publication, 2015.

[58] D. Flore, B. Bertenyi, "5G Timeline in 3GPP", SP-150140, 3GPP TSG RAN#67, Shanghai, China, March 2015.

[59] K. Chang, et al. , "In-band Full Duplex Radios and System Performance", IEEE 802.11-15-0043-01-00ax, Jan. 2015.

[60] M. Ghoraishi, W. Jiang, P. Xiao, R. Tafazolli, "Subband Approach for Wideband Self-Interference Cancellation in Full-Duplex Transceiver", *IEEE International Wireless Communications & Mobile Computing Conference (IWCMC) 2015*, Dubrovnik, Croatia , Aug. 2015.

[61] D. Schreurs, M. O'Droma, A.A. Goacher, M. Gadringer (Ed.), RF Power Amplifier Behavioral Modeling, Cambridge University Press. 2009.

[62] P. Xiao, M. Sellathurai, "Improved linear transmit processing for single-user and multi-user MIMO communications systems," *IEEE Transactions on Signal Processing*, vol. 58, no. 3, pp. 1768–1779, March 2010.